UNIVERSITY OF CALIFORNIA
SANTA CRUZ

BIOLOGICAL AND PHYSICAL MODIFICATIONS TO THE ONSET OF SEDIMENT TRANSPORT

A dissertation submitted in partial satisfaction
of the requirements for the degree

DOCTOR OF PHILOSOPHY

in

EARTH AND PLANETARY SCIENCES

by

Claire C. Masteller

December 2017

The Dissertation of Claire C. Masteller is approved:

Associate Professor Noah Finnegan, chair

Professor Emily Brodsky

Dr. David Rubin

Professor Leonard Sklar

Tyrus Miller
Vice Provost and Dean of Graduate Studies

List of Figures

List of Tables

ABSTRACT

Biological and physical modifications to the onset of sediment transport

by

Claire C. Masteller

Virtually all mechanistic predictions of landscape evolution are underpinned by predictions of sediment transport rates. Sediment transport via bedload is the primary way by which coarse sediment is transported through landscapes, and thus, accurate prediction of bedload transport represents a fundamental topic in the study of earth surface processes. Specifically, predictions of coarse sediment transport are strongly dependent on the selection of the threshold for motion, or the forcing at which sediment transport begins. However, it is well known that the threshold for motion varies in space and time, and in response to a number of processes. This dissertation aims to identify and quantify the effects of biology and prior flow history on the onset of coarse particle motion through a combination of mathematical modeling, novel physical experiments, and continuous bedload transport measurements in the field. Chapter 2 develops and tests a mechanistic model for the entrainment of coarse sediment by attached kelp, highlighting the significance of biology in setting coastal sediment transport rates. In Chapter 3, we explore the effects of below-threshold, antecedent flow history on gravel bed structure, grain protrusion, and bedload transport through a series of flume experiments. We find that bedload flux, and by extension, the onset of motion, is extremely sensitive to the duration of prior below-threshold flow. This reduction in bedload transport rates is

related to the reduction in the population of high protruding grains, related to the pivoting of precariously placed, highly mobile particles into nearby pockets. In Chapter 4, we carry out a systematic analysis of the temporal evolution of the threshold for motion in a natural channel though the analysis of a unique record of continuous bedload transport measurements. We observe that variations in the threshold for motion are significantly linked to previous flow magnitude, highlighting that the onset of motion is a history-dependent quantity. Collectively, these studies provide new observations and approaches towards predicting the temporal and spatial evolution of the threshold for motion, providing a basis for improved bedload transport models.

For my tremendous parents, George and Sandy, whose encouragement and support I could not have done without.

Acknowledgements

It's frankly impossible to thank everyone that has played a role in my dissertation experience in the following pages. Nonetheless, I will try my best.

First and foremost, I'd like to thank my advisor, Noah Finnegan. First, for changing his mind and accepting me as a graduate student five years ago. Hopefully he does not regret it! Noah's excitement to explore new ideas, evidenced by the range of problems that I have seen him work on over the last five years, has really been inspiring. I hope that one day I can maintain the same breadth of research. I want to thank Noah for giving me the space and freedom to explore throughout my graduate experience. Noah truly let me be the driver of my own dissertation, but was always there to pull out the map when I veered a little too far off course. Noah, thank you for your continued support, excitement, and willingness to explore – this thesis would not be what it is without you. I am truly grateful to have had you as my advisor.

I'd also like to thank the other members of my committee: Emily Brodsky, Leonard Sklar, and Dave Rubin. Emily, thank you for entertaining multiple reading groups through the years. From granular mechanics to fatigue, your encouragement to expand my views beyond geomorphology has played an enormous role in my graduate studies, and frankly, how I approach scientific research. I'd like to thank Leonard Sklar for opening Richmond Field Station to me, for his incredible kindness, and for his generous, insightful comments and ideas. Dave Rubin's enthusiasm has

been a constant source of support throughout my dissertation, and a constant reminder of the world beyond the flume.

The Finnegan geomorphology group has been a continuous source of motivation and friendship throughout this process. Thanks to you all – Jon Perkins, Kerri Johnson, Danica Roth, Allison Pfeiffer, Rachael Klier, Dave Santaniello, and Christian Braudrick. Though Luca Malatesta has only joined our group recently, his openness and excitement has made an enormous difference in these final months. Thank you for pushing me to explain my sweeping scientific claims, I am glad to call you my friend. The most special thanks are reserved for Alex Nereson, whose unwavering friendship, willingness to let me disrupt his work with frantic whiteboard drawings and arm-waving, and seemingly endless supply of both patience (and wine), has meant the world.

Numerous other colleagues have contributed significantly to this document. Thank you to Jonathan Warrick and Ian Miller, co-authors of Chapter 2, for your shared enthusiasm for kelp. Chapter 3 benefited greatly from help with regarding experimental design and data collection from Christian Braudrick. Without the generosity of Jens Turowski and Dieter Rickenmann, Chapter 4 would not have been possible. Joel Johnson, whose work has been a constant source of inspiration and encouragement, has also generously provided advice and comments on Chapters 3 and 4.

Many friends and family members have carried me through this thesis. Mom and Dad, thank you for your love and support through this process, I wouldn't be

where I am or who I am without you. Thank you for being so understanding, even if you didn't always understand my work. To all of my friends who have celebrated my successes and been there for me when things didn't go my way, I can't thank you enough. To name only a few – Stephanie and Tali, thank you for always listening; Neil and Earl, thank you for always making me laugh; Andrew, thanks for being my most reliable drinking buddy. To Peter, Jackie, and Hannah, thanks for sticking with me through the thick of it.

Colin Phillips has truly become a great friend, mentor, and integral support system over these years. Colin has always had my best interests at heart and has looked out for me in more ways that I can count. As an undergraduate, Colin guided me through my first AGU, making a point to teach me how to network. As a third-year graduate student, Colin went out of his way to bring me to St. Anthony Falls Laboratory to support my experimental endeavors, and bought me multiple dinners when he deemed my graduate-student budget diet (mostly Cliff Bars) unacceptable. Most recently, Colin's willingness to endure numerous two to three-hour phone calls (sometimes on weekends), to talk me through proposal applications, difficult career decisions, and potential scientific directions has been invaluable. Thank you, Colin, for holding me to a high standard of scientific rigor via text message, for always providing a proverbial open-door, and for some of the most valuable advice.

I would remiss to not acknowledge Doug Jerolmack – a hefty task, that I saved for last. Words cannot express how I am lucky to have found such a tenacious advocate and mentor so early in my career (before I had a career, even). I walked

into Doug's class as a fine art major looking to fulfill a general education requirement. I walked out a budding geomorphologist. Doug's passion for science and for geomorphology is infectious – it hooked me almost immediately and I have never looked back. If it were not for Doug's willingness to give me the opportunity to explore Earth's surface through the lens of his lab, his encouragement to pursue a PhD, and going above and beyond as an advocate for me, I would not be where I am today.

Funding support *for my graduate education was supported by National Science Foundation Graduate Research Fellowship grant DGE-1339067, the ARCS Foundation Fellowship from the Northern California Chapter, and numerous UCSC Graduate Student Association travel grants.*

Chapter 1

Introduction

Landscapes evolve through the complex interplay of tectonics and climate over geologic timescales. However, the evolution of a landscape, in its simplest form, occurs through the redistribution of mass over time. Rivers represent the main conduit by which tectonic and climatic signals can be transferred across the entire landscape. Through the transport of sediment, signals from mountainous regions are propagated downstream, until they are finally deposited in the ocean and archived into the stratigraphic record. Thus, it is of fundamental importance to determine the conditions under which sediment transport begins.

Sediment mobility is the thread that connects the projects in my dissertation, which together address the fundamental question: *under what conditions does sediment move?* While a simple question, observations of sediment transport rates in the field commonly diverge strongly from model predictions (Gomez and Church, 1989; Recking et al., 2012). This discrepancy has broad ramifications for how rivers and ecosystems evolve, including their response to changes in climate. With improved sediment mobility models, these environments can be understood more completely and managed more effectively, for instance, by optimizing timed dam releases in order to maintain aquatic habitats. The goal of my dissertation is to identify and quantify processes, both biological and physical, that result in varying

sediment mobility, through a combination of mathematical modeling, field observations, and novel physical experiments.

While the patterns and processes that shape landscapes are intimately connected to the biology that colonizes them (Dietrich and Perron, 2006), sediment transport and landscape evolution models do not explicitly account for its impact on model physics. The first chapter of my dissertation begins to address this knowledge gap by quantifying the impacts of kelp on the onset of motion for coarse particles. Specifically, I developed and implemented an analytical model accounting for the added forces of drag and lift by kelp, quantifying the role of attached kelp on the onset of motion for coarse sediments for the first time. Observations at a site in the Strait of Juan de Fuca confirm the model predictions, demonstrating that kelp increases sediment mobility by as much as 92%. These results highlight that biology is fundamental to the physical processes shaping the coastal zone in this setting. My findings were published in *Geology* in April 2015.

In fluvial systems, predictions of sediment transport rates are routinely made with empirical models using large-scale characteristics of rivers, such as channel width, depth, and slope (Shields, 1936; Wong and Parker, 2006; Lamb et al., 2008b). These models ignore the complex packing of sediment on a riverbed and the physics associated with the evolution of these granular packings. For my second chapter, I designed and carried out flume experiments to constrain the impact of sediment packing arrangements on grain mobility. I, for the first time, tested a 25-year old hypothesis regarding the influence of grain protrusion on bedload sediment transport

rates (Kirchner et al., 1990). A synthesis of high-resolution topographic surveys generated from digital images paired with experimental transport data show that the proportion of particles protruding highest into the flow, ~1% of the total riverbed, govern sediment flux. This result emphasizes that subtle changes in bed topography have dramatic effects on sediment transport. This work was published in the *Journal of Geophysical Research: Earth Surface* in December 2016.

Landscape and riverbed structure reflect not only their formative processes, but also the operative timescales over which memory of previous history persists. However, fluvial bedload transport is typically treated as a process that is independent of any previous time step, and is solely dependent on concurrent flow strength (Meyer-Peter and Müller, 1948; Wong and Parker, 2006). However, in some well-documented examples, bedload sediment transport clearly displays short- and long-term dependence on prior flow history (Yager et al., 2012b; Saletti et al., 2015). Thus, it is natural to ask what processes cause the threshold for motion to vary over time. My third chapter builds on results from my flume experiments, which suggest that alluvial riverbeds are sensitive to their prior flow history (Masteller and Finnegan, 2017), incorporating field observations from a steep mountain stream in the Swiss Prealps, and highlighting seasonal signatures of riverbed aging, evidenced by systematic, seasonal increases in the threshold of sediment motion, consistent over a 20-year period. This work represents the first, systematic analysis of history-dependence of the threshold for motion in a natural channel. We identify a class of below- and near-threshold flows over which memory of past flow magnitude is reflected by threshold for

motion. Further, we identify a range of flows which disrupt the aging process, and result in a loss of correlation, or the destruction of the memory of prior flow magnitude related to the onset of motion.

A universal finding, which spans all three chapters of this dissertation, is that the variation in individual particle mobility has significant effects on bedload transport rates in both coastal and fluvial environments. This dissertation attempts to identify and quantify some of the processes that result in this variability in sediment mobility. Further, this work provides new approaches and directions towards more accurate predictions of sediment transport rates by drawing from scientific disciplines outside of geomorphology, including biomechanics and granular physics.

Chapter 2

Kelp, cobbles, and currents: Biologic reduction of coarse grain entrainment stress

Previously published as:

Masteller, C.C., Finnegan, N.J., Warrick, J.A., and Miller, I.M., 2015, Kelp, cobbles, and currents: Biologic reduction of coarse grain entrainment stress: Geology, v. 43, no. 6, p. 543–546, doi: 10.1130/G36616.1.

2.1 Abstract

Models quantifying the onset of sediment motion do not typically account for the effect of biotic processes, as it is typically difficult to isolate and quantify in relation to physical processes. Here, we investigate an example of the interaction of kelp (Order Laminariales) and coarse sediment transport in the coastal zone where it is possible to directly quantify and test its effect. Kelp are ubiquitous along rocky coastlines and their impact on ecosystems has been well studied. We develop a physical model to explore the reduction in critical shear stress of large cobbles colonized by *Nereocystis luetkeana*, or bull kelp. Observations of coarse sediment motion at a site in the Strait of Juan de Fuca confirm the model prediction and show that kelp reduces the critical stress required for transport of a given grain size by up to

92%, enabling annual coarse sediment transport rates comparable to fluvial systems. We demonstrate that biology is fundamental to the physical processes that shape the coastal zone in this setting.

2.2 Introduction

Biological activity is pervasive across seascapes and living organisms influence its topographic evolution. In cool mid and high-latitude waters, kelp forests colonize the sublittoral zone and play a vital role in coastal ecosystems (Pearse and Hines, 1979; Harrold and Reed, 1985; Estes and Duggins, 1995; Steneck et al., 2003). Kelp colonize hard substrate such as bedrock, boulders, or cobbles (Emery and Tschudy, 1941; Morrison et al., 2009). Unlike organisms that have evolved to reduce their size to withstand high-energy environments, kelp are generally large and flexible, allowing them to endure high wave and current stresses (Friedland and Denny, 1995). Kelp holdfasts anchor the plant in place by attaching to bedrock or large grains through a chemical weathering process in which metabolites from the plant dissolve the rock, allowing the holdfast to penetrate up to 10 mm (Morrison et al., 2009). This attachment also allows for the hydrodynamic forces from the frond, which is suspended in the water column, to be transferred to the underlying substrate through a stem-like stipe (Figure 2.1). This transfer of forces may aid in the transport of coarse sediment by altering the net driving force acting on the grain, subsequently reducing the bottom stress required for entrainment.

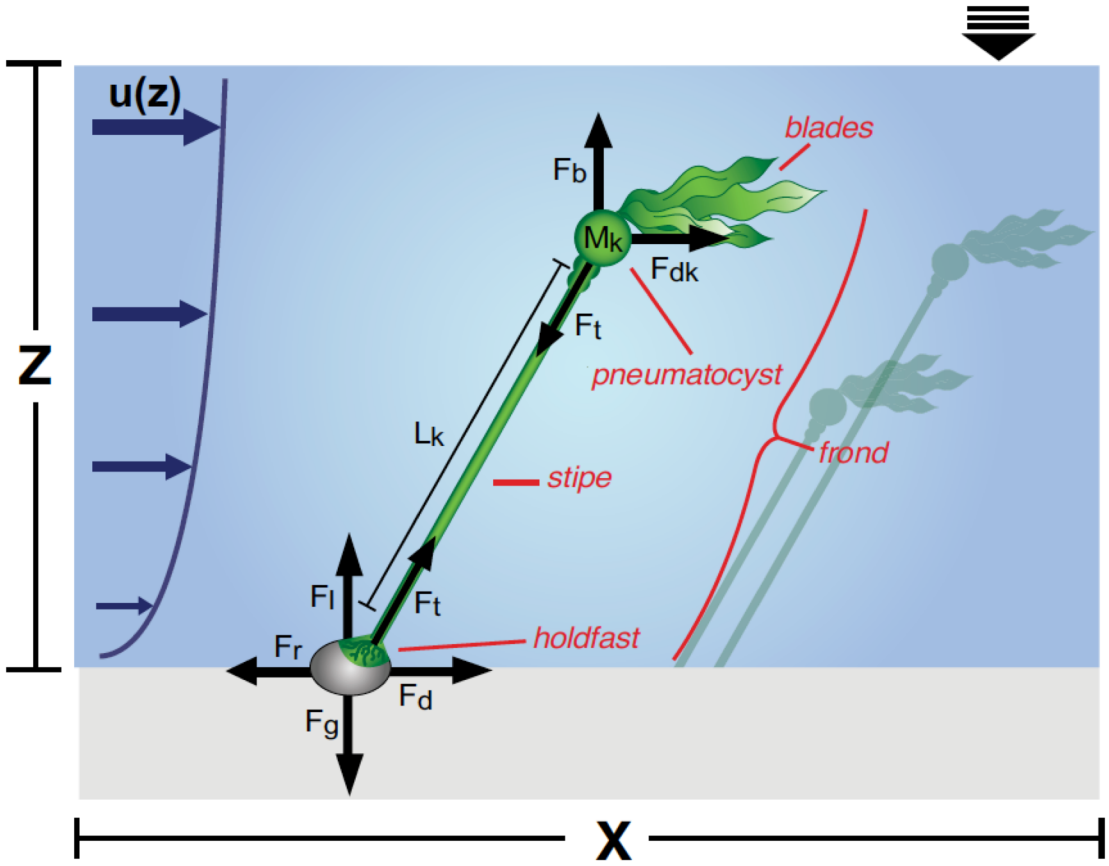

Figure 2.1. Model schematic. Bull kelp frond with grain attached, relevant forces labeled. Model components include kelp mass, M_k, kelp length, L_k, unidirectional velocity profile, u(z), and forces acting on the grain and the kelp. The drag, F_d, lift, F_l, resisting, F_r, and gravitational force, F_g, acting on the grain are highlighted, as well as the buoyant force, F_b, and the drag force, $F_{d\ kelp}$, acting on the kelp. The tension force, F_t, acts along the kelp stipe and is transferred to the grain.

Kelp-assisted transport of large cobbles has been observed across the globe, including in southern Africa (Woodborne et al., 1989), northern Europe (Naylor et al., 2012), New Zealand (Garden and Smith, 2011), Antarctic regions (Emery and Tschudy, 1941), and both coasts of North America (Scheibling et al., 2009; Frey and Dashtgard, 2012) and has also been studied in experiments (Kudrass, 1974; Gilbert, 1984; Carling, 2014). The transport of large grains in anomalously low current conditions has been noted by a number of these studies (Kudrass, 1974; Woodborne

et al., 1989; Garden and Smith, 2011; Frey and Dashtgard, 2012), and deposits of large cobbles with kelp attached have been found in an estuary where current velocities are typically sufficient to only transport silt (Woodborne et al., 1989). These observations suggest that the attachment of large kelp fronds can substantially reduce the threshold for motion for large grains. An experimental flume study found that this addition reduces critical stress of all size fractions examined (Carling, 2014). Further, a single in situ observation has shown that kelp-assisted transport can occur at current velocities far below the critical threshold for motion predicted by entrainment models that do not consider the impact of kelp (Frey and Dashtgard, 2012). However, a quantitative, mechanistic model for kelp-assisted entrainment has not been previously presented.

It is worth noting that there are many species of kelp (Order Laminariales) globally, with variable characteristics, including size, morphology, physical properties (e.g. stiffness), and habitat (e.g. depth and substrate preferences). Here, we examine the potential transport properties of *Nereocystis luetkeana,* or Northeast Pacific Ocean bull kelp, which occurs in depths 10 – 17 m from Alaska to Central California (Denny et al., 1997). The adult bull kelp plants reach 20 – 45 m in height and have blades that are concentrated near one large pneumatocyst near the tip of the stipe, a flexible, stem-like structure (Denny et al., 1997). For the remainder of this study, we use bull kelp to calibrate a model we develop for kelp-assisted grain entrainment and focus on observations of bull kelp assisted transport from the Strait of Juan de Fuca in Washington State.

2.3 The model

The threshold for incipient motion is typically determined by balancing the driving forces of drag and lift against the resisting forces of gravity and friction acting on a grain (Wiberg and Smith, 1987). This model does not account for the forces translated from attached frond to its underlying substrate, and thus these must be quantified and applied to this preexisting model to better capture the effect of kelp. The response of kelp to hydrodynamic forces of both waves and currents is well-studied (Utter and Denny, 1996; Denny et al., 1997; Gaylord and Denny, 1997; Denny et al., 1998; Stevens et al., 2001; Gaylord et al., 2008), and the main forces applied to the kelp frond include a buoyant force, drag force, and tension force (Figure 2.1).

The buoyant force, F_b, is generated by a density difference between the kelp and the surrounding water due to the pneumatocysts, or large gas-filled bladders, which allow the plant to float in the water column (Utter and Denny, 1996). The buoyant force is dependent on the material properties of the kelp, which generates a density difference, and acts in the upward direction. As the density of kelp is not well-reported, we rely on empirical measurements of the mean buoyant force for bull kelp, and apply a large range of buoyant forces surrounding that mean (Friedland and Denny, 1995; Utter and Denny, 1996; Denny et al., 1997; Stevens et al., 2001).

As water flows past kelp, there is a drag force, F_d, over the area of the frond in the direction of flow (Utter and Denny, 1996). The drag formulation for a kelp frond

is species specific, accounting for variability in plant shape and size and is generally given by:

$$F_d = 0.5\rho_f u^{\beta} A_k S_d \qquad (1)$$

where u is current velocity (m/s), β is an empirically determined exponent that changes with the shape of the kelp frond. For non-streamlined objects, β = 2, while for streamlined objects and plates oriented parallel to the flow, β~1.5 (Vogel, 1984). A_k is the area of the kelp frond (m^2), and S_d is an empirically determined, dimensionless shape parameter similar to the drag coefficient (Friedland and Denny, 1995; Utter and Denny, 1996; Denny et al., 1997).

As kelp stretches and flexes in response to the flow, the tension across the plant increases. When the kelp is stretched beyond its initial length, the tension force, F_t, which extends in the direction of stretching, is dependent on the overall change in length, the material stiffness, and the cross-sectional area of the frond and is given by:

$$F_t = E[(L_k+\Delta L_k)/L_k]^c A_{xs} \qquad (2)$$

where E is the stiffness of the kelp stipe (MPa), a measured empirical property, L_k is the unstretched length of the kelp frond (m), ΔL_k is the change in length of the kelp frond (m), c is an empirically determined exponent, and A_{xs} is the cross-sectional area (m^2) (Utter and Denny, 1996; Denny et al., 1997).

We take advantage of the previous models of kelp frond hydrodynamics (Utter and Denny, 1996) and combine it with an existing model for entrainment (Wiberg and Smith, 1987) to determine the impact of a frond on the force balance considered for the initiation of motion. A full derivation of this revised force balance

is presented in the Supplementary Material. Specifically, using a finite difference approach, we numerically solve for the static force balance between drag and buoyancy, as well as kelp angle and stretch that balances the frictional resistance of that grain for a given current velocity. We assume a unidirectional, steady current, which follows a "law of the wall" logarithmic velocity profile, noting that the extrapolation of the profile to the entire water column may result in slightly elevated velocities in the upper portion of the water column (Yalin, 1972). For our application, the unidirectional current resulting in sediment transport is assumed to be tidal in origin. We apply this modified force balance in order to determine the reduction in entrainment stress for a range of grain sizes and current conditions.

2.4 Methods

In order to test the model predictions, we compare model output to field observations of kelp-assisted transport at the mouth of the Elwha River, in the Strait of Juan de Fuca in Washington State. The recent removals of the Elwha Dam and Glines Canyon Dam have garnered widespread attention due to the enormous volume of sediment liberated by these projects (East et al., 2015; Gelfenbaum et al., 2015). Consequently, a number of studies have focused on the transport and fate of sediment and the response of the coastal landscape to sediment loading (Duda et al., 2011; Miller et al., 2011). To support these investigations, an Acoustic Doppler Current Profiler (ADCP) was deployed at the mouth of the Elwha River to measure current

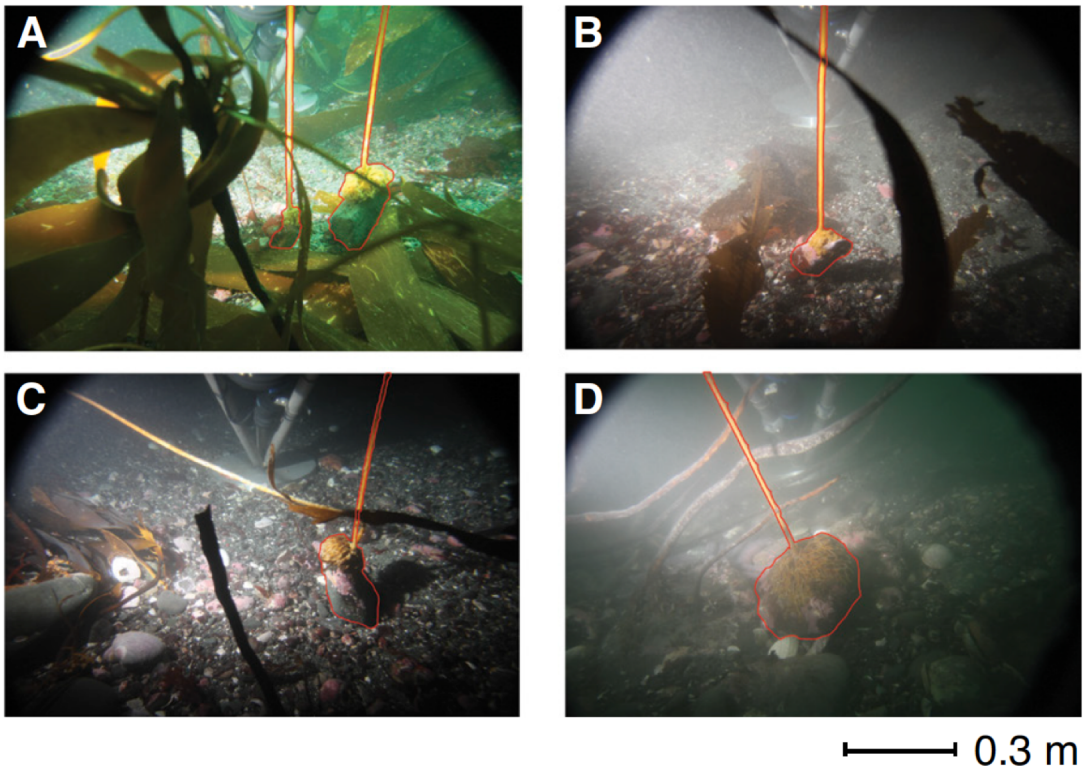

Figure 2.2 A-D. **Kelp-assisted transport observations.** Underwater observations of kelp-assisted transport events, with rocks with kelp attached outlined in red. Scale set by 0.3 m diameter tripod foot in background.

velocity, direction, and turbidity at five-minute intervals. The sampling tripod was outfitted with a camera, which captures oblique images of the bed every four hours. Between October 2011 and October 2012, 71 kelp-assisted sediment transport events were identified from the tripod photos. The grain size of the transported cobbles was estimated from the images by comparing the cobble to the tripod foot, which has a known diameter of 0.3 m (Figure 2.2). These 71 observations were on the same image plane as the tripod foot in order to minimize error introduced into grain size measurements due to camera perspective. All other rocks with attached kelp were ignored. The maximum surface current velocity for the preceding four-hour period is assigned to the identified transport event.

Table 2.1. Model parameters for *Nereocystis luetkeana*

Variable	Description	Value
F_b	Buoyant force (N)	2, 12, 25
β	Drag coefficient	1.6
S_d	Shape coefficient	0.016
E	Stipe stiffness (Pa)	1.2×10^7
c	Tension exponent	1
A_{xs}	Cross-sectional area of stipe (m^2)	4.1×10^{-5}
L_k	Stipe length (m)	2, 4, 6, 8
A_k	Area, function of length (m^2)	$0.14\ L_k^{1.27}$
M_k	Mass, function of area (kg)	$0.124\ A_k^{1.391}$

Note: Species-specific, empirically determined parameters for *Nereocystis luetkeana* for kelp-assisted entrainment model (Denny et al., 1997).

We parameterize the model for *Nereocystis luetkeana*, or bull kelp, the kelp species most frequently observed in the underwater photos (Table 2.1). We assign a water depth of 9 m, consistent with the average water depth at the site, and explore a range of kelp lengths from 2 to 8 m, well within the range for *Nereocystis luetkeana*, as direct measurement was impossible (Stevens et al., 2001). Bracketing one known direct measurement of bull kelp buoyant force of 12.51 N, we explore a larger range of buoyant forces from 2N to 25 N (Denny et al., 1997). We consider a steady, uniform current and do not incorporate forces due to waves in this first-order model. Waves do occur in this Strait of Juan de Fuca study area, although at heights considerably smaller than those observed along the outer Pacific Ocean coast (Duda et al., 2011; Miller et al., 2011). We assess wave action by looking for trends between significant wave height, surface current velocity, and grain size for the identified transport events (Figure 2.3a). We observed no clear relation between significant wave height, grain size, and surface current velocity. Further, the majority of the transport events show small values for corresponding significant wave height measurements. These findings indicate that waves are not likely to drive kelp-assisted transport at this location and further reinforces the choice to consider a unidirectional,

steady current in the model. That said, we acknowledge the clear potential for waves to influence transport in shallower water or where waves are higher.

2.5 Results

Model results indicate that the addition of kelp drastically reduces the current velocity necessary for entrainment for all grain sizes considered (Figure 2.3). Grain sizes range from 0.02 m to 0.25 m with a mean size of 0.09 m. The grain-only model for incipient motion overpredicts the velocity required for transport of the measured grain sizes by a mean value of 81% and a maximum of 92%. These findings agree well with the 92% reduction in velocity observed by a previous study in the Strait of Juan de Fuca (Frey and Dashtgard, 2012). None of the observations of kelp-assisted transport can be reconciled with the grain-only model for entrainment (Figure 2.3). Current velocities recorded during transport are 44% higher than the mean surface current velocities measured between October 2011 and October 2012, indicating that entrainment is a threshold process, and that rocks with kelp attached are not simply floating in the water column (Figure 2.3b-c).

The model presented here, which considers the force translated from the kelp frond to the attached grain, encompasses 87% of the ADCP observations of transport. It is worth noting that the model predictions presented here are conservative, as we do not consider wave effects and only account for a fraction of the variation of both buoyant force and kelp length. We consider bull kelp fronds up to 8 m in length, as

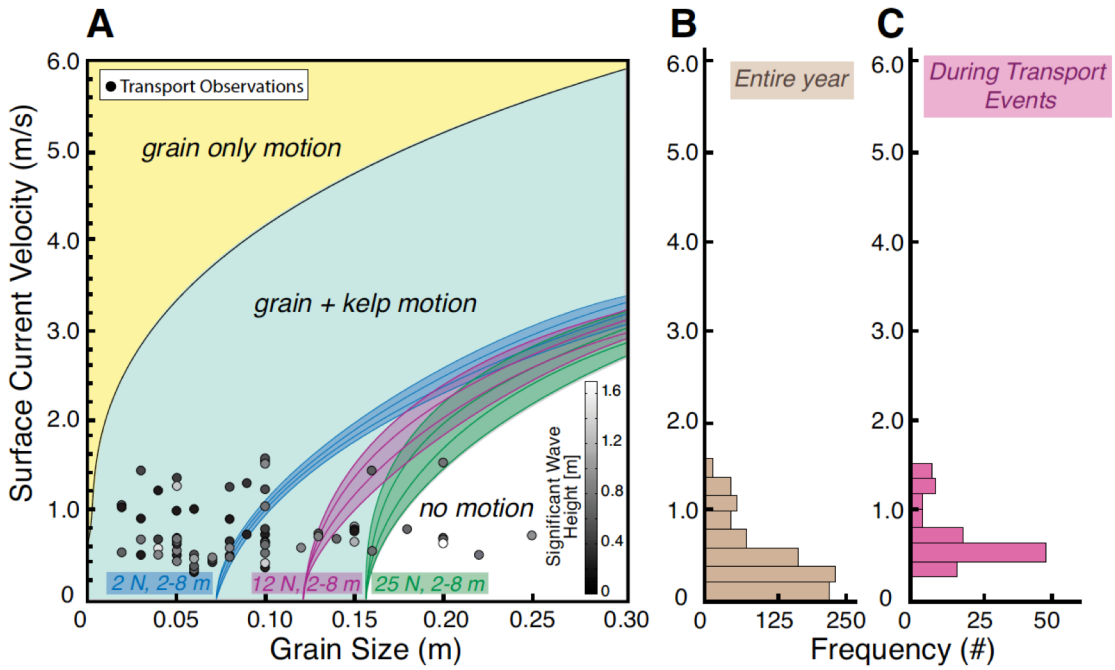

Figure 2.3. Model predictions and field observations. A) Model output for both the grain-only force balance and the grain and kelp force balance models for incipient motion with consideration of a range of frond lengths (2–8 m) and buoyant forces (2–25 N). Lines show the maximum transportable grain size for each combination of length and buoyant force for a range of surface current velocities. Transport observations are plotted over model results with corresponding colors representing measured significant wave heights for each transport event. **B)** Distribution of surface current velocities for the entire year of sampling. **C)** Distribution of surface current velocities during observed kelp-assisted transport events.

the average water depth at our study site is only 9 m. However, bull kelp can grow up to 20–45 m in length (Stevens et al., 2001). An increase in kelp length increases the drag force, encompassing a larger fraction of the ADCP observations (Figure 2.3). An increased buoyant force has similar effects, as the increase in upward force will more effectively oppose the downward force due to the weight of the grain, thereby reducing the frictional resistance to grain motion (Woodborne et al., 1989).

2.6 Discussion

Model results indicate that the addition of kelp drastically reduces the entrainment stress required for motion. We show that a model for incipient motion without the consideration of the attached kelp is not consistent with any of the field observations of kelp-assisted transport from the Strait of Juan de Fuca. The model presented here, while conservative, can reconcile the majority of underwater observations.

To determine the contribution of kelp-assisted transport towards overall sediment flux within the coastal zone, we approximate the coarse sediment transport rate from tripod observations. We estimate the total volume of observed rocks with kelp attached from the photos and normalize by the width of the photo to calculate the total annual coarse sediment transport rate of 1.5×10^3 kg/m/yr from observations, assuming a density of 2650 kg/m^3, typical of quartz sand. We note that this annual transport rate is a conservative estimate, as photos were taken every four hours and only encompass a very small fraction of the year. Nevertheless, our estimate of the coarse flux here is comparable to an estimate of fluvial transport rate (3×10^3 kg/m/yr) from a perennial, armored lowland stream (Laronne et al., 2003). Remarkably, kelp-assisted transport rates are similar to those in fluvial systems. Yet, regions of kelp-assisted transport likely extend hundreds of meters in the across-shore (i.e., normal to the current) direction, a length scale much greater than most gravel transporting fluvial systems. Thus, biology plays a key role in controlling both coarse sediment

fluxes and morphodynamics within the coastal zone of this, and potentially many other settings.

Due to the linkage between kelp and coarse sediment transport at the mouth of the Elwha River, the recent dam removals are likely to impact the frequency of future kelp-assisted coarse transport. In the near-term, high turbidity and increased scour in the coastal waters around the river mouth will likely prevent the recruitment or growth of kelp (Duda et al., 2011). In the long-term, a shift in substrate toward finer sediment size classes that aren't utilized by kelp around the Elwha River delta may lead to a reduction in kelp density (Gelfenbaum et al., 2015). Thus, at this location, independent of current conditions, the maximum transportable grain size can change drastically depending on the structure and spatial distribution of the kelp population.

2.7 Conclusion

We have shown that kelp facilitates the transport of large grains at anomalously low current velocities. Kelp or seaweed assisted transport may therefore explain the process by which incongruously large grains can be deposited in relatively low energy environments (Emery and Tschudy, 1941; Woodborne et al., 1989). These results suggest that kelp may facilitate significant sediment transport rates, and therefore may play a fundamental role in structuring the morphology of the coastal environment in temperate seas. It is worth emphasizing that the influence of biology on coarse sediment transport may be overlooked in the rock record, given that kelps and seaweeds decompose quickly and are rarely preserved (Emery and Tschudy,

1941). Without considering this mechanism of transport, it is possible to misinterpret past environmental conditions. These results highlight the important link between biology and the processes that shape the landscape upon which life colonizes.

2.8 Acknowledgements

This material is based upon work supported by the National Science Foundation Graduate Research Fellowship under Grant No. NSF DGE-1339067. We thank Melissa Foley of USGS Santa Cruz for supplying ADCP photos. Jessica Lacy provided a review of an earlier version of this paper. Tripods were funded by the USGS Coastal and Marine Geology Program and a grant from the Puget Sound Partnership / U.S. Environmental Protection Agency

Chapter 3

Interplay of grain protrusion and bedload transport in a laboratory flume

Previously published as:

Masteller, C.C., and Finnegan, N.J., 2017, Interplay between grain protrusion and sediment entrainment in an experimental flume: Journal of Geophysical Research: Earth Surface, v. 122, no. 1, p. 274–289, doi: 10.1002/2016JF003943.

3.1 Abstract

Bedload sediment transport is typically formulated as a nonlinear function of the shear stress exerted on the bed in excess of a critical value. However, because of the inherent spatial variability in both grain packing and protrusion on waterworked beds, the critical stress used in transport models represents a spatial averaging of the critical stresses for the entrainment of many individual particles on the bed. We perform a series of flume experiments in which we quantify, for the first time, the evolution of grain-scale topography during low flow periods and its controls on bedload sediment transport rates and hence critical stresses. By exploiting the observed dependence of bedload flux on antecedent low flow duration,

we experimentally simulate a wide array of transport rates at the same applied Shields stress in order to isolate the relationship between grain protrusion and bedload flux. A synthesis of high-resolution bed topography surveys and bedload flux data show that bedload transport rates characteristic of gravel bedded channels are governed by the proportion of particles that protrude highest above the bed, a population that corresponds to ~1% of the total bed elevation distribution in our experiments. This result supports the argument that only a small portion grain entrainment thresholds for a riverbed are exceed during transport and controls bedload transport rates. Further, these results emphasize that subtle changes in bed topography can have dramatic effects on bedload sediment transport. We also find that the transport of these highest protruding particles enhances the local erosion of surrounding grains.

3.2 Introduction

Bedload transport is a regime of sediment transport in which particles roll, slide, or saltate in a series of successive low hops along the streambed. Impacts from saltating bedload can result in the incision of bedrock channels and contribute to the evolution of bedrock channel morphology (Sklar and Dietrich, 2004; Hsu et al., 2008; Lamb et al., 2008; Sklar and Dietrich, 2008). In gravel-bedded river channels, the necessity of transporting the coarse load is likely a key control on channel morphology (Parker, 1979; Phillips et al., 2016). By modifying river morphology,

bedload sediment transport also impacts aquatic habitat suitability for freshwater organisms (Montgomery et al., 2011; Albertson et al., 2014; Riebe et al., 2014; East et al., 2015). Despite the large body of scientific work focused on bedload transport, it remains difficult to predict accurately. This difficulty lies in the complex coupling between fluid and granular processes at the interface of a flow and an underlying deformable sediment boundary (e.g. Dancey et al., 2002; Papanicolaou et al., 2002; Charru et al., 2004; Jerolmack and Paola, 2010), resulting in a wide range of conditions for the onset of sediment motion.

The concept of a singular value for the critical stress at which sediment transport begins originates from the experimental work of Shields (1936), and has subsequently been studied theoretically (Wiberg and Smith, 1987). Typically, a single value for this critical stress, commonly non-dimensionalized as the critical Shields stress, or τ^*_c, is assigned in the calculation of sediment flux from bedload transport formulas (e.g., Meyer-Peter and Müller, 1948). However, a compilation of eight decades of incipient motion studies reveals considerable scatter in cited values of τ^*_c in both field and laboratory observations (Buffington and Montgomery, 1997). Further, time-series observations from single channels also show a wide range of conditions for the initiation of sediment motion (Reid et al., 1985; Turowski et al., 2011). Put simply, the use of a single value of critical Shields stress in the prediction of bedload flux does not fully capture the complex processes that control bedload transport rates. Previous studies have shown that variability in critical shear stress may be due to changes in bed pocket geometry (Wiberg and Smith, 1987; Kirchner et

al., 1990), grain exposure and protrusion (Fenton and Abbott, 1977; Kirchner et al., 1990), bed grain size distribution (Parker and Sutherland, 1990; Ferguson, 1994; Wilcock and Crowe, 2003), channel slope (Lamb et al., 2008), and even biological organisms (Albertson et al., 2014; Masteller et al., 2015).

Kirchner et al. (1990) advocated that the critical stress for the entrainment of natural particles should not be treated as a single value, but rather as a probability distribution of entrainment thresholds to encompass the wide range of grain packing and protrusion on a natural bed. Kirchner et al. (1990) argued that only the tail of this distribution of critical stresses, representing a very small fraction of the particles that comprise water-worked beds, have low enough entrainment stresses to be moved by typical flows. These most mobile particles include those that protrude highest above the bed, as they experience the highest fluid drag (Fenton and Abbott, 1977; Wiberg and Smith, 1987) and have the lowest grain friction angles. A consequence of this hypothesis is that the availability of these highest protruding particles should control bedload flux during transport. Thus, an accurate prediction of sediment transport requires both a quantification of bed topography at the particle scale, as well as the processes that shape and modify this bed topography.

Several studies (Kirchner et al., 1990; Buffington et al., 1992) have characterized the distribution of both protrusion and friction angle on gravel beds. However, the relationship between the distribution of protrusion heights and bedload transport rates has not been examined previously. This gap in previous work is likely

due to the difficulty of measuring the protrusion of many, individual grains. The recent advent of high-resolution laser scanning and photogrammetric methods has allowed for better quantification of particle-scale topography. For example, a recent study utilized high-resolution topographic measurements of a gravel bed to illustrate spatial variations in predicted entrainment stress due to differences in grain packing between pool and riffle sequences (Hodge et al., 2013). However, a more direct quantitative test of Kirchner et al. (1990) that links experimental measurements of bedload transport and the details of bed topography has not been undertaken prior to this work.

Although Kirchner argued that only the highest protruding grains are mobilized during typical flows, the result of their motion may modify the protrusion, and subsequently, the mobility of surrounding particles. *Brayshaw* (1985) showed that neighboring grains influence the initial motion of approximately 70% of moving particles by altering the relative protrusion of the surrounding particles. This local instability drives collective entrainment and group transport of the surrounding grains (Ancey et al., 2006; Heyman et al., 2013). Thus, the relative availability of high protruding grains should control bedload transport rates in two fundamental ways. First, Protruding grains are relatively more mobile themselves. Second, Protruding grains, when transported, can destabilize their neighbors.

More recently, studies have also focused on the temporal variation of sediment mobility due to stress history. Both field (Reid et al., 1985; Turowski et al.,

2011) and experimental studies (Monteith and Pender, 2005; Paphitis and Collins, 2005; Haynes and Pender, 2007) demonstrate large changes in the rate and timing of bedload transport as a function of antecedent low flow duration, when little to no transport was evident on the bed. Specifically, the results of these studies find that bedload transport rates decrease with increased antecedent periods of low flow. These studies suggest that the observed temporal patterns in sediment mobility are related to changes in bed structure, namely bed compaction (Paphitis and Collins, 2005; Ockelford and Haynes, 2013) or reduction in bed roughness (Ockelford and Haynes, 2013). The work presented here builds on previous work in this area by explicitly linking changes in bed structure during low flow to subsequent changes in bedload flux during transport flows. Further, this work moves beyond bulk characteristics of bed topography and focuses on the scale of individual particles.

Variability in the arrangement of particles on the bed surface during transport can result in variability in sediment mobility. The formation of gravel clusters (Brayshaw, 1984; Church et al., 1998), imbricated stone lines, and other interlocked arrangements (Laronne and Carson, 1976), as well as fluvial armor (Parker and Klingeman, 1982), all tend to stabilize gravel channels and decrease bed mobility. However, the formation of these structures tends to require above threshold transport (e.g. Parker and Klingeman, 1982). This work explores the ability of below threshold flows to stabilize the bed in the absence of these gravel structures, which has not been explored previously at the particle scale.

This study focuses on how the development of stabilizing bed structure is dependent on prior stress history; namely the duration of an antecedent low flow. We examine how this variation in riverbed particle arrangement impacts bedload transport at the onset of motion. We link the temporal and spatial variation in the distribution of mobile particles to bedload transport through the analysis of high-resolution measurements of grain protrusion using Structure from Motion (SFM) Photogrammetry (Westoby et al., 2012). Specifically, we exploit these temporal effects to test the hypothesis of Kirchner et al. (1990) which states that only small portions of the bed protrude high enough to be mobile during typical transporting flows, and, consequently, observed changes in grain protrusion should correlate to variation in bedload transport rates.

3.3 Experimental Methods

3.3.1 Experimental set-up and workflow

A series of 10 flume experiments were completed in a 5 m long, 0.3 m wide flume with a slope of 0.008 at the Richmond Field Station, University of California, Berkeley. In order to isolate the impacts of grain-scale bed topography on bedload transport, we seek to generate a wide range of bedload transport rates at an identical transport stress. By eliminating any variation in fluid forcing, we hypothesize that changes in transport should be reflected in bed surface topography. Following previous experiments (Monteith and Pender, 2005; Haynes and Pender, 2007), the

bed is exposed to a low flow conditioning period for various antecedent durations to induce small-scale topographic changes in the experimental alluvial river in the absence of bedload transport. In order to explore the connection between grain-scale topography and gravel transport, we then measure the resultant changes in surface topography and bedload flux during a subsequent transport event.

More specifically, the experiments occur in three phases: bed preparation, conditioning, and transport. To prepare the bed, we hand mixed and screeded gravels ranging from 2-24 mm (D_{50} = 8.5 mm, and geometric standard deviation, σ = 4.3 mm) in the flume in order to yield the least packed, least sorted bed possible. This initial, "loosely packed" bed surface should generate the strongest response to low flow conditioning on short timescales. This preparation was repeated before the beginning of each experiment. After mixing, to begin the conditioning stage water was then fed into the flume and the flow rate was slowly increased until it achieved a bed Shields stress (τ^*_{50}) of ~0.039. Bed Shields stress measurements were calculated using the hydraulic radius calculated from six point measurements of water depth taken longitudinally along the flume at 0.5 m intervals. Depth at each point varies by less than 1 cm (0.05-0.06 m), resulting in less than a 10% variation in applied Shields stress between experimental runs. Water surface slope in each experiment was added to the overall slope of the flume, yielding on average, a slope approximately equal to 0.011. This calculated slope, as well as the median grain size of the sediment mixture (D_{50} = 8.5 mm), was used for the calculation of τ_{*50}. The applied Shields stress approaches the lower bound of the range of critical Shields stress identified by

Buffington and Montgomery (1997) and did not generate any measureable bedload flux out of the flume. We then varied the duration of this low flow conditioning time over four intervals: 1 minute (2 runs), 10 minutes (3 runs), 100 minutes (3 runs), and 200 minutes (2 runs). The selection of this longest flow duration was based on observations from previous studies, in which the most pronounced changes in critical Shields stress and bedload flux occur over short time scales (Monteith and Pender, 2005; Paphitis and Collins, 2005; Haynes and Pender, 2007).

Following this conditioning period, we increased the flow to a bed Shields stress (τ_{*50}) of ~0.051, which is comparable to values of τ_{*c} that correspond to bankfull conditions for gravel rivers (Parker et al., 2007; Phillips et al., 2016). Bedload is caught by a basket placed at the end of the flume and weighed at the end of the three-minute transport period. This time period represents a compromise between allowing enough time to quantify bedload transport and avoiding significant removal of surface sediments, which would complicate the interpretation of the effects of surface topography on measured transport rates.

To ensure that no significant grain displacement occurred during the filling and draining of the flume, we filled the flume slowly; increasing the flow over a 30 second period prior to the conditioning and transport stages. This also avoided a significant flood bore at the onset of flow. Painted tracer particles were placed in the flume at the beginning of each experiment and showed no displacement between draining and refilling of the flume during experiments.

3.3.2 Measuring bed topography

Structure From Motion (SFM) surveys were completed when the flume was drained following the initial preparation of the bed, the conditioning period, and again following the transport period. Thirty-nine permanent benchmarks were placed in the flume to facilitate processing. Ninety digital photos of a 150 cm long section at the bottom of the flume were processed using the software Agisoft Photoscan to yield a high-resolution, three-dimensional point cloud of the sample area. This point cloud was then transformed into a 2 mm x 2 mm gridded digital elevation model (DEM) of the flume area in the open source software CloudCompare (www.danielgm.net/cc/).

To quantify the repeatability of SFM measurements, we conducted a test in which we constructed multiple DEMs of the same experimental bed from two sets of repeat images. The DEMs were then compared at each grid point, from which we calculated a root mean square error of 1.4 mm (Figure B.2). We cropped 7 cm from each side of all of the experimental DEMs, resulting in a 16 cm by 150 cm DEM area of the flume bed to avoid increased spatial errors or distortion near the flume walls and in areas where photo coverage is sparse. In order to facilitate the analysis of local bed topography, we detrend the bed DEM by removing the best-fit plane to the bed topography. We then measured protrusion by locating local maxima exceeding elevation thresholds spaced in 1 mm increments from the mean bed elevation (protrusion threshold of 0 mm) to 15 mm above mean bed elevation (Figure 3.1).

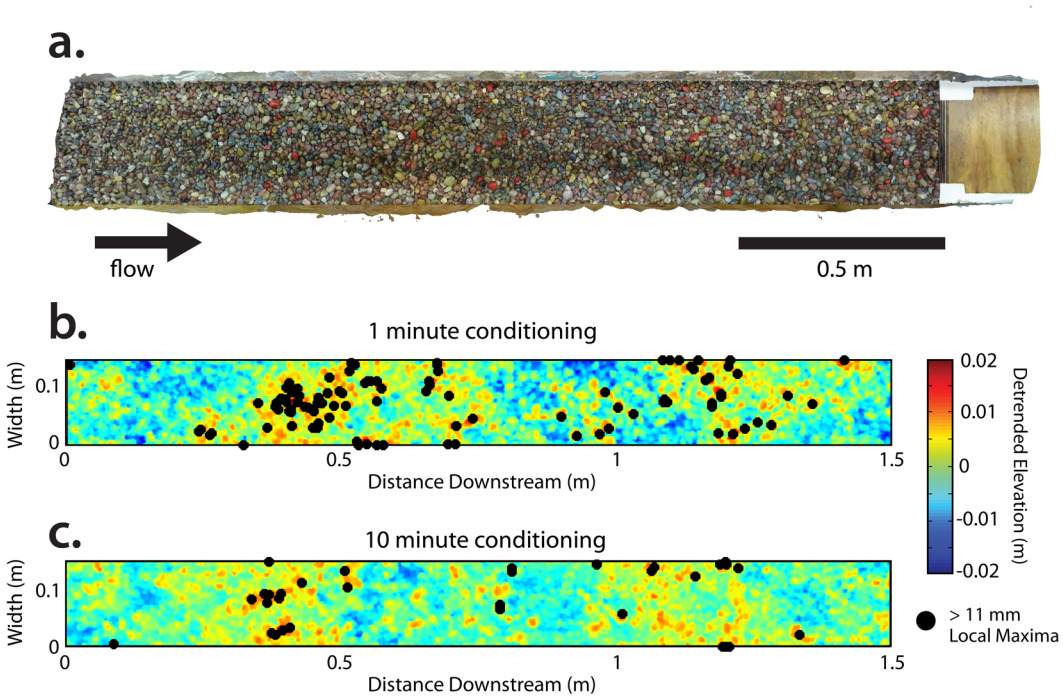

Figure 3.1. a) High-resolution photomosaic of the flume bed. Structure From Motion (SFM) derived, detrended, Digital Elevation Model (DEM) of the flume bed following a low flow conditioning period of **b)** 1 minute and **c)** 10 minutes. Black circles represent local elevation maxima in excess of 11 mm above the mean bed elevation.

Local maxima were found by searching along the columns, rows, and the diagonals crossing each location on the DEM. Local maxima are identified at a minimum spacing of 4 mm due to the resolution of the gridded DEM. The measured protrusion is relative to mean bed elevation, and does not impart any information regarding the size of the grain associated with the identified local maxima.

Bed surface grain-size distributions were measured to determine if any significant armoring occurred during any phase of the experiment, as changes in surface grain size could impact sediment transport rates (Wiberg and Smith, 1987; Parker and Sutherland, 1990). Photos of the bed were taken to carry out automated

grain size measurements by implementing the digital grain-size algorithm described in Buscombe (2013). This algorithm uses the spatial distribution of pixel intensity from photos of the bed to capture the scales of variability that exist in the image. It then approximates the full grain size using a global wavelet power spectrum. For more details on the automated grain-size algorithm see Buscombe (2013). We calibrate the algorithm by determining the resolution of each image in ImageJ (imagej.nih.gov/ij/) and find that the average resolution of the images used in our analysis is 0.1 mm/pixel. With this calibration, the RMS error of the grain size analysis is, on average, less than 1 mm (~0.75 mm) (Buscombe, 2013). Thus, we round our grain size measurements to the nearest millimeter.

3.3.3 Linking grain protrusion to bedload transport rates

To assess the relationship between sediment transport rates and protrusion, Pearson's linear correlation coefficients were computed between the total bedload flux during the transport stage and the density of protruding points at or above each specified elevation threshold after the conditioning phase of each experiment. We calculated the correlation coefficient at 1 mm intervals from the mean bed elevation (protrusion threshold of 0 mm) to 15 mm above mean bed elevation. We then focus our analysis on the protrusion thresholds that exhibit a significant relationship with bedload measurements ($p<0.05$).

We calculate bed elevation changes during the transport phase by differencing

the DEMs from after the conditioning and transport phases. This allows us to examine the mobility of the grains with a significant correlation with bedload transport relative to the rest of the bed. In addition, patterns of erosion and deposition measured from these DEMs are also used to assess the potential for these grains to act as "keystones", whose removal enhances collective erosion of the surrounding grains. We use the term keystone grain after Booth et al., (2014), only in the sense that their removal impacts the mobility and subsequent transport of surrounding grains.

To determine if there is heightened erosion driven by the removal of these protruding grains, we examine the local elevation changes surrounding any particle with a significant correlation with bedload flux. To avoid the erosion signal of the keystone grain itself, represented by the local maxima in this analysis, we do not sample within a 0.016 m (~2 median grain diameters) x 0.016 m square surrounding the identified local maxima. This length scale was selected to account for the uncertainty in the position of the local maxima relative to the edge of the particle. Further, the selection of twice the D_{50} encompasses a large range of the grain sizes that may be represented by the identified local maxima.

To isolate the impact of removing a keystone on only its nearest neighbors, we measure the elevation change of the area immediately surrounding a protruding particle. This sample region restricts the sample area to a one D_{50}-wide ring around the grain, with dimensions of 0.032 m x 0.032 m, excluding the inner 0.016 m x 0.016 m square. While there may be further reaching hydrodynamic effects from the

removal of these grains (e.g. Brayshaw et al., 1983; Lacey and Roy, 2008), our sample area represents a conservative estimate of the potential mass contribution associated with the removal of the local maxima, as it only considers the grains directly surrounding the keystone. While some sheltering may occur between closely spaced local maxima, we eliminate any local maxima that are spaced more closely to one another than a single grain diameter (0.0085 m) from the analysis in order to avoid overlap of erosion signals. The number of grains eliminated due to overlap is, on average, about 20 grains, or about 30% of the population. Distributions of elevation change surrounding these high points are then compared to elevation changes observed at all points of the differenced DEMs to determine both how mobile different protruding grain populations are during transport, as well as the impact of these grains on the transport of their neighbors.

3.4 Results

3.4.1 Bedload transport rates

Cumulative bedload flux during the transport phase of the experiments decreases linearly as a function of increased conditioning time (Figure 3.2, Table 3.1). These observations are qualitatively consistent with previous studies (Monteith and Pender, 2005; Haynes and Pender, 2007) in that bedload flux decreases as a function of low flow conditioning time. A linear fit line produces the best-fit value to the data (R^2=0.86), but an exponential fit also has good agreement (R^2=0.76). Given this, paired with the differences in conditioning time between this work (1-200 minutes)

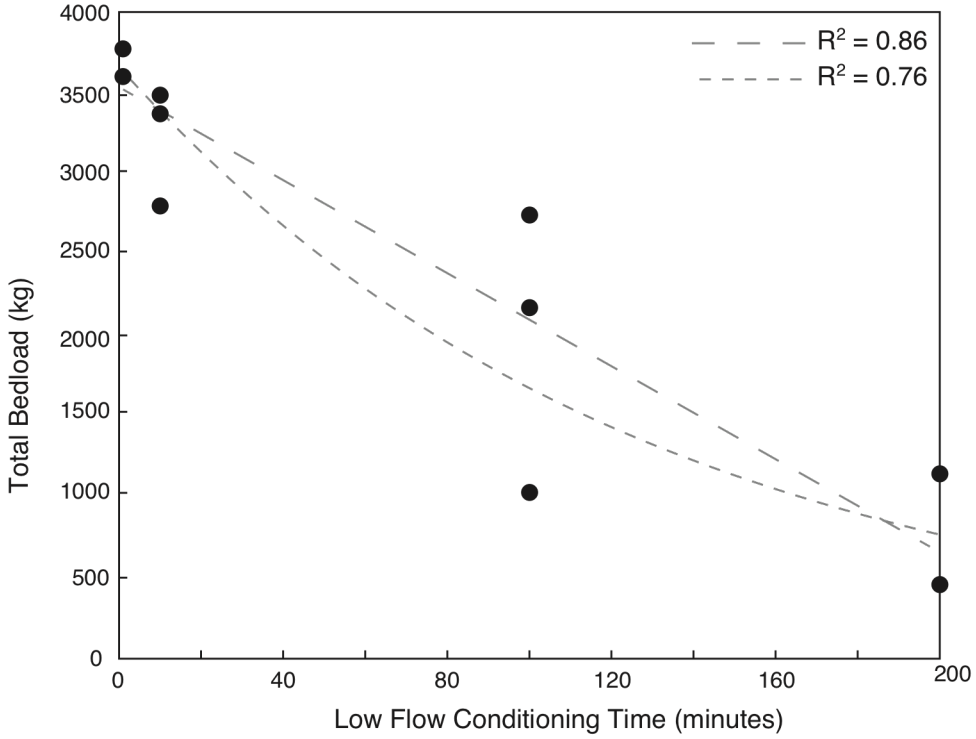

Figure 3.2. Total bedload as a function of low flow antecedent conditioning time for 10 experiments with linear (dashed) and exponential (dotted) best-fit lines. Bedload flux was measured over a 3-minute time period.

and previous studies (1,440 minutes (Haynes and Pender, 2007)), we do not compare our quantitative relationship directly. These results are consistent with an overall reduction in grain mobility, implying an increase in critical Shields stress with increased conditioning time. Bedload flux does not approach a constant value during our experiments, but rather, continues to decrease as a function of low flow antecedent conditioning time. After one minute of low flow conditioning, transport rates are high, with a maximum flux, $q_s = 0.066$ kgm^{-1}s^{-1}. After 200 minutes of low flow conditioning, bedload flux decreases by a factor of seven to a minimum value, q_s

Table 3.1. Bed Load Transport, Grain Size, and Slope Data for the Initial, Conditioned, and Transport Phases of All 10 Experiments[a]

Table 1. Bed Load Transport, Grain Size, and Slope Data for the Initial, Conditioned, and Transport Phases of All 10 Experiments[a]

		Initial				After Conditioning				After Transport			
Conditioning Time	Bed Load Flux (kg/m/s)	D_{16} (m)	D_{50} (m)	D_{84} (m)	Slope	D_{16} (m)	D_{50} (m)	D_{84} (m)	Slope	D_{16} (m)	D_{50} (m)	D_{84} (m)	Slope
1	0.063	0.004	0.010	0.019	0.015	0.005	0.011	0.021	0.017	0.005	0.010	0.020	0.022
1	0.066	0.004	0.010	0.018	0.011	0.005	0.011	0.020	0.012	0.004	0.009	0.018	0.015
10	0.049	0.005	0.011	0.020	0.013	0.005	0.011	0.019	0.013	0.005	0.011	0.021	0.010
10	0.061	0.005	0.011	0.019	0.026	0.005	0.010	0.019	0.027	0.005	0.012	0.019	0.010
10	0.059	0.004	0.009	0.016	0.016	0.004	0.009	0.018	0.019	0.004	0.008	0.018	0.013
100	0.038	0.004	0.009	0.017	0.019	0.005	0.011	0.020	0.018	0.005	0.011	0.021	0.005
100	0.048	0.006	0.011	0.018	0.017	0.005	0.010	0.018	0.019	0.005	0.009	0.020	0.017
100	0.018	0.005	0.011	0.020	0.014	0.005	0.011	0.020	0.014	0.005	0.011	0.020	0.013
200	0.020	0.004	0.010	0.019	0.016	0.005	0.011	0.018	0.017	0.005	0.010	0.021	0.011
200	0.008	0.006	0.012	0.022	0.012	0.005	0.010	0.018	0.010	0.005	0.011	0.019	0.016
Correlation coefficient flux versus slope					0.26				0.44				0.18
P value ($\alpha = 0.05$)					0.476				0.204				0.627

[a]Correlation coefficients and *p* values between observed bed load flux and slope.

= 0.009 $kgm^{-1}s^{-1}$. The dimensionless Einstein bedload numbers (q_*) (Einstein, 1950) for the experiments range from q_*= 0.001 to q_*= 0.008, and are consistent with observations of transport in gravel bed rivers (e.g. Reid and Laronne, 1995).

Distributions of bed elevation range, on average, from a minimum value of 2 cm below mean bed elevation to 2 cm above mean bed elevation, which is approximately equivalent to the size of the largest grains present in the experiments (D_{max} ~2 cm). Contrary to previous studies, mean bed elevation does not evolve as a function of conditioning time, as observed by Ockelford and Haynes (2013) (Table 3.2). Further, the changes in the standard deviation of surface topography are subtle, on the order of 0.01-0.1 mm (at a maximum, 3.5% of D_{50}) (Table 3.2, Figure 3.3), and within the range of error of the topographic measurements. These results suggest that on short timescales, changes in mean bed elevation and standard deviation do not reflect the duration of low flow conditioning time.

Table 3.2. Changes in standard deviation and mean bed elevation between initial and conditioning phases of each experiment

Table 2. Changes in Standard Deviation and Mean Bed Elevation Between Initial and Conditioning Phases of Each Experiment

Conditioning Time	Change in Standard Deviation of Bed Elevation (m)	Change in Mean Bed Elevation (m)
1	3.00E-04	−3.14E-04
1	4.24E-05	8.29E-04
10	1.51E-04	3.31E-04
10	2.23E-04	−2.61E-03
10	1.18E-04	−4.44E-03
100	8.84E-05	1.91E-03
100	8.34E-05	1.80E-03
100	1.42E-04	−1.03E-02
200	3.02E-05	−1.85E-03
200	1.11E-04	9.05E-04

In each experimental run, the largest change in the elevation distribution occurs in the tails of the distribution, or at the highest and lowest elevations across the bed (Figure 3.3). This reduction in the highest elevations suggests that precariously placed grains are pivoting into nearby available pockets. The filling of pockets by these displaced grains would also increase the elevations of the lowest elevations, narrowing the entire elevation distribution. We also observed grains oscillating in place throughout the conditioning period of the experiments. This observed vibration might also enable individual grains to reorient themselves into a more streamlined position, reducing their relative protrusion.

Despite the range of antecedent low flow conditioning times, surface grain size measurements do not reveal a consistent pattern of coarsening or fining of surface bed material between the initial and conditioned phases of the experiments, indicating that armor formation did not occur during antecedent conditioning periods (Table 3.1). Further, we do not find any significant correlation between values of D_{16},

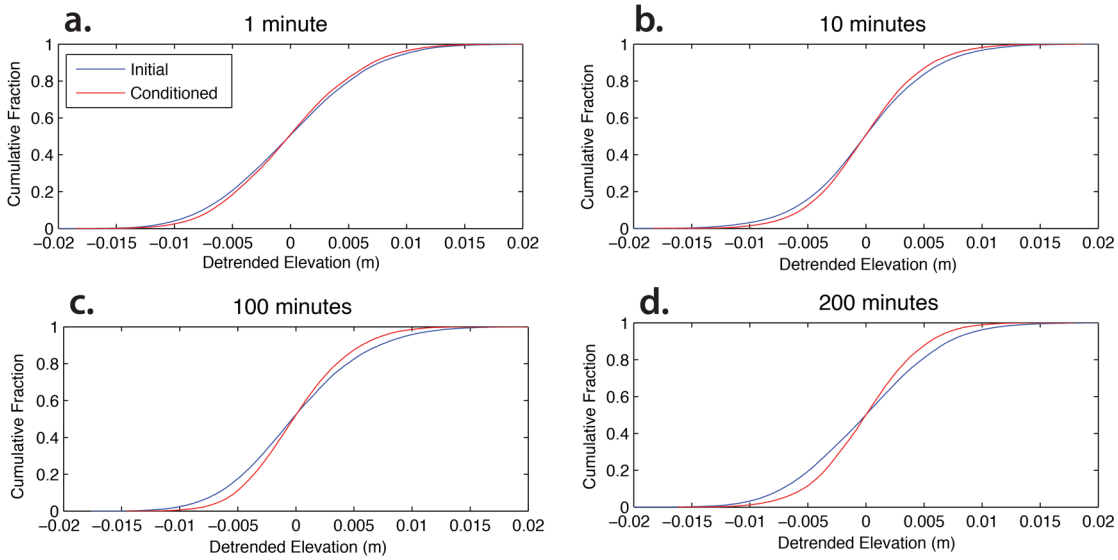

Figure 3.3. Cumulative elevation distributions for the initial (blue) and conditioned (red) beds for **a)** 1 minute conditioning, **b)** 10 minute conditioning, **c)** 100 minute conditioning, and **d)** 200 minute conditioning duration.

D_{50}, or D_{84} during the initial or conditioning phases with observed flux out of the flume (Table 3.1). No significant changes in bed slope between the initial and conditioning phases of the experiments occur (Figure B.3). This observation is consistent with the lack of observed transport out of the flume during conditioning stage. Despite our best efforts, the local bed slope, which was measured using SFM over 30% of the overall flume length, varied between experiments from 0.011 to 0.026 (Table 3.1). This variation of slope between experimental runs is due to the hand mixing of the bed during the preparation stage. That said, there is no significant relationship between conditioning slope and observed bedload transport rates (R^2 = 0.18, p = 0.204) (Table 3.1). Hence, grain size and slope do not appear to exert strong controls on the observed differences in sediment transport rates.

To assess how much reworking or regrading of the bed occurs during transport, we compare the total volume transported out of the flume to the volume of a single layer of sediment in the flume, as defined by the median bedload grain size (0.0085 m) multiplied by the total area of the flume bed (0.3 m x 5 m). During transport, this ratio shows that even at the highest observed transport rates, the material removed from the flume during transport is equivalent to only 11.1% of the volume of the experimental bed surface. At a minimum, the volume eroded is equivalent to only 1.3% of the volume of the bed surface. This finding indicates that degradation of the bed is minimal during the three-minute period, such that only surface or near-surface grains are eroded during the transport stage. By limiting erosion to near-surface sediments, we can link any observed changes in bedload transport to details of bed topography resultant from the conditioning phase.

3.4.2 Linking bedload transport and grain protrusion

The number of local maxima, which we interpret as a proxy for the number of grains protruding at or above a designated elevation threshold, decreases with increasing elevation threshold. At low protrusions, we identify thousands of grains per square meter. As the specified elevation threshold increases, the number of protruding grains per square meter decreases nonlinearly (Figure 3.4).

We use the bedload flux and bed topography data to explore the relationship between grain protrusion and the observed variation in bedload flux. Specifically, we compute the correlation coefficient between the observed sediment flux during the

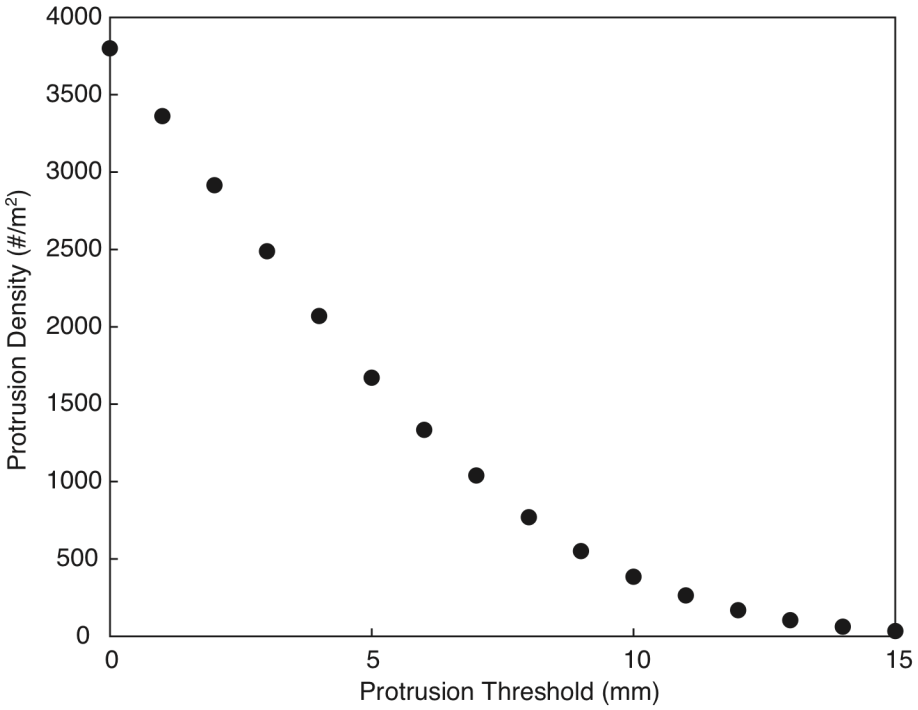

Figure 3.4. Average grain denstiy across all experiments as a function of the protrusion elevation threshold. Each dot represents the average number of local maxima per square meter at or above the specified elevation threshold across all 10 experiments. A protrusion threshold of zero is equivalent to mean bed elevation.

transport phase, which varies linearly with time, and the logarithm of the density of points, as we observe that the protrusion density varies logarithmically with time (Figure 3.5). We observe a peak in the correlation coefficient between bedload and the number of protruding grains at 11 mm and 12 mm above mean bed elevation, with respective values of R = 0.65 and R = 0.66 (Figure 3.6, Table 3.3). The correlation coefficient between flux and protrusion is statistically significant at these protrusions ($\alpha = 0.05$), with p values of p = 0.044 and p = 0.037, respectively (Figure 3.6, Table 3.3). Any population of protruding grains with a $p<0.05$ is suggestive of a significant

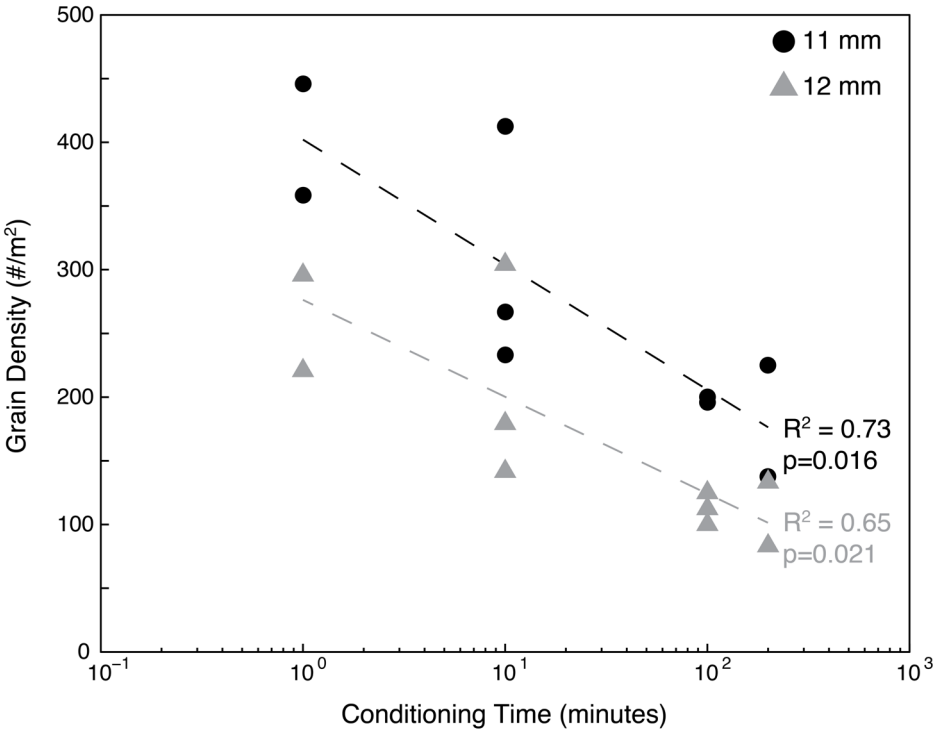

Figure 3.5. Number of local maxima at or above 11 mm (black circles) and 12 mm (grey triangles) per unit area as a function of low flow antecedent conditioning time for all 10 experiments.

effect that warrants further examination. Aside from protrusion values of 11 mm and 12 mm, the observed correlation coefficient between flux and protrusion is not significant for any other elevation range (Figure 3.6, Table B.2).

Notably, after amalgamating all of the experimental data, we calculate that protrusions at or above 11 mm correspond to the 95th to 99th percentiles of the elevation distributions across all experiments (Table 3.3). These protruding grains represent 1-5% of the full elevation distribution. We then estimate the percentage of total mass that this portion of the flume bed contributes to the total transport out of the flume. Assuming that each local maxima represents a single spherical grain with a diameter, D_{50} = 0.0085 m, we calculate the mass contribution of these protruding

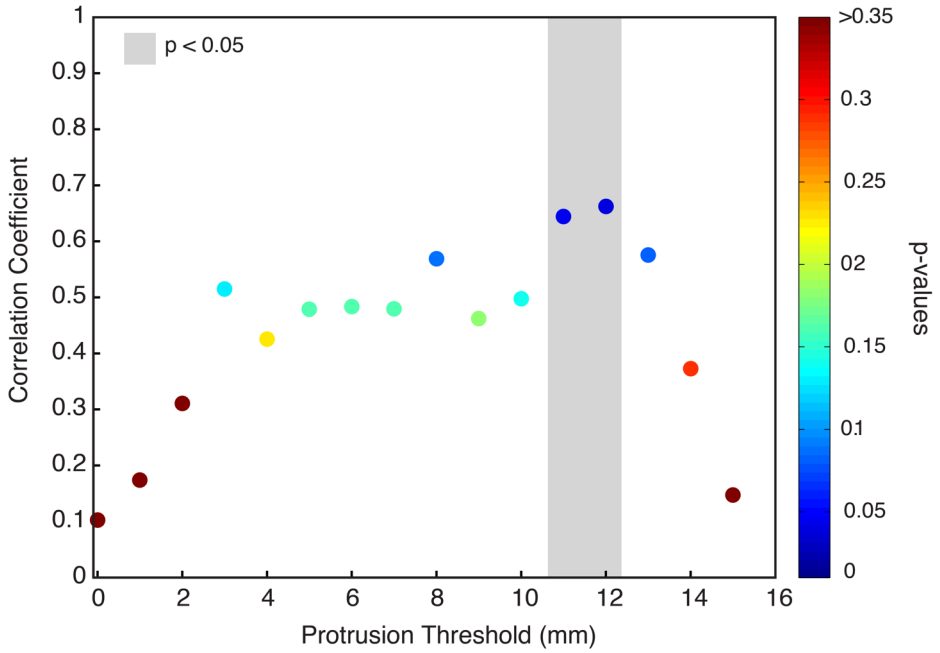

Figure 3.6. Correlation coefficient between the logarithm of the density of local maxima at or above each elevation and observed bedload flux rates. Color of dots correspond to calculated p-values of the correlation coefficients. P-values less than α= 0.05 are highlighted by a grey box.

grains to total bedload by multiplying the volume of a single grain by the number of local maxima protruding >11 mm above mean bed elevation. We assume that all grains with this protrusion threshold are eroded during transport. Assigning a grain density, ρ=2650 kg/m^3, we convert this volume estimate to a mass estimate and compare to total mass transported out of the flume (Table B.1). On average, the mass contributed by the population of

grains protruding 11 mm or more above mean bed elevation makes up only 20.5% of total mass flux during the transport stage of the experiments (Table B.1).

Local maxima protruding more than 11 mm undergo significant erosion during the transport phase, with an average of 93.9% experiencing erosion of >2 mm.

Table 3.3. Bed Load Transport and 11 and 12 mm Protrusion Data for the Initial, Conditioned, and Transport Phases of All 10 Experiments[a]

Table 3. Bed Load Transport and 11 and 12 mm Protrusion Data for the Initial, Conditioned, and Transport Phases of All 10 Experiments[a]

		Initial				After Conditioning				After Transport			
		11 mm Protrusion		12 mm Protrusion		11 mm Protrusion		12 mm Protrusion		11 mm Protrusion		12 mm Protrusion	
Conditioning Time	Bed Load Flux During Transport Phase (kg/m/s)	Grain Density ($\#/m^2$)	Percentile	Grain Density ($\#/m^2$)	Percentile	Grain Density ($\#/m^2$)	Percentile	Grain Density ($\#/m^2$)	Percentile	Grain Density ($\#/m^2$)	Percentile	Grain Density ($\#/m^2$)	Percentile
1	0.063	523.8	96.5	368.0	97.5	445.8	97.5	295.8	98.5	333.3	98	212.1	99
1	0.066	411.3	97.5	272.7	98.5	358.3	98.5	220.8	99	428.6	97	320.3	98
10	0.049	502.2	96	389.6	97	412.5	97.5	304.2	98.5	294.4	97.5	194.8	98.5
10	0.061	372.3	97.7	281.4	98.5	233.3	99	141.7	99.5	116.9	99.5	77.9	99.7
10	0.059	298.7	98.5	207.8	99	266.7	98.5	179.2	99	324.7	97.5	303.0	98.5
100	0.038	393.9	97	290.0	98	200.0	99.5	125.0	99.6	186.1	98	242.4	98.5
100	0.048	164.5	99	108.2	99.3	195.8	99.5	112.5	99.7	190.5	99	129.9	99.5
100	0.018	419.9	97.5	281.4	98.5	200.0	99	100.0	99.3	272.7	98	207.8	99
200	0.020	428.6	97.5	324.7	98	137.5	99.5	83.3	99.7	207.8	99	125.5	99.5
200	0.008	298.7	98	203.5	99	225.0	99	133.3	99.3	355.0	99	108.2	99.5
Correlation coefficient flux versus log(grain density)		0.073		0.072		0.650		0.662		−0.010		0.339	
P value ($\alpha = 0.05$)		0.846		0.849		0.044		0.037		0.987		0.339	

[a]Correlation coefficients and p values between observed bed load flux and grain density at 11 mm and 12 mm protrusion thresholds.

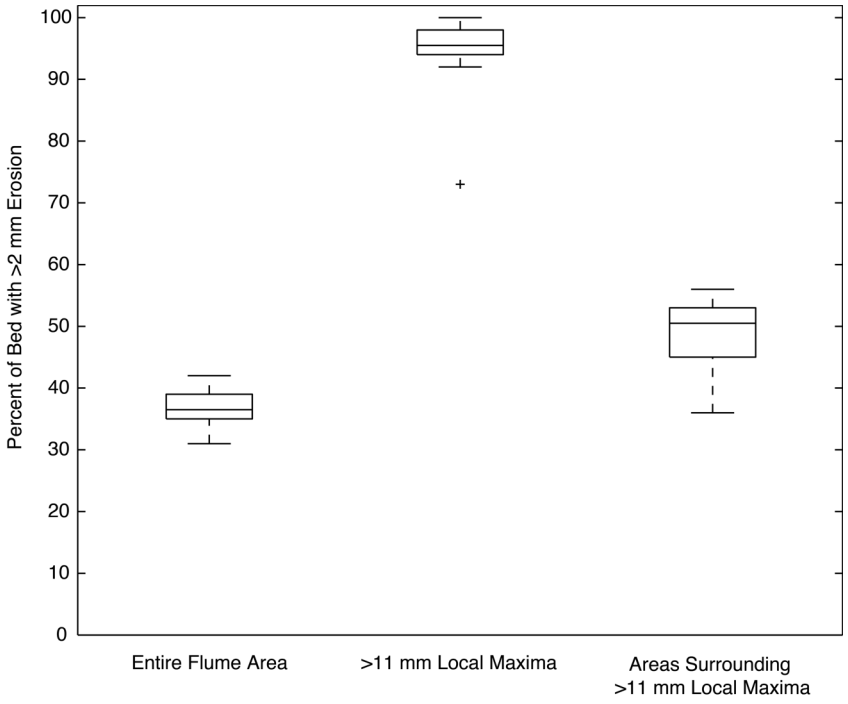

Figure 3.7. Comparison of percent area eroded across 1) the entire experimental DEM, 2) only >11 mm local maxima, and 3) the areas surrounding the >11 mm local maxima. Erosion was classified as a decrease in elevation of more than 2 mm during transport. Both the distribution of erosive high points and their surrounding areas are significantly higher than the percent of erosion across all points in the DEM ($p = 2.1 \times 10^{-14}$ and $p = 1.1 \times 10^{-6}$, respectively)

Any changes less than 2 mm fall within the RMS error of the SFM measurements. Two mm of erosion is also equivalent to the erosion of the smallest grains of the experimental grain size distribution. These high protruding points experience significantly higher erosion compared to the entirety of each DEM, where, an average of 36.6% of all points experience >2 mm of erosion. Further, the elevation changes observed in areas surrounding these high points is increased compared to background, with an average of 48.5% of points experiencing >2 mm of erosion (Figure 3.7, Figure B.5, B.6). The erosion of high points and their surrounding areas is

significantly higher than the erosion across the entire flume bed ($p = 2.1 \times 10^{-14}$ and $p = 1.1 \times 10^{-6}$, respectively) (Figure 3.7, Figure B.5, B.6).

The additional contribution to the cumulative mass flux by the nearest neighbors of these keystone grains can be estimated from DEM analysis. We calculate the average change in elevation across all points of each sample area. For each experimental run, the average erosion depth over these samples ranges from -0.002 m to -0.0048 m. We apply this average change in elevation across the 0.032 x 0.032 sample area (excluding the 0.016 x 0.016 area surrounding the local maxima) and multiply by the total number of high protruding points across the entire flume area for each experiment. The volume is then converted into a mass to estimate the proportion of the observed bedload flux from erosion from the areas surrounding the highest protruding grains. We find that, on average, these areas contribute an estimated 80% of the total mass transport out of the flume (excluding one extreme outlier) (Table B.2). There is considerable scatter in the data, with estimated mass contribution from these areas ranging from 37%-148% (Table B.1). Any values over 100% indicate that deposition of some particles occurs within the flume.

3.4.3 Response of grain protrusion during transport

To explore how changes in bed grain-scale topography are affected by transport, we compare the number of high protruding grains on the bed after the three-minute transport phase to the number of protruding grains following low flow

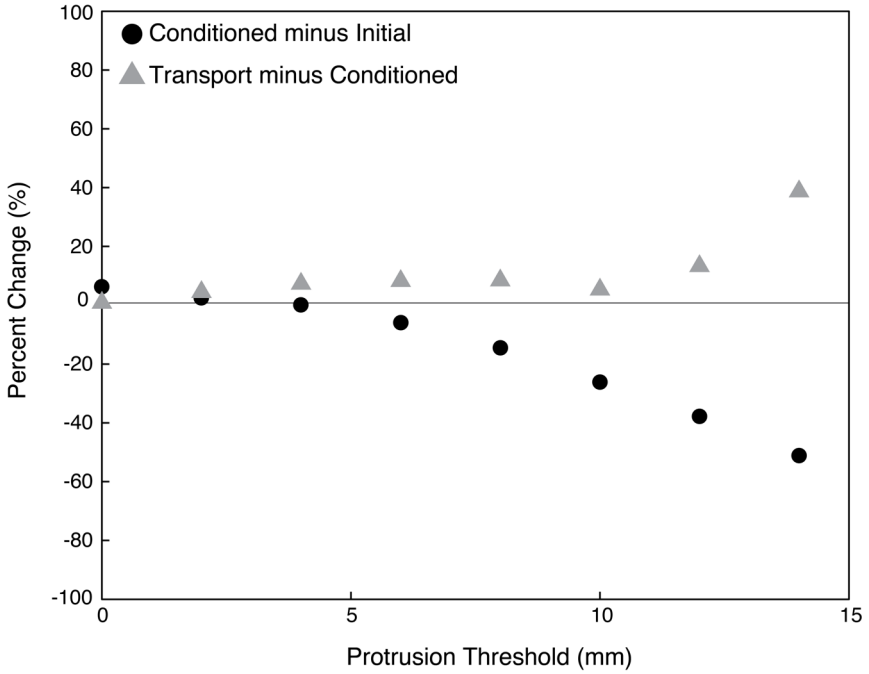

Figure 3.8. Summary of changes in protrusion density between different experimental stages averaged over all experiments. Percent change in number of local maxima with >11 mm protrusions between initial and conditioning phases (black dots) and conditioning and transport phases (grey triangles) averaged over all experiments.

conditioning (Figure 3.8). We find that over three minutes, the number of all protruding points increases, suggesting that the bed is locally dilating under the imposed transporting flow (Figure 3.8). In this case, we define local dilation as an increase in the density of high protruding particles on the sample bed. This is consistent with previous studies, which observe compaction of granular media at low shear rates and dilation at high shear rates (van der Elst et al., 2012; Houssais et al., 2015). Other studies have suggested that grain dilation in gravels may be tied to a winnowing of fine grains from the surface and into available pore spaces during transport (Allan and Frostick, 1999; Middleton et al., 2000). However, we do not see any consistent increase in the D_{16} between the conditioning and transport phases of

our experiments, indicating that smaller grains are not preferentially transported to the subsurface during transport. This suggests that winnowing of finer material is not driving dilation in our experiments, and that the local dilation we observed is likely a consequence of increased flow strength. That said, the original protrusion densities were not fully recovered during the three-minute transport event. We speculate that with a longer transport period there would be further replenishment of high protruding points. This indicates that low flow and transporting flows have significantly different impacts on shaping bed topography, and the subsequent mobility of grains during transport.

3.5 Discussion

3.5.1 Low flow conditioning modifies grain protrusion and bedload transport rates at the onset of motion

Our experiments directly link, for the first time, measured changes in bedload flux to observed changes in grain-scale bed topography induced by variation in low flow. We find that the number of the highest protruding grains decreases with increased low flow conditioning time. This modification of bed structure during low flow results in a factor of seven variation in bedload flux at the onset of transport. We find that the number of highest protruding grains, on average about 1-5% of the total bed area, correlates significantly with variations in bedload transport (Figure 3.6). This result agrees well with the predictions of Kirchner et al. (1990) that only a small

fraction of a water-worked bed is mobile under typical flows, and thus contributes to bedload transport observations. These results suggest a direct link between the number of available, protruding grains and the number of grains in transport.

The observation that increased low flow conditioning results in reduced sediment transport rates is qualitatively consistent with previous studies (Monteith and Pender, 2005; Paphitis and Collins, 2005; Haynes and Pender, 2007). In our work, we have shown a linear decrease in bedload transport as a function of low flow conditioning, as it provides the best fit to our data. However, an exponential fit also agrees well with the data (R^2=0.76). Over short conditioning timescales, bedload transport rates decrease as the bed stabilizes and the number of high protruding grains is reduced. This reduction is captured well by both best-fit lines. However, over long timescales it is unclear whether bedload transport rates will continue to decrease until transport ceases, or if bedload flux approaches a constant, non-zero value.

The linear fit to the data suggests that bedload transport rates should approach zero over longer conditioning durations. A cessation of transport would imply that all of the highest protruding grains are able to find more stable positions, rendering the entire bed immobile at τ_{*50} = 0.051. Thus, the shear stress applied to the bed must increase to transport material. Conversely, the exponential fit to our data implies a constant, non-zero transport rate at long timescales. The approach to a constant flux, as found by previous work (Monteith and Pender, 2005; Paphitis and Collins, 2005; Haynes and Pender, 2007), suggests that under antecedent conditioning, the bed is

never fully stabilized, and that a population of high-protruding grains is always available for transport. Constant transport rates may also reflect that the number of depositional pockets is a potential limitation to bed stabilization. However, the data from the experiments presented here is limited, and we are unable to determine which scenario may arise over extended conditioning timescales. Further experiments should be carried out in the future to determine the temporal evolution of bedload transport rates over long conditioning times. Future studies should also be undertaken to explore the factors limiting alluvial bed stabilization.

We do not observe a spatially uniform deflation of the bed with increased low flow conditioning (Table 3.2). Instead, we find that the density of high protruding grains decreases with increased low flow conditioning time, which is a new result. The changes in the standard deviation of surface topography (Table 3.2) we observe are less than 10% of the median grain size, much less than observed in previous work (Ockelford and Haynes, 2013). However, previous gravel-bed experiments ran conditioning times on the order of 1000 minutes (Monteith and Pender, 2005; Haynes and Pender, 2007; Ockelford and Haynes, 2013), whereas the maximum conditioning time in our experiments is 200 minutes. We expect that if the duration of the low flow antecedent conditioning was extended, that larger topographic changes might occur, as described by previous studies.

During low flow, we infer that high protruding grains are rotated into nearby pockets, causing local compaction that is not reflected by a larger change in mean bed

elevation due to short conditioning times (Table 3.2). The logarithmic reduction of the highest protruding particles with time (Figure 3.5) is consistent with the compaction of dry granular media as observed by other studies (Knight et al., 1995; Richard et al., 2005). Previous flume experiments that have observed measurable compaction required several days of run time (Charru et al., 2004). Over longer timescales, it is possible that this reduction in high protruding particles can be related to a bulk deflation of the bed, as observed by Ockelford and Haynes (2013).

The finding that the availability of grains with higher protrusion controls bedload transport rates is not surprising. Grains that protrude further away from the mean bed elevation, on average, have lower friction angles (Kirchner et al., 1990). In addition, they are exposed to higher fluid drag, also resulting in increased mobility (Fenton and Abbott, 1977). In the experiments presented here, the most drastic elevation changes during low flow conditioning manifest themselves in the extreme tails of the elevation distribution and go undetected in bulk measurements, such as in the mean bed elevation or standard deviation of bed surface topography. However, we show that these small changes result in significant differences in total bedload over the transport phase of our experiments.

This result highlights the difficulty in applying a single value of critical Shields stress, whether to a gravel patch, a river reach, or an entire fluvial landscape. While this simplification may be appropriate for some applications, it is clear from our observations that subtle changes in grain-scale topography can result in order of

magnitude differences in bedload transport rates under a constant driving stress. Empirical relations used in the prediction of bedload transport are framed as a function of excess shear stress above a singular, critical value specific to the empirical relation used (e.g. Meyer-Peter and Müller, 1948). However, predictions of bedload flux based solely on this excess stress do not capture the important effects of grain-scale topography that have been observed by this work and others (i.e. Ockelford and Haynes, 2013).

Typically, the critical Shields stress for the onset of motion is related to large-scale river characteristics, including grain size, channel depth, width, and slope (Buffington and Montgomery, 1997; Parker et al., 2007, Lamb et al., 2008). These channel characteristics are relatively easy to measure in the field, and thus, provide a useful framework for predicting bedload transport rates. However, changes to these channel characteristics require sediment transport to occur. We have shown in our experiments that variations in bed structure at the particle scale can emerge even in the absence of significant bedload transport. Further, we have shown that these subtle changes in topography are directly related to bedload flux, with a higher density of protruding particles resulting in increased transport rates. This observation implies a range of critical Shields stresses and may account for some divergence between predictions of transport using existing empirical relations and observations of sediment flux.

3.5.2 Removal of high protruding grains enhance erosion of their neighbors

While the density of grains with the highest protrusion is significantly correlated to bedload transport rates, this population of grains is not the sole source of the observed transport out of the flume. As shown, on average, the erosion of these highest highs can explain only 20.5% of the mass flux out of the flume (Table B.1). There simply are not enough grains with these protrusions to generate the observed mass flux. Even under the assumption that every grain protruding at or above 11 mm moves during transport and exits the flume, only considering this population vastly underestimates transport out of the flume. We show that these most mobile grains act as "keystone" grains, enhancing erosion of the surrounding sediment. When these most mobile grains are dislodged, their neighbors, whose own protrusion may vary widely, are also destabilized and are entrained by the flow. The transport of these neighboring grains, on average, accounts for 80% of the total mass out of the flume.

This destabilization of many grains due to the dislodgement of a single, highly mobile keystone grain is consistent with the idea that particles are collectively entrained, and are transported in groups (Ancey et al., 2006; Heyman et al., 2013). While in place, the highest protruding particle shelters its lower protruding neighbors, but its removal both lowers the particle friction angles of upstream particles and exposes all surrounding particles to higher fluid velocities, potentially destabilizing the entire cluster (Brayshaw et al., 1985). Collective entrainment of particle clusters may explain why the density of grains with the highest protrusion correlate most

significantly with bedload transport rates, but only make up a small percentage of the total volume eroded.

While we have shown that there is indeed enhanced erosion in the areas surrounding the highest highs, the estimates of the contribution of mass to observed flux out of the flume have a large scatter (37%-148%, excluding one extreme outlier) (Table B.1). Mass estimates exceeding 100% are due to deposition of eroded material in the flume. A fraction of transported grains encounter pockets and are deposited rather than exiting the flume. Underestimates of mass contribution are likely due to the entrainment of grains protruding <11 mm above mean bed elevation, which are not accounted for in our mass estimates. While there is not a significant correlation between lower protruding grains and flux, this does not preclude their motion. A fraction of these populations may still be mobile during typical transporting flows, but have a lower probability of entrainment, leading to reduced correlation with the observed bedload transport rates. Regardless, we have shown that the areas surrounding these highest points have an increased probability of entrainment, further underscoring the importance of these most mobile grains as keystones for collective entrainment.

The keystone grain analysis done here is fairly simple, as it only considers a small area directly around the grain. By concentrating on this area, we do not consider the hydraulic effects that the removal of the high protruding grain may have on an expanded surrounding area. Previous work suggests that particles roughly 2.5 grain

diameters downstream from an obstacle may be relatively unaffected by sheltering effects (Brayshaw et al., 1983; Lacey and Roy, 2008). We also do not directly address the grain sheltering that may occur when two local maxima with similar protrusion values are closely spaced. In future work, the analysis presented here could be expanded to examine the impact of the erosion of high protruding grains over larger length scales to address grain hiding or sheltering more directly.

3.5.3 Response of grain protrusion during transport

Smoothing of the bed surface occurs during low flow periods, while, conversely, an increase in surface roughness occurs under transporting flows. These observations are consistent with a transition from compaction under low shear rates to dilation under high shear rates observed in previous studies (van der Elst et al., 2012; Houssais et al., 2015). Further, we have shown that the changes in bed surface topography during the conditioning phase is not fully erased, or reset, by transport. These results suggest the potential for the signature of low flow durations to be long-lived, or remembered across multiple transport events. Thus, it is possible that bed surface topography may integrate the effects of numerous low flow events between transport periods.

The transport phases explored here have short durations, and capture bedload transport rates at the onset of motion. However, we have not fully explored how long-lived the patterns in bed structure reflecting low flow conditioning duration may be

under extended transport conditions. We expect that a more stable surface layer with fewer protruding points would require longer transport durations to restore the roughness that has been reduced during low flow. Because there are a reduced number of high protruding particles following longer conditioning durations, the bedload flux at the onset of transport is reduced, requiring a longer transport event to remove the entire stabilized surface layer and reset the bed topography and increase the density of high protruding particles. However, we have not explicitly tested this in the experiments presented here. The strength of the topographic signature of low flow conditioning during longer transport events is a potential area of future work.

3.5.4 Future work

It is unclear how the relationship between density of high protruding particles and bedload transport that we have identified here would vary with a range of other experimental parameters. Future work should consider how the initial bed conditions, experimental grain size distribution, conditioning flow magnitude, and magnitude and duration of transport conditions may impact the temporal evolution of grain-scale topography and subsequent effects on bedload transport rates. First, the initial condition of the experiments presented here was a hand mixed, screed bed. This initial condition is not water-worked, and thus will likely have the largest response to changes in low flow duration. Future work should include conducting similar experiments on a water-worked bed to address how the relation between changes in

bed structure and low flow duration may change as a function of the initial conditions of the experimental bed. We expect that repeating the experiments presented here on a bed evolved to an equilibrium state during transport may damp the changes in bed structure presented here, as some development may be integrated from previous transport events.

We did not measure the relationship between the relative size of the surface grains and their protrusion. We find that the protrusion values with the most significant relationship to bedload flux are 11 and 12 mm (Figure 3.6), indicating that grains are protruding more than one D_{50} above the bed. However, while we do not see a significant change in the surface D_{50} across different stages of the experiments, surface D_{50} is, on average, 11 mm. This indicates that the surface layer of all of the experiments is slightly coarser than the subsurface through all stages of the experiment, more similar to the protrusion values that correlate best with transport. Further, it is likely that larger grains can sustain higher protrusion elevations, increasing their relative mobility. However, larger grains are also more massive, resulting in their reduced mobility relative to smaller grains. By not accounting for grain size variation in our analysis, these two competing effects may introduce considerable scatter into the relationship between protrusion and bedload flux if the grain size of these highest particles varies. We expect that if protrusion were normalized by local grain size, the relation would improve.

In the future, a larger phase space of experimental parameters should be explored to determine how the development of bed structure during low flow and its affect on bedload transport vary. Experimental grain size distribution and both conditioning and transport flow strength should be varied to assess the conditions under which low flow conditioning becomes significant. The experiments performed here were designed to apply a transport stress very near the commonly cited threshold for transport, as most equilibrium channels are thought to be near threshold (Parker, 1979). However, it is likely that at higher transport stresses, as more of the bed becomes mobile, the signal of the highest protruding grains will become less significant as increased fluid drag will be able to effectively move grains in more stable configurations. The range of flows over which the observed dependence of bedload transport rates on the highest protruding grains is a future avenue of exploration.

3.6 Conclusions

The formulations of numerous frequently used models to predict bedload transport rates rely on the assumption of a single critical value of shear stress (e.g Meyer-Peter and Müller, 1948; Engelund and Fredsøe, 1975; Wong and Parker, 2006; Fernandez Luque and Van Beek, 2010). Kirchner et al. (1990) argued that the critical entrainment should be represented as a distribution, rather than a single value, in order to encompass the complexity of a natural bed and account for the effects of

grain packing and variation in protrusion. Further, Kirchner (1990) hypothesized that only a small fraction of a river bed has low enough critical stresses to be transported. A prediction of this hypothesis is that the availability of highest protruding, most mobile grains, should be well correlated to bedload transport rates. The study presented here tests this hypothesis by directly linking detailed measurements of grain protrusion and measurements of bedload transport for the first time using high-resolution measurements of bed topography generated with Structure from Motion Photogrammetry.

Here, we have exploited the observation that variation in a low flow antecedent conditioning time is able to generate a wide range of bedload transport rates with the same transporting flow. Using this approach we show that the availability of the highest protruding grains (1-5% of the entire experimental bed) is well correlated with the order of magnitude variation in bedload transport rates that result under an identical driving stress. Further, we show that these grains are highly mobile, as almost the entire population is eroded during transport, resulting in a high correlation between the number of these grains available for transport and the total mass eroded from the experimental bed. Lastly, we show that these grains act as keystone grains, and that their transport dislodges the surrounding grains, which amplifies their importance in governing bedload transport rates.

3.7 Acknowledgments

This material is based upon work supported by National Science Foundation Graduate Research Fellowship grant DGE-1339067. We thank Christian Braudrick, Leonard Sklar, and Emily Brodsky, whose input greatly benefited the work. We also thank Joel Johnson, Rebecca Hodge, and two anonymous reviewers for their helpful comments. Two data tables used to create Figures 2, 4, 5, 6, and 7 are included as part of the Supplementary Material, any additional data may be obtained from CCM (cmastell@ucsc.edu).

Chapter 4

History-dependent threshold for motion revealed by continuous bedload transport measurements in a steep mountain stream

In preparation for publication

Claire C. Masteller, Noah J. Finnegan, Jens M. Turowski, Dieter Rickenmann

4.1 Introduction

Bedload transport is the key process that governs channel change. This mode of transport represents an important portion of the sediment load, especially for a gravel river (up to 60%) (Métivier et al., 2004; Meunier et al., 2006; Liu et al., 2008). Virtually all problems related to fluvial morphodynamics, from understanding alluvial channel geometry (Parker, 1979) to predicting bedrock incision rates (Sklar and Dietrich, 2004), require some prediction of bedload transport rates. Despite over a century of work related to this problem, beginning with Gilbert and Murphy (1914), predicting bedload transport rates represents a fundamental difficulty in geomorphology because of the complex interactions of individual sediment grains and the surrounding flow (Wilcock and Crowe, 2003; Chen and Stone, 2008; Frey

and Church, 2009; Jerolmack and Paola, 2010). A significant reason for this difficulty is the well-documented variation in the shear stress associated with the onset of sediment motion (Buffington and Montgomery, 1997), a quantity which underpins most existing predictive models. Widely-used formulas for bedload flux are semi-empirical equations derived from data from flume experiments or field observations (i.e. Meyer-Peter and Müller, 1948; Engelund and Fredsøe, 1975; Wong and Parker, 2006; Fernandez Luque and Van Beek, 2010). A majority of these models take the following form:

$$qs^* = c(\tau^* - \tau^*_c)^b \qquad (1)$$

where the instantaneous, dimensionless bedload flux per unit width (qs^*), is a power function (b) of the dimensionless shear stress (τ^*) in excess of a defined critical dimensionless stress (τ^*_c), modified by an empirically-derived coefficient (c). This critical dimensionless stress, τ^*_c, describes the flow conditions necessary for the onset of motion, above which measurable sediment transport occurs. Based on the pioneering work of Shields (1936), this critical dimensionless stress, also termed Shield's stress, is defined as

$$\tau^*_c = \tau_b/[(\rho_s - \rho)gD_{50}] \qquad (2)$$

where τ_b is the total boundary shear stress acting on the bed (Pa), ρ_s is sediment density (kg/m^3), ρ is fluid density (kg/m^3), g is acceleration due to gravity (m/s^2), and D_{50} is the median surface grain size (m). Typically, a single value for τ^*_c is

assigned in the calculation of sediment flux using bedload transport formulas of the form of Equation 1. While these models have significant utility, due to the minimal number of input parameters required, they offer limited physical insight related to processes operative on the channel bed. Additionally, model predictions of bedload flux result in up to two orders of magnitude of error when compared to direct transport measurements (Gomez and Church, 1989; Lenzi et al., 2006; Bathurst, 2007; Recking et al., 2012; Scheingross et al., 2013). This significant mismatch highlights that the assumptions of these simple models do not adequately capture bedload transport dynamics, especially, in steep streams (Lenzi et al., 2006; Scheingross et al., 2013) and for flows very close to the identified threshold for motion (Gomez et al., 1989; Recking et al., 2012). This disagreement between predictions of bedload flux and direct observations represents a significant problem, as the majority of sediment transport occurs during near-threshold conditions (Phillips et al., 2016).

A significant assumption of these widely-used models is the treatment of bedload transport as a threshold process. Imposing a threshold for transport, as reflected in Equation 1, artificially divides the hydrograph into two distinct states: transport and no transport. This division implies that during times when flow conditions do not exceed τ^*_c, no motion occurs and the channel remains fixed. In this below-threshold state, these models predict that any discharge that the channel experiences has no impact on subsequent sediment transport rates. Further, it is known that even when boundary shear stress does exceed τ^*_c, not all sediment is

mobilized, and partial transport occurs (Frey and Church, 2009), likely as a result of the complex arrangement of particles on the bed (Kirchner et al., 1990). Thus, the treatment of bedload transport as a binary system, with a sharp transition from no transport to transport, may be the cause of the known errors associated with this class of models.

While this division of the hydrograph has been widely utilized by sediment transport studies for decades (e.g. Meyer-Peter and Müller, 1948;), recent work has suggested that rather than the channel bed occupying one of two distinct "states" separated by τ^*_c, the shift to measurable bedload transport is a continuous transition (Houssais et al., 2015). Indeed, sheared granular flow rheology displays a range of behavior akin to a solid, a liquid, or a gas (Jaeger et al., 1996), behaviors which are thought to also be relevant for fluvial systems (Frey and Church, 2009). Further, previous studies on dry granular flows observe a continuous transition from a jammed state to an un-jammed, dense flow, rather than an abrupt one (Katsuragi et al., 2010). This transition is characterized by low-velocity creep, accommodating shear over a length scale that exceeds the experimental grain size, indicating that the transition from no motion to motion is progressive, rather than discontinuous (Katsuragi et al., 2010; Houssais et al., 2015). Given this, the treatment of bedload transport as a process with a sharp threshold is not appropriate, and rather, suggests that the full range of forcing conditions contributes to setting bedload transport rates, and by extension, channel evolution.

A second significant implication of bedload transport predictions in the form of Equation 1 lies in the assumption that τ^*_c remains constant both spatially and temporally (e.g Wong and Parker, 2006). It is widely acknowledged that a constant threshold for motion does not effectively capture the full complexity the onset of sediment motion in fluvial systems (Lavelle and Mofjeld, 1987; Buffington and Montgomery, 1997; Johnson, 2016). Specifically, the onset of motion has been shown to vary as a function of surface grain size (Moog and Whiting, 1998; Chen and Stone, 2008), sediment supply (Dietrich et al., 1989), the degree of previous bed compaction (Charru et al., 2004; Houssais et al., 2015), and flood intermittency (Haynes and Pender, 2007; Ockelford and Haynes, 2013; Masteller and Finnegan, 2017). Further, a major consequence of a temporally invariant τ^*_c is that instantaneous bedload transport rates are completely independent of any previous events, such that a channel system exhibits no memory of previous flow or transport history.

Because of these clear shortcomings with a constant critical Shields stress assumption, a more physically realistic treatment of the onset of motion represents a key knowledge gap in fluvial geomorphology. New approaches to this problem include probabilistic models for sediment transport (i.e. Furbish et al., 2012; Monsalve et al., 2016) that treat particle activity as a stochastic quantity, rather that modeling transport in a deterministic way. In a sense, stochastic approaches address the potential variations in the onset of motion in space and time, as individual particle response to an applied forcing is allowed to vary. However, stochastic models do not typically account for temporal effects directly, and instead focus on instantaneous

transport rates (Furbish et al., 2012). More recently, Johnson (2016) developed a state-function to model an evolving threshold for motion as a function of net erosion and deposition. This formalization assumes that the threshold for motion is a memory-dependent quantity and its variation is a function of previous history. This model is the first of its kind to explicitly frame the threshold for motion as a state variable. However, both the degree of sensitivity to previous conditions and the timescale over which the proposed history-dependence of τ^*_c persists has not been well-defined for a natural channel.

Although the treatment of the threshold for motion as a history-dependent quantity has only been formalized recently, the dependence of the threshold for motion on prior flow history was first suggested, to our knowledge, by Reid et al. (1985). The study observed that bedload transport rates in a perennial gravel stream during more temporally isolated transport events were reduced when compared to those that were closely spaced. Reid et al. (1985) hypothesized that, rather than the bed remaining completely fixed during sustained subthreshold flows, local sediment rearrangement occurs, increasing particle interlocking and as a result, the threshold for motion. This observation both challenges the assumption that no considerable change to bed structure can occur in the absence of measureable bedload transport, and highlights the need to consider the role of the full hydrograph in modifying channel conditions.

Previous laboratory experiments explored the sensitivity of bedload transport to subthreshold antecedent flows and show that bedload flux is indeed sensitive to the magnitude of prior subthreshold, inter-event flow (Monteith and Pender, 2005; Paphitis and Collins, 2005; Haynes and Pender, 2007). Specifically, Monteith and Pender (2005) showed that for a graded gravel bed, increased magnitude and duration of an antecedent low flow resulted in a decrease in total sediment flux during the following transport event, consistent with the field observations of Reid et al. (1985). Building on this observation, Masteller and Finnegan (2017) show that while these flows are incapable of transporting grains significant distances downstream, they are able to pivot the most precariously placed grains into nearby pockets, reducing overall grain protrusion. This reduction in grain exposure both reduces the drag and lift forces on these particles and increases the interparticle friction angles, resulting in an increase in the boundary shear stress required for the onset of motion, leading to decreased bedload flux.

Additionally, previous studies illustrate that sediment mobility is also altered by the history of previous high discharge, transporting flows. Exceptionally high discharge events drastically reorganize channel bed structure by mobilizing boulders and breaking step pools, ultimately disrupting particle interlocking and reducing τ^*_c (Turowski et al., 2009; Yager et al., 2012b). The effects of this substantial reorganization can persist across numerous, consecutive transport events, leading to long-lived increases in bedload transport rates associated with reduced channel stability (Yager et al., 2012b). Additionally, Masteller and Finnegan (2017) found

experimentally that in response to above-threshold, transporting flows, bed roughness increased, suggesting a concurrent decrease in τ^*_c due the increased population of highly mobile, high protruding grains. This suite of observations suggest that gravel beds integrate the effects of both inter-event and transporting flows through a reorganization of surface grains, resulting in a discharge-dependent threshold for motion.

These observations of the divergence in response of τ^*_c to high and low flows is analogous to the evolution of granular materials under shear, where low shear rates result in compaction and increased order, and high shear rates result in dilation and disorder (i.e. Jaeger et al., 1996; Iverson, 1997; Campbell, 2006; van der Elst et al., 2012). In particular, this similarity suggests that the threshold for motion is indeed a history-dependent quantity, exhibiting memory of past flow conditions. However, the degree of sensitivity of the threshold for motion on previous flow magnitude has not been explored systematically in a natural channel. In this contribution, we explore the temporal evolution of the onset of motion utilizing a unique dataset of continuous bedload transport measurements from a natural gravel channel. Specifically, we find that the threshold for motion is indeed dependent on previous flow magnitude, exhibiting memory of prior conditions. We apply the findings of previous laboratory experiments (e.g. Monteith and Pender, 2005), which highlight the importance of subthreshold, inter-event flows, to explore the effect of this portion of the hydrograph on the onset of motion in a natural channel for the first time. Further, we show that near-threshold, transporting flows result in a similar dependence as inter-event flows

without measurable transport, providing support to the idea that the onset of motion is a continuous transition. In particular, we identify a transition from strengthening to weakening behabvior with increasing boundary shear stress, similar to observations in dry granular flows. We then assess the potential physical mechanisms that underpin the observed discharge dependence of the onset of motion, and show that while no transport is independently measured during inter-event periods, grain rearrangement is physically possible. Finally, we discuss the implications of these findings in the development of a history-dependent model for bedload transport.

4.2 The Erlenbach torrent, Swiss Prealps

The Erlenbach torrent in the Swiss Prealps is a small step-pool channel with a drainage area of 0.74 m^2 and an average gradient of 10%. Sediment transport events at the Erlenbach are driven by summer thunderstorms, leading to variable spacing between transport events from hours to weeks (Turowski et al., 2011). The Erlenbach is one of the best-instrumented rivers in the world, as high-resolution sediment transport, hydrologic, and meteorologic data has been recorded for over 30 years (Hegg et al., 2006; Rickenmann and McArdell, 2007; Rickenmann and McArdell, 2008). Bedload impact sensors have been in place since 1986 to continuously monitor individual sediment impacts at 1-minute resolution. The first generation of piezoelectric impact sensors was installed in 1986, which were replaced in 1999 by geophones (see Rickenmann and McArdell, 2007; 2008 for full description of

instrumentation). Both generations of instruments recorded the number of sediment impulses exceeding one centimeter in diameter (Turowski et al., 2009). Channel discharge is recorded concurrently at 10 minute intervals by a stream gage situated about 30 m upstream of the impact sensors (Rickenmann and McArdell, 2007). Given that discharge is not entirely representative of the total force acting on the channel bed, as it does not account for channel geometry, boundary shear stress is a more appropriate quantity to characterize the strength of the flow. With this consideration, flow strength will be characterized in terms of boundary shear stress rather than discharge for the remainder of this contribution. Boundary shear stress is calculated using a rating curve from Yager (2006), which calculates boundary shear stress as a function of measured flow depth, paired with concurrent discharge measurements.

Turowski et al. (2011) compiled a dataset of the discharge at the onset and cessation of bedload transport for individual sediment transport events from 1987-1999 and 2002-2009. Sediment impacts are measured directly by the geophones, and the threshold for motion is defined by the discharge or boundary shear stress at the advent of a non-zero number of geophone impacts, independent of any observer, model, or extrapolation. We utilize this dataset, focusing our analysis on the onset of motion, and add three additional sample years to extend the record to 2012. We do not include years with <10 transport events, due to their low sample size, resulting in a 19-year record from 1987-1999 and 2007-2012, with a total of 445 transport events (median of 21 events per year). To avoid the effects of snowmelt or the freezing of the channel, we restrict our analysis to transport events that occur between the months

of March and September. In this time series, periods of observed sediment transport comprise only 1.21% of the full record, whereas, below threshold, inter-event periods occupy the remaining 98.79% of time. In terms of discharge, only 16.6% of the total discharge occurs during transport events, with the remaining 83.4% discharge occurring in inter-event times without measurable coarse sediment transport. It is worth noting that due to the detection threshold of the geophones, fine-grained bedload transport and suspended transport are not captured in this dataset. However, fine (<1 cm) grains comprise about 8% of the total grain size distribution (Yager et al., 2012a), so this dataset likely captures the bulk behavior of the channel.

4.3 Seasonal variations in the onset of motion (analysis by year)

In the time series, we note clear seasonal patterns in the boundary shear stress at the onset of motion in many of the years on record (Figure 4.1). We observe that the boundary shear stress at the onset of motion increases by up to 159 Pa, or a maximum of 250%, from March to September of each year. Across the 19 years on record, there is an average annual increase of the threshold for motion of 53% each spring and summer from the first transport event to the last.

Across the entire record, the threshold for motion is observed to vary by an order of magnitude, as previously noted by (Turowski et al., 2011). The boundary shear stress at the onset of motion ranges from 39.5 Pa to 340 Pa, corresponding to a wide range of critical Shields stresses, assuming a constant median

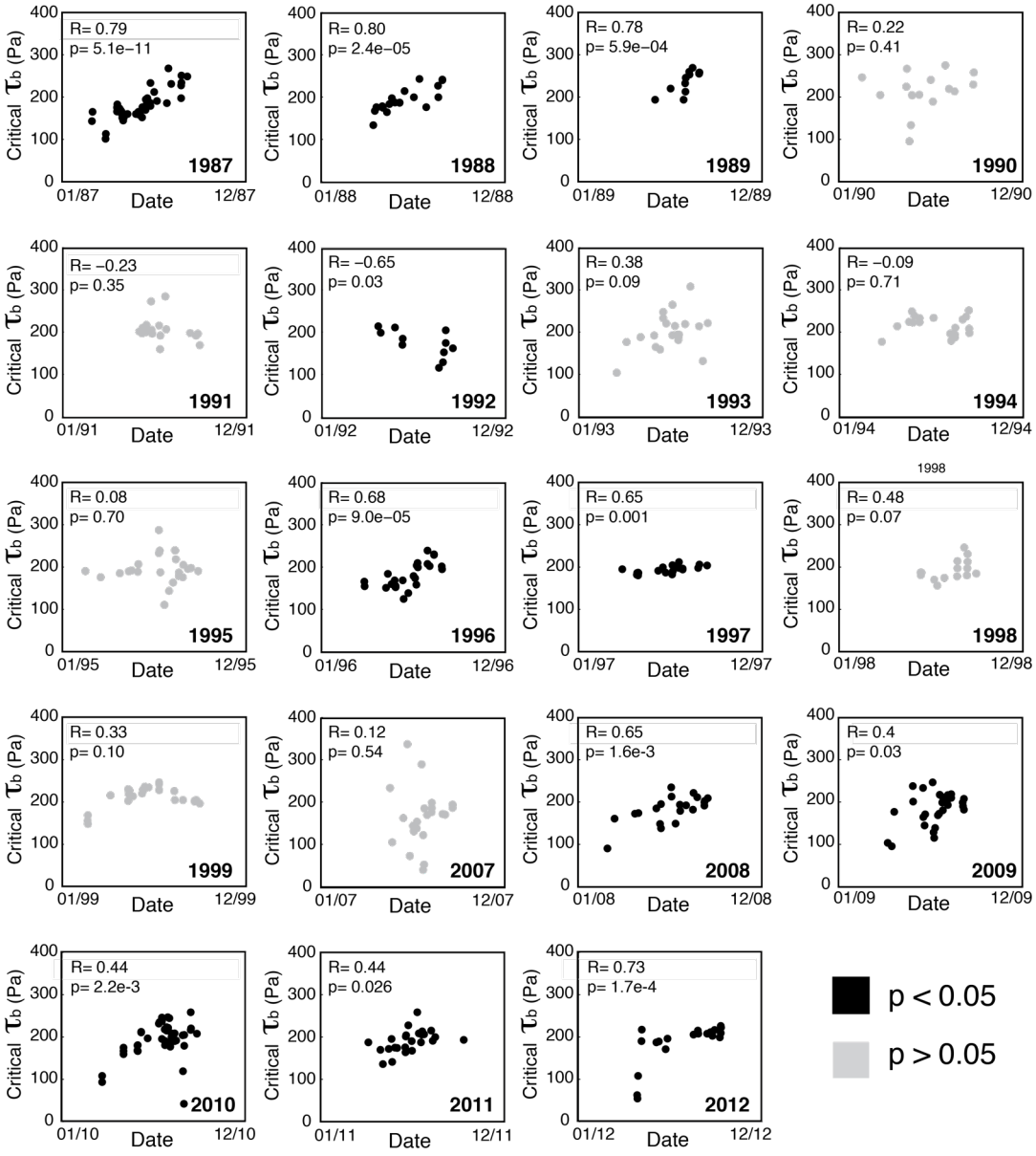

Figure 4.1. Time series of critical boundary shear stress (τ_b) at the onset of sediment motion for each year of continuous bedload transport measurements at the Erlenbach. Years where the correlation coefficient (R) between the critical τ_b and time is significant ($p<0.05$) are shown in black, years without significant correlation ($p>0.05$) are in grey.

surface grain size (D_{50} = 0.08 m), of τ^*_c = 0.03-0.28. This variation of τ^*_c is consistent with previous data compilations of the threshold for motion (Buffington and Montgomery, 1997; Lamb et al., 2008b). The data are normally distributed, with a median threshold stress of 192 Pa and a standard deviation of 39 Pa.

To quantify the strength of this observation, we calculate the Pearson correlation coefficient between the boundary shear stress at the onset of coarse bedload transport and time for each year on record. We find that for 11 of the 19 years on record (58%), variations in the threshold for motion are significantly correlated with time (Figure 4.1, Table 4.1). Ten of these years show significant increases in the threshold for motion from March to September. One year on record, 1992, the threshold for motion decreases significantly through the summer months (Figure 4.1, Table 4.1).

To determine the average timescale over which the threshold for motion remains significantly correlated between transport events, we also perform an autocorrelation analysis on the entire record. Due to the data gap in impulse data, we divide the time series into two separate groups, (1) events prior to 2000 (n = 281) and (2) events from 2007-2012 (n = 174). As there is variable spacing between transport events, we characterize the lag of the autocorrelation as an integer number of transport events. For the 1987-1999 time series, the threshold for motion remains significantly correlated over 13 transport events, whereas from 2007-2012 the threshold is correlated over 10 transport events (Figure 4.2). This long-lived, inter-

Table 4.1. Correlation coefficient analysis of threshold for motion with time of year, cumulative total shear stress, cumulative transport shear stress, cumulative above threshold transport stress, and cumulative inter-event flow shear stress

		Time of year		Cumulative shear stress		Cumulative transport shear stress		Cumulative > τ_{*c} shear stress		Cumulative < τ_{*c} shear stress	
Year	*n*	*Corr. Coef.*	*P-val*	*Corr. Coef.*	*P-val*	*Corr. Coef.*	*P-val*	*Corr. Coef.*	*P-val*	*Corr. Coef.*	*P-val*
1987	46	0.79	5.1E-11	0.77	4.2E-10	0.06	0.711	0.07	0.671	0.78	3.9E-10
1988	20	0.80	2.3E-05	0.76	1.5E-04	0.30	0.216	0.19	0.431	0.76	1.5E-04
1989	15	0.78	5.9E-04	0.74	2.5E-03	0.24	0.408	-0.03	0.925	0.73	3.0E-03
1990	16	0.22	0.410	0.30	0.284	-0.07	0.807	-0.02	0.938	0.29	0.287
1991	18	-0.23	0.352	-0.25	0.328	0.01	0.971	0.02	0.925	-0.26	0.317
1992	11	-0.65	0.032	-0.42	0.222	0.50	0.144	0.13	0.728	-0.43	0.217
1993	21	0.38	0.093	0.23	0.332	0.20	0.401	0.36	1.2E-01	0.23	0.325
1994	20	-0.09	0.711	-0.26	0.283	0.38	0.113	0.33	0.161	-0.26	0.286
1995	24	0.08	0.704	0.06	0.788	-0.06	0.788	-0.06	0.783	0.06	0.773
1996	27	0.68	9.0E-05	0.66	2.5E-04	0.14	0.487	0.13	0.532	0.64	4.5E-04
1997	22	0.65	1.0E-03	0.74	1.2E-04	0.29	0.200	0.21	0.366	0.74	1.2E-04
1998	15	0.48	0.073	0.51	0.061	0.53	0.052	0.41	0.142	0.51	0.061
1999	47	0.33	0.101	0.37	0.072	0.07	0.735	0.09	0.674	0.36	0.074
2007	28	0.12	0.541	-0.12	0.555	0.14	0.478	0.33	0.089	-0.13	0.531
2008	21	0.65	1.6E-03	0.47	0.038	0.28	0.225	0.17	0.480	0.46	0.039
2009	29	0.40	0.034	0.20	0.300	0.05	0.805	0.02	0.916	0.20	0.312
2010	45	0.44	2.2E-03	0.33	0.030	0.17	0.265	0.16	0.298	0.35	0.021
2011	25	0.44	0.026	0.50	0.013	0.48	1.8E-02	0.48	0.017	0.50	0.013
2012	20	0.73	1.7E-04	0.70	5.8E-04	0.12	0.614	0.05	0.826	0.70	5.7E-04

event correlation illustrates that small, systematic changes in the onset of motion result in significant change in the threshold for motion from March to September, rather than a single event dominating the signal.

We also calculate the Pearson correlation coefficient of the threshold for motion as a function of total cumulative shear stress, which we use as a proxy for the potential work or possible rearrangement done on the channel bed (Table 4.1). We find significant correlations between the onset of motion with time of year, similar to those captured by the total cumulative shear stress in the channel. Nine years (49%) on record show a significant, positive correlation between the total cumulative discharge and the boundary stress at the onset of motion (Table 4.1). All nine years

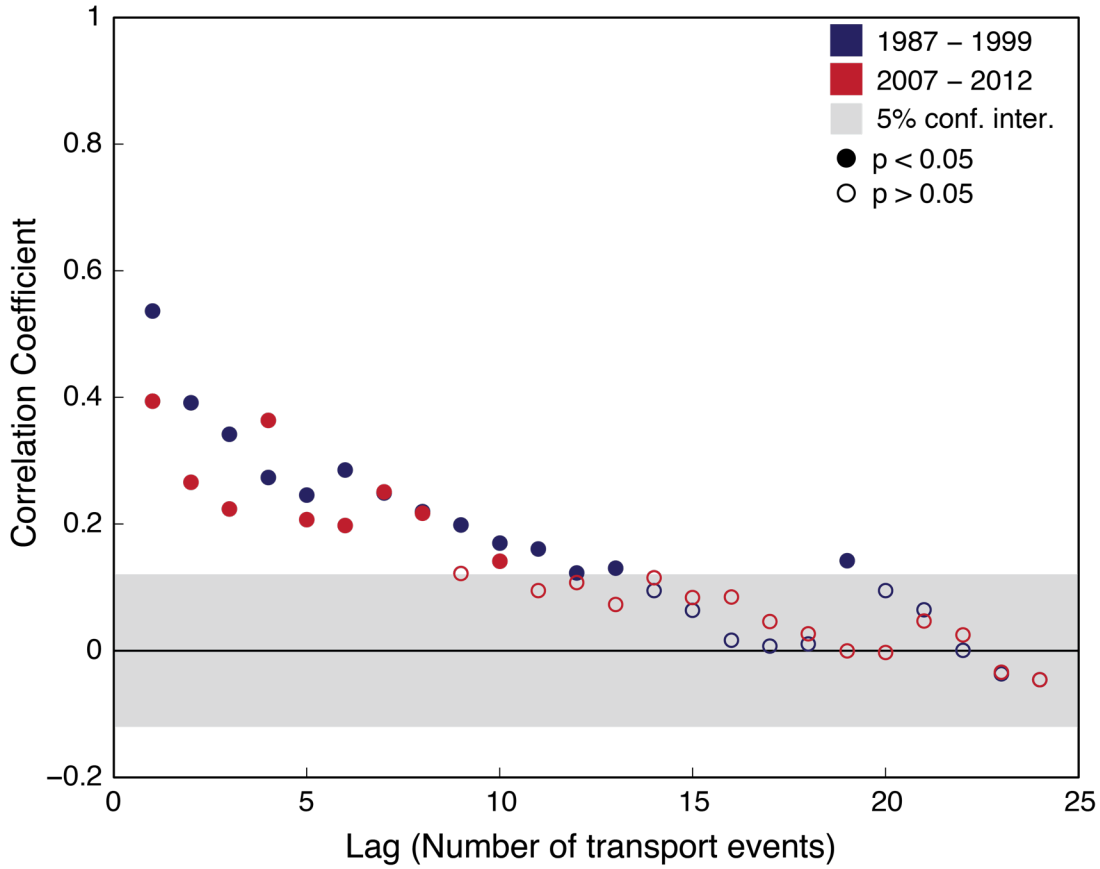

Figure 4.2. Autocorrelation of threshold for motion time series for years 1987-1999 (blue) and 2007-2012 (red) at the Erlenbach. Filled circles indicated a significant correlation ($p<0.05$), open circles represent correlations with no statistical significance ($p>0.05$).

also display a significant, positive correlation with time. Further, 1992, the one year with a negative temporal correlation is not captured by this analysis. However, these results suggest, overall, that the total boundary shear stress that the channel experiences across both transport events and low flows is an important driver of the temporal evolution of the threshold for motion.

Variation in the onset of motion is thought to result from a reworking of the channel bed, both to increased particle interlocking during below threshold, inter-event periods (Reid et al., 1985; Masteller and Finnegan, 2017) as well as significant

reorganization of channel morphology, disrupting this interlocking, during exceptional peak flows (Turowski et al., 2009; Yager et al., 2012b). However, the functional relationship between prior flow magnitude, across both inter-event and transporting flows, and the subsequent response of the threshold for motion as not previously been explored in a natural channel. Previous work predicts a divergence in the response of the onset of motion as a function of prior flow magnitude (Turowski et al., 2009; Houssais et al., 2015; Masteller and Finnegan, 2017), with increases in the threshold for motion expected following relatively low boundary shear stresses transitioning to a decrease in the threhsold in response to elevated boundary shear stress. To explore the role of above- and below-threshold flows on the observed patterns in the onset of motion, we separate the hydrograph into two portions, cumulative transporting discharge, and cumulative inter-event, low flow discharge, and perform the same correlation coefficient analysis (Table 4.1).

Notably, only one year (5.3%) on record shows a significant correlation between the magnitude of the threshold for motion and the cumulative shear stress during transporting flows. The correlation between transporting flows and the threshold for motion improves slightly when only the cumulative stress exceeding the onset of motion for individual events is considered, with two years (11%) of displaying a significant dependence of the threshold for motion on discharge. However, only one of these years reflects the patterns observed with time. Given this, it appears that transporting flows do not adequately capture the temporal evolution of the threshold for motion.

In contrast, 9 years of the time series (49%) demonstrate a significant correlation between the threshold for motion and cumulative low flow shear stress, consistent with the relationship between the onset of motion and both total stress and time. Given that 83.4% of total discharge occurs during inter-event low flows, this similarity in the correlation analysis is not entirely surprising. However, this result is of note, as it challenges the widely held idea that the bed remains completely fixed between transport events, and shows that subthreshold, inter-event periods are a significant driver for setting the threshold for motion.

4.4 Inter-event flow and the onset of motion

This apparent dependence of the threshold for motion on below-threshold flows suggests that grain rearrangement significant enough to alter the stability of the channel bed is possible, even in the absence of measurable coarse bedload transport. To explore this dependence, we focus on the relationship between the critical boundary shear stress and the average magnitude of the prior inter-event period. We classify a low flow period as any time separating two transport events as identified by Turowski et al. (2011). We exclude the first event of each year, to avoid any uncertainty in quantifying the previous low flow period. Average low flow shear stress spans an order of magnitude, from 25 Pa to 253 Pa with a mean value of 96 Pa.

We observe a strong dependence of the magnitude of the threshold for motion on the magnitude of inter-event low-flows for discharges >104 Pa (Figure 4.3a). In

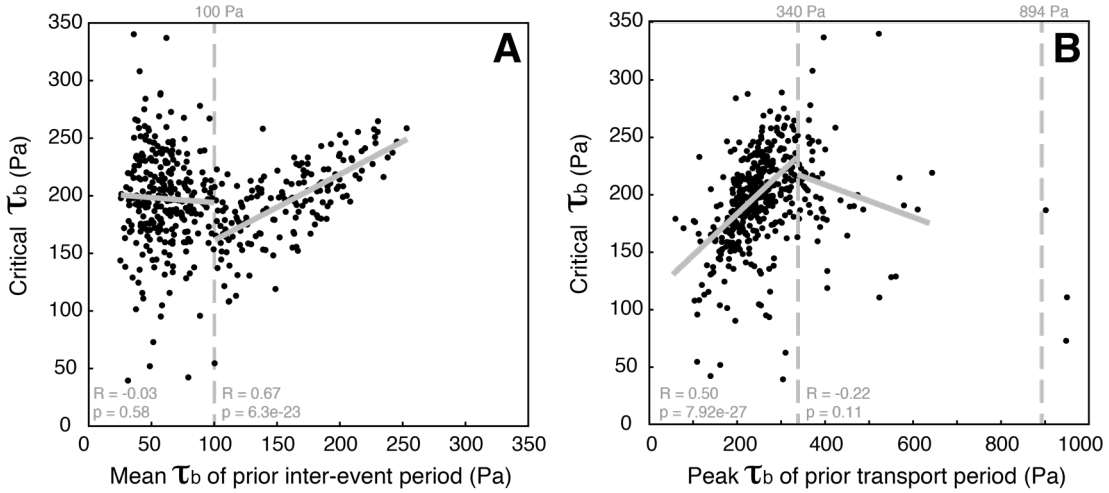

Figure 4.3. Threshold for motion as a function of (a) mean prior inter-event flow magnitude and (b) peak transporting flow magnitude of previous transport event

this region, the threshold for motion increases following an elevated discharge inter-event period (R = 0.69, p = 4.3e-24). It is worth stressing here that no coarse (>1 cm) bedload transport is observed during these low flow periods. For inter-event flows <104 Pa, there is no correlation between the threshold for motion and the magnitude of inter-event low-flows (R = -0.03, p = 0.58).

This result is notable, as it highlights the importance of inter-event discharge on the temporal evolution of the threshold for sediment motion and reinforces the importance of prior flow history on determining sediment mobility and setting bedload transport rates. Further, we identify a lower bound on the magnitude of the antecedent boundary shear stress which exerts control on the threshold for transport of 104 Pa. We hypothesize that below this discharge, no significant rearrangement of the bed can occur.

We also find that the range of mean inter-event discharges (25 Pa to 253 Pa) has significant overlap with the observed thresholds for the onset of motion (39.5 Pa to 340 Pa), such that ~90% of the distributions overlap. This overlap indicates that the range of flows that exert control on the threshold for motion includes a range under which transport can occur. This finding is consistent with the findings of Charru et al. (2004), who observed a slow transition from active bedload transport to no observable transport at a constant boundary shear stress in an experimental flume. This result implies that both inter-event flows and low discharge, transporting flows, likely contribute to an increase in the threshold for motion of the following transport event.

4.5 Transporting flow and the onset of motion

In contrast, exceptional, high discharge, events, are known to decrease the threshold for motion at the Erlenbach (Turowski et al., 2009; Yager et al., 2012b). Specifically, Turowski et al. (2009) classified exceptional events as high discharge events (peak discharge > 9 m^3/s, 894 Pa) that rearrange the step pool morphology of the channel. As jammed step pools are broken, particle interlocking is reduced, increasing bed mobility and resulting in an increased sediment yield. This reduction in the threshold for motion can persist across multiple subsequent transport events, with effects observable for up to year (Yager et al., 2007). This apparent decrease of the threshold for motion differs from the increase in the threshold for motion in

response to low discharge, inter-event and transporting flows, suggesting that there is a transition in the response of the channel bed at high discharge flows compared to below- or near-threshold flows.

To explore the role of high discharge and pervasive sediment transport in the Erlenbach time series, we focus on the dependence of the threshold for motion on the peak boundary shear stress of the previous transport event (Figure 4.3b). Peak shear stress values range from 60 Pa to 950 Pa, with an average peak boundary shear stress of 274 Pa. There is considerable overlap between peak boundary shear stress values and the range of critical stresses at the threshold for motion (~85%), but the maximum values for peak transporting stress far exceed this range. Within this range of overlap, where peak stress during transport is near the threshold for motion, trends similar to those observed for the below-threshold data emerge (Figure 4.3b). In this range of near-threshold flows, the critical stress at the onset of motion increases as a function of the magnitude of previous peak stress, significantly ($R = 0.5$, $p = 7.9 \times 10^{-27}$). This relationship highlights the similar effect of near-threshold, transporting flows and below-threshold, inter-event flows on the threshold for motion. These results are consistent with findings from Charru et al. (2004), which show that near-threshold transport events have a stabilizing effect on the bed, ultimately resulting in reduced bedload transport rates and in increase in the threshold for motion. Further, this result supports the idea that the division of the hydrograph by models of the form of Equation 1 is arbitrary and that the onset of sediment motion is a more continuous transition (Houssais et al., 2015).

Transport events with a peak boundary shear stress exceeding 340 Pa do not overlap with the distribution of measured critical stresses and include the exceptional events described by Turowski et al. (2009a). This subset of data comprises about 11.6% of the full transport time series, indicating that most transporting flows only slightly exceed the threshold for motion (Phillips et al., 2016). Across 19 years, any flow event with a peak boundary shear stress exceeding 340 Pa resulted in measurable transport in the channel, suggesting that a significant portion of the bed is mobilized during these events. We find that there is a significant, inverse relationship between the magnitude of the threshold for motion and the magnitude of these highest discharge transporting flows ($R = -0.43$, $p = 6.2e\text{-}4$). However, we note that this signal is dominated by three exceptionally high discharge events exceeding 894 Pa. These three events have a relatively low average threshold for motion, about 31.2 Pa, when compared to the full population, falling in the 6^{th} percentile of the distribution of critical shear stresses. This result is consistent with previous studies at the Erlenbach, which illustrate that these highest flows result in disorder and weakening of the bed (Turowski et al., 2009; Yager et al., 2012b). Removing these extreme events from the record, we find that there is no significant relationship between the magnitude of the threshold for motion and the magnitude of the remaining population of high peak discharges ($R = -0.22$, $p = 0.11$).

It is worth noting here that the range of critical shear stresses above and below this observed break in correlation at 340 Pa is not significantly different. For the entire dataset, the mean critical boundary shear stress is 192 Pa. For the portion of

the critical stress distribution following near-threshold peak shear stresses, below 340 Pa, the mean critical stress is 198 Pa. The mean critical stress is 196 Pa for the onset of transport following transport events with a peak shear stress exceeding 340 Pa. Thus, though there is an observed loss of dependence, the observed threshold for motion occupies the same range above and below this value, suggesting that the threshold for motion does not approach a steady or constant maximum value.

The loss of a significant correlation between the peak shear stress of the previous transport event and the threshold for motion is, nonetheless, notable (Figure 4.3b). The disruption of the strengthening pattern observed at below- and near-threshold flows suggests that the physical mechanisms for strengthening observed at below-threshold (e.g. Masteller and Finnegan, 2017) and near-threshold discharges (e.g. Charru et al., 2004), are not as effective as the magnitude of the flow increases well about the threshold for motion, as pervasive transport begins. This is not entirely surprising, as these higher flows are able to dislodge more stable particles, overcoming larger friction angles (Wiberg and Smith, 1987), and potentially result in dilation (van der Elst et al., 2012; Houssais et al., 2015). Pervasive transport also results in increased bed roughness and the restoration of high protruding, highly mobile particles, which may also result in a decreased threshold for motion (Kirchner et al., 1990; Masteller and Finnegan, 2017).

These results highlight that there is a transition in the response of the evolution of threshold for motion as a function of prior flow history. We find that the

threshold of motion increases with flow magnitude in response to below- and near-threshold flows. This pattern is disrupted at intermediate and high discharges, resulting in a loss of correlation between the threshold for motion and previous transporting flow. Notably, this transition appears to occur across a range of discharges, and is independent of the occurrence of measurable sediment transport, providing further support for the onset of motion as a continuous process.

4.5 A physical mechanism for discharge-dependent evolution of the threshold for motion

We have observed that the threshold for coarse bedload transport at the Erlenbach is dependent on the magnitude of previous flow history, and sensitive to a range of boundary shear stresses from 104 Pa to 340 Pa (Figure 4.3). In this range, the threshold for motion is positively correlated with prior stress, with a larger antecedent boundary shear stress resulting in an increased threshold for motion. Above an antecedent boundary shear stress of 340 Pa, measurable bedload transport always occurs. Following these transport events, we find no significant relationship between prior flow history and the boundary shear stress at the onset of motion. However, following the largest discharge events (>895 Pa), the threshold for motion is reduced, representing the 6^{th} percentile of the full distribution of critical boundary shear stresses.

There are a number of physical mechanisms that may result in the observed variations in variations in the onset of motion, including (1) changes in surface grain size (Moog and Whiting, 1998; Chen and Stone, 2008), (2) changes in sediment supply (Dietrich et al., 1989; Yager et al., 2012b), or (3) changes to particle surface arrangement or packing (Kirchner et al., 1990; Charru et al., 2004; Masteller and Finnegan, 2017). However, due to the strong correlation between cumulative inter-event flow discharge and the threshold for motion, as well as the clear dependence of the threshold for motion on low flow magnitude, it is clear that no measurable transport is required to modify the mobility of surface sediments.

Previous work has shown that subtle reworking of the bed during below- and near-threshold flows, when intermittent to no transport occurs, increases interlocking on the channel bed, increasing order and bed stability (Ockelford and Haynes, 2013; Masteller and Finnegan, 2017). As the degree of transport increases, we hypothesize that significant transport more effectively removes grains from stable pockets, disrupting interlocking and resulting in increased disorder on the channel bed, ultimately resulting in a loss of correlation between previous flow and the threshold for motion of the following transport event (Masteller and Finnegan, 2017).

To explore these hypotheses, we utilize a physical model for sediment entrainment from Wiberg and Smith (1987), to determine under what conditions coarse grains can, theoretically, be mobilized at the Erlenbach. This model calculates the force balance on individual sediment grains, incorporating both hydraulic forces

and particle geometry on the bed. Specifically, the model resolves four major forces: the drag force, the lift force, the gravitational force due to grain weight, and the resisting force due to pocket geometry and particle friction angle (Wiberg and Smith, 1987). When the driving forces of drag and lift just exceed the weight of the particle and overcome the interparticle friction angle, the grain will begin to move.

The model calculates the maximum friction angle that a can be overcome for a given grain size and boundary shear stress (Table 4.2). To capture the full range of observed flow conditions at the Erlenbach we utilize a range of boundary shear stresses from 0 Pa to 1000 Pa. We focus on three grain sizes, the smallest detectable grain size by the geophones (D_{min} = 0.01 m), the 30th percentile of the surface grain size distribution (D_{30} = 0.03m), and the median surface grain size (D_{50} = 0.08 m) (Table 2) (Turowski et al., 2011). The minimum detectable grain size should require, given its mass, the least amount of boundary shear stress to be entrained, and as such, represents the most mobile population of surface grains (Wiberg and Smith, 1987). In contrast, if the median surface grain size is predicted to be mobile, we expect that a significant portion of the channel bed can be transported, resulting in significant rearrangement of the bed.

Model results are sensitive to the selection of the length scale representative of bed roughness, k_s, which modifies the near-surface velocity profile, affecting both the drag and lift force acting on the channel bed. For hydraulically rough flows, where the Reynold's number exceeds 100, the base of the logarithmic, near-bed velocity

profile, z_0, is characterized by $k_s/30$ (Rouse, 1961). It is difficult to assign a single value for bed roughness across the Erlenbach, as it is a step-pool channel, characterized by a wide range of grain sizes, spanning from 1 mm sand (Yager et al., 2012b) to boulders over 1 m in diameter (Turowski et al., 2009; Yager et al., 2012b). To account for this variability, we select a minimum roughness value of 1 cm, consistent with the smallest detectable grain size, to capture the most mobile portions of the bed, where large grains would have high protrusion and low friction angles. To account for larger roughness elements, the maximum roughness that we consider is 8 cm, or equivalent to the median surface grain size, as well as an intermediate roughness of 3 cm, equivalent to the D_{30} (Turowski et al., 2009) (Table 4.2). For 1 cm grains, this maximum roughness should hamper mobility significantly, as grain hiding effects can be significant, resulting in large friction angles and reduced exposure to the flow. This range of roughness values reflects the grain size distribution of mobile patches as characterized by Yager et al. (2012a), where 80% of the grains in these mobile patches are less than 9 cm in diameter. These patches are likely to be the only portions of the bed mobile at flows well below bankfull conditions (Yager et al., 2012a).

Model solutions calculate the maximum interparticle friction angle that a grain of a given size can overcome to be entrained into an imposed flow, with a maximum possible friction angle of 90 degrees, indicating that the majority of grains of a given size can be transported. We find that 1 cm grains in homogenous patches (k_s = 1 cm) are predicted to be mobile at a boundary shear stress of 123 Pa (Figure 4.4). This is

Table 4.2. Entrainment model parameters

Input Parameter	Value	Units
Boundary shear stress, τ_b	0-1000	Pa
Slope	0.1	
Grain size	0.01; 0.08	m
Roughness length scale, k_s	0.01; 0.04; 0.08	m
Drag coefficient	0.4	
Lift coefficient	0.2	
Sediment density	2650	kg/m^3
Water density	1000	kg/m^3
von Karmon's constant	0.407	

notable, as this boundary shear stress is equivalent to the minimum boundary shears stress for which we observe the onset of dependence of the threshold for motion on prior below- and near-threshold stress. This suggests that while no transport is measured by the geophones at this boundary shear stress, it is physically possible for 1 cm grains and smaller to be dislodged and rearranged on the bed. This result is consistent with the idea that the least stable grains can be transported to nearby, more stable pockets, resulting in an increase in the threshold for motion (Reid et al., 1985; Monteith and Pender, 2005; Masteller and Finnegan, 2017).

In contrast, we find that the boundary shear stress associated with the loss of correlation between the threshold for motion and the magnitude of previous flow above 340 Pa is consistent with the mobilization of larger grains, both the D_{30} and D_{50}, with varying bed roughness (Figure 4.4). For intermediate roughness values (k_s = 0.03 m), we find that all grains of size D30 are predicted to be mobile at a boundary shear stress of 374 Pa (Figure 4.4). Similarly, for the minimum roughness (k_s = 0.01m), we find that the D50 is predicted to be mobile, regardless of friction angle, at a boundary shear stress of 380 Pa (Figure 4.4). These results suggest that a large portion of the grains which comprise mobile patches are predicted to be mobile during flows exceeding 340 Pa. This result confirms that above 340 Pa, indeed, a large portion of the bed is active, suggesting that significant reorganization of the bed can occur, essentially resetting the bed, consistent with the idea that significant transport essentially "resets" the bed, through the restoration of highly mobile, precariously placed particles (Masteller and Finnegan, 2017).

While these results only provide a rough estimate of the mobility of each grain size class, they identify the discharge range of interest for future studies, and show that rearrangement at low shear stresses is possible, even the absence of measurable bedload transport. We have focused on size-selective transport, as we are chiefly interested in the range of boundary shear stresses that approach or overlap with the shear stress at onset of motion. Previous studies show that near-threshold flows

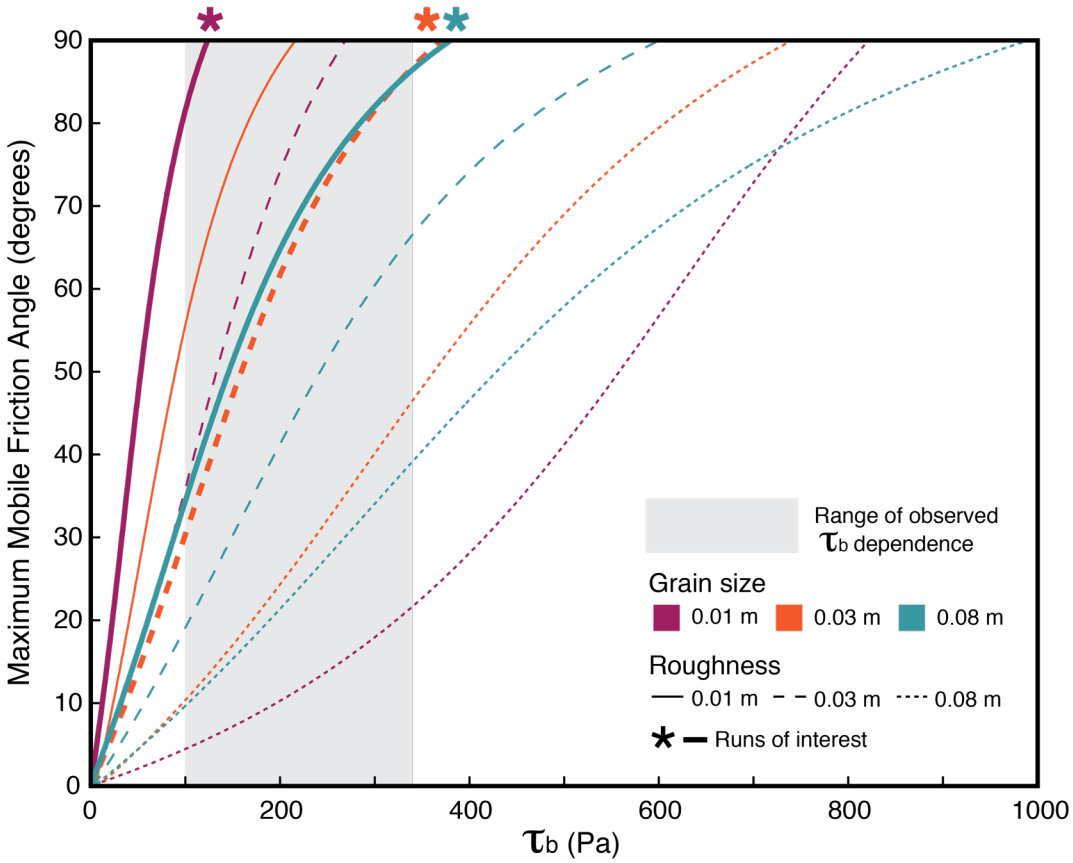

Figure 4.4. Model predictions of maximum mobile friction angle as a function of applied boundary shear stress for grain sizes of 0.01 m (purple), 0.03 m (orange), and 0.08 m (teal), with roughness values of 0.01 m (solid line), 0.03 m (dashed line), and 0.08 m (dotted line). Range of boundary shear stress values over which the threshold for motion is correlated to prior stress denoted in grey.

typically result in size-selective, partial transport, and thus this focus is appropriate (Lenzi et al., 1999). Further, these calculations are consistent with the findings of Yager et al. (2012a), who observed that largest transported grain size increased with peak boundary shear stress at the Erlenbach. Further, for six storms with peak boundary shear stresses ranging from 187-304 Pa, the range of mobilized trace grain

sizes was from 1-11 cm, consistent with the range we predict to be entrained with our simple analysis (Yager et al., 2012a).

In contrast, bedload transport in response to flows significantly above the threshold for motion appear to result in an equal mobilization of all grain size classes (Lenzi et al., 1999). This potential transition towards full mobility of surface sediments is likely associated with significant rearrangement of the channel, and may be related to the loss of correlation that we observe between the threshold for motion and previous discharge. However, the ability to test this idea is beyond the scope of this work and not possible with the dataset we utilize.

While there are many complicating factors not accounted for in the analysis that we present here, it suggests that rearrangement is physically possible under these boundary shear stresses, even in the absence of measurable coarse grain transport, and is consistent with previous observations of grain motion at the Erlenbach. Given this, we expect that the local rearrangement of gravel patches at the Erlenbach exerts a primary control on the evolution of the threshold for motion through each season. We anticipate a decrease in surface roughness (Ockelford and Haynes, 2013), and the abundance of high protruding grains (Masteller and Finnegan, 2017), as a function of previous low flow magnitude, resulting in a modified threshold for motion. We have identified a range of inter-event and transporting flow over which we anticipate a response of bed microtopography, chiefly through variations in surface roughness.

Thus, monitoring of local bed structure at the Erlenbach represents a fruitful avenue of future work.

Changes to surface grain size or available sediment supply may also result in variations in the threshold for motion (Moog and Whiting, 1998; Yager et al., 2012b). Surface grain size evolution and variations in sediment supply are known to be tightly linked to one another (Buffington and Montgomery, 1999), with decreases in sediment supply resulting in bed surface coarsening and a reduction in bedload transport rates (Dietrich et al., 1989). However, bed armoring (Parker and Klingeman, 1982) or the destruction of the armor layer, requires significant transport to occur. Parker and Klingeman (1982) note that gravel pavement, or an armored bed surface, is a mobile-bed phenomenon. As we observe minimal correlation between above-threshold discharge and the onset of motion (Table 4.1), as well as a strong dependence of the threshold for motion on inter-event flows and in lieu of any detectable bedload transport (Figure 4.3a), it is unlikely that bed armoring is the dominant process by which the threshold for motion evolves at the Erlenbach. Additionally, because surface grain size is tightly linked to changes in sediment supply, where reduced supply results in coarsening via winnowing of mobile fine grains (Dietrich et al., 1989) and sediment supply above transport capacity results in sediment deposition, ultimately fining the bed surface (Buffington and Montgomery, 1999). However, both of these effects also require significant transport to occur, and thus, are likely unrelated to the dependence of the threshold for motion on low- and near-threshold flow magnitude. Recent work at the Erlenbach has allowed for grain

size to be inferred from bedload impact amplitude as recorded by the geophone monitoring system (e.g. Wyss et al., 2016). This advance allows this potential mechanism to be explored in more detail in future work.

4.6 Conclusions

We observe a transition in the relationship between prior flow magnitude and the evolution of the threshold for motion with increasing boundary shear stress. In response to below- and near-threshold flows, we observe an increase in the threshold for motion, related to an apparent strengthening of the bed. In response to above-threshold, transporting flows, we observe a loss of correlation between the magnitude of the flow and the threshold for motion of the following event. The seemingly random response of the bed during at these intermediate stresses suggests a disruption in the strengthening behavior observed at low flows, and perhaps, a transition in the dominant process operative on the channel bed. Though the sample size is small (n=3), in response to the most extreme flows, we observed a reduction in the threshold for motion, suggestive of a weakening or destabilizing of bed structure, consistent with observations of boulder transport and step rearrangement in the study reach (Turowski et al., 2009; Yager et al., 2012b).

These observations draw parallels to previous studies of dry granular flows under shear. A similar transition from strengthening to weakening behavior with increased shear stress has been observed by previous studies of dry granular flows,

where low shear stresses result in compaction and an apparent increase in effective friction (Boyer et al., 2011; van der Elst et al., 2012; Houssais et al., 2015) and high shear stresses result in dilation and a decrease in friction (Jaeger et al., 1996; van der Elst et al., 2012; Houssais et al., 2015). Furthermore, this divergent response in the channel bed to the magnitude of applied boundary shear has been observed experimentally by Houssais et al. (2015) in a laminar flume, where a bed of glass beads was exposed to a range of boundary shear stresses. The study observes a transition from creeping behavior at low boundary shear stresses, characterized by slow deformation of the bed in the downstream direction, to active bedload at increased boundary shear stress. Between these two states, the study suggests that there is a continuous transition from slow strengthening and compaction by creep towards bed dilation and active bedload. The results exhibit similar trends to those exposed in this idealized set of experiments, and suggest that the same transition may be relevant for natural channels composed of a wide size range of non-spherical grains exposed to turbulent flow.

We have shown that the threshold of motion is dependent on prior flow magnitude, even in the absence of measurable sediment transport. This result highlights the failure of current, state-of-the-art, sediment transport models of the form of Equation 1, and the assumption of a constant threshold for motion, to accurately capture and predict bedload transport rates. Specifically, we have shown that the implicit assumption of these models, that the bed remains "fixed" below an assigned τ^*_c, is likely false. Further, consistent with recent experiment studies (e.g.

Houssais et al., 2015; Masteller and Finnegan, 2017), this work suggests that the division of the hydrograph at a particular τ^*_c is artificial, and that sediment transport, while subtle, can still occur below this threshold, contributing to variations in observed bedload transport rates by modifying the overall stability of the channel bed.

Instead, these results provide support for the treatment of the onset of motion as a state-dependent quantity, as recently formalized by Johnson (2016). State functions have long been used to successfully describe frictional sliding (Scholz, 1998), earthquake nucleation (Dieterich, 1994), and damage accumulation in materials (Grady and Kipp, 1987). This study shows that the threshold for motion varies as a function of prior flow history, providing support for the further implementation and formulation of the model of Johnson (2016). We have identified the range of discharges over which we observed a strong dependence on prior flow, and a range of discharge over which this dependence appears to break down, providing insight into the range of conditions over which a state-dependent model may more accurately capture the temporal evolution of the onset of motion.

Through the consideration of a simple force-balance model for the entrainment of individual grains, we predict that the onset of discharge-dependence is consistent with local transport of grains less than 1 cm in diameter into more stable configurations. In contrast, we predict that the loss of correlation between the threshold for motion and prior flow occurs when a large portion of the surface grain size distribution and be entrained, pervasive transport restores high protruding particles. Future work

should focus on testing these predictions in the field, and linking changes in bed microtopography in natural channels to the observed variations in the onset of motion.

4.7 Acknowledgements

This material is based upon work supported by National Science Foundation Graduate Research Fellowship grant DGE-1339067 and the ARCS Foundation Northern California Chapter. Conversations with Dr. Joel Johnson and Dr. Colin Phillips greatly benefited this work.

Chapter 5

Concluding remarks

In this thesis, I have attempted to illuminate some of the processes which modify the threshold for particle motion and provide new approaches to quantify these effects. The driving question behind this research is: *when does sediment transport begin*? To address this question, this work has utilized a range of tools and approaches, including mathematical modeling (Chapter 2), novel physical experiments (Chapter 3), and field observations (Chapter 4). The threshold for motion underpins the most widely-used relations for sediment transport predictions, and is known to vary widely (Buffington and Montgomery, 1997), potentially resulting in a significant mismatch between predictions and observations of sediment flux (Gomez and Church, 1989; Recking et al., 2012). Thus, the identification and quantification of the processes that lead to these observed variations in the threshold for motion will contribute to improved predictions of sediment transport rates.

In Chapter 2, we've shown that the colonization of coarse sediment by kelp drastically reduces the threshold for motion. To quantify this effect, we develop a mechanistic model, which accounts for the added effects of drag and lift translated from the kelp frond to the attached cobble via tension in the kelp frond. We then test this model against novel observations of kelp-assisted sediment transport paired with

current velocity measurements from the Strait of Juan de Fuca. We find that the standard model for particle entrainment cannot account for any of our observations of coarse sediment transport. In contrast, our revised model for kelp-assisted entrainment captures 92% of field observations. This new mechanistic model for entrainment of coarse grains by kelp is one of the first attempts to incorporate and apply the forces imparted by biology to the process of sediment transport. This work not only identifies and quantifies a novel means of coarse sediment transport in coastal systems, but it also presents a new approach towards incorporating the effects of biology on particle entrainment and sediment transport rates.

Chapters 3 and 4 turn their focus towards coarse sediment transport in fluvial systems, concentrating on the dependence of the threshold for motion on previous flow history. Chapter 3 explores the role of below-threshold, antecedent flows on gravel bed structure and subsequent bedload transport rates. While previous work has shown that the threshold for motion can vary as a function of prior storm intermittency, the changes to the channel bed that result in these variations has not been previously explored. By varying the duration of an antecedent low flow period, we are able to isolate the relationship between grain protrusion and bedload flux, testing the almost 30-year old hypothesis of Kirchner et al. (1990). Specifically, we demonstrate that (1) the number of high-protruding grains decreases systematically with increased low-flow duration, (2) a decreased number of high protruding particles results in decreased bedload transport rates, related to an increased threshold for motion, and (3) only these highest protruding particles contribute significantly to

bedload flux. Additionally, this study showed that transporting flows are able to restore the population of high protruding particles, effectively decreasing the threshold for motion and disrupting the observed history effects observed at low flow. These results link prior flow history and its topographic signature on the channel bed for the first time experimentally, and provide a framework for the consideration and further quantification of flow history effects on the onset of motion.

Chapter 4 continues to explore the role of inter-event, below-threshold flows, and applies experimental findings from Chapter 3 to a natural channel. For this chapter, we focus on data from the Erlenbach torrent in the Swiss Prealps, where strong seasonal variations in the threshold for motion are observed. Utilizing a unique dataset of continuous bedload transport measurements made over 19 years, we find that the temporal variations in the onset of motion is not captured solely by transport flows, but rather, inter-event low flows. This finding is significant, as it highlights that the consideration of only transporting flows, a common practice, does not capture the full complexity of an evolving threshold for motion. We identify a strong correlation between prior inter-event flow magnitude and the onset of transport during the following transport event, where an increased inter-event boundary shear stress leads to an increase in the threshold for motion. Similar dependence is observed for near-threshold, transporting flows, suggesting that the transition from no measurable bedload flux to active transport is actually a continuous process. Additionally, we observe that the pattern of increasing critical Shields Stress is

disrupted after large storm events, where subsequent variations in the threshold for motion appear to be random.

These findings draw parallels to previous work on granular media, where compaction and strengthening occurs at low shear rates and dilation and disorder occurs at high shear rates. We hypothesize that below- and near-threshold memory, resulting in an increased threshold, reflects local compaction and strengthening of the bed in the absence of measureable bedload flux. Preliminary calculations suggest that this threshold for memory formation corresponds with the mobilization of <10% of the bed, consistent with previous experimental work from Chapter 3. In contrast, we hypothesize that high discharge transporting flows where pervasive sediment transport occurs resets memory by depositing grains randomly, increasing the number of high-protruding grains, resulting in discharge-independent variations in the threshold for motion. Preliminary calculations suggest that this threshold for memory destruction corresponds with the mobilization of ~50% of the bed. We provide support for the use of a state-function to describe an evolving threshold for motion, as proposed by Johnson (2016), and provide insight on the range of memory forming discharges that should be considered when implementing this model.

This work has identified that significant changes to the channel bed can occur in the absence of any measurable sediment transport, and shows that the full hydrograph should be considered in the prediction of bedload transport rates. Currently, fluvial bedload transport is typically treated as a process that is independent of any previous time step, and is solely dependent on concurrent flow

strength. However, Chapters 3 and 4 have shown that prior flow history has a significant effect on the threshold for motion. Findings from this work have opened up a wide array of future research questions related to history-dependence in fluvial systems. Future work should focus on the sensitivity of history effects to variations in multiple parameters, including grain size, sorting, and other environmental conditions, as well as the topographic signature of these prior flows on the channel bed.

Appendix A

Chapter 2 Supplementary Information

Kelp Model

Initation of motion of a grain begins when the driving forces acting on that grain, $F_{driving}$, are equal to the resisting forces acting on the grain, $F_{resisting}$.

$$F_{driving} = F_{resisting} \qquad [1]$$

In this case, kelp contributes to the driving forces of the grain by translating a tension force, F_t, along its stipe, modifying this balance to the following

$$F_{driving} + F_t = F_{resisting} \qquad [2]$$

First, we quantify the force balance acting on the kelp frond, in which the buoyant force, F_b, the drag force, $F_{d\,k}$, result in the tension force, F_t, acting along the length of the kelp stipe. We then quantify the force balance acting on only the grain. We then apply the tension force to the force balance acting on the grain to determine the onset of motion of

Forces on Kelp

The Buoyant Force

Since the kelp frond has a different density than that of the water surrounding it, a net buoyant force acts in the upward direction. This density difference is partially attributed to the pneumatocysts, or large gas-filled bladders, which allow kelp fronds to float within the water column. The buoyant force is given by

$$F_b = (\rho_k - \rho_f)gV \qquad [3]$$

where ρ_k is the kelp density (kg/m^3), ρ_f is the fluid density (kg/m^3), g is acceleration due to gravity (m/s^2) and V is the volume of the kelp frond (m^3). Due to the buoyant force's dependence on material properties, it remains constant and acts in the upward direction regardless of current conditions.

For bull kelp specifically:

$$F_b = 2\ N;\ 12\ N;\ 25\ N \qquad [4]$$

The density of kelp is not well-reported, and thus, instead we rely on empirical measurements of the mean buoyant force for each kelp species we consider (Friedland and Denny, 1995; Utter and Denny, 1996; Denny et al., 1997; Stevens et al., 2001) . However, the relationship of the buoyant force and the size of the kelp frond are not well correlated. Here, we utilize empirical measurements of kelp

buoyant force made in past studies (Friedland and Denny, 1995; Utter and Denny, 1996; Denny et al., 1997).

The Drag Force

A drag force acts over the cross sectional area of a kelp frond in the direction of flow as the fluid moves past the frond. The drag calculation for a kelp frond varies from species to species, as plant shape and size is highly variable, and can be modeled by the following generalized relationship (Utter and Denny, 1996).

$$F_d = 0.5\rho_f u^{\beta} A_k S \qquad [5]$$

Where u is the current velocity (m/s), β is an empirically determined exponent that changes based on the shape of the kelp frond. A value of β=2 is assigned for non streamlined objects, while for streamlined objects and plates oriented parallel to the flow β=1.5 is typical [*Vogel*, 1984]. β determines how quickly drag increases as a function of the current velocity. A_k is the area of the kelp frond (m^2), and S_d is an empirically determined shape parameter similar to the drag coefficient (Friedland and Denny, 1995; Utter and Denny, 1996).

For bull kelp specifically:

$$F_{d\,k} = 0.5\rho_f u^{1.6} A_k 0.016 \qquad [6]$$

The Tension Force

A tension force is generated in the kelp frond as the kelp stretches in the flow. As such, when a stipe is not being stretched, or equal to or less than its original length, the tension force on the frond is zero(Utter and Denny, 1996). However, when the kelp is stretched beyond its initial length, a tension force extends along the stipe in the direction of stretching. The tension force depends on the overall change in length of the kelp stipe, the kelp stiffness, and the cross sectional area of the frond. The general formulation of the tension force is as follows

$$F_t = E[(L_k+\Delta L_k)/L_k]^c A_{xs\,k} \qquad [7]$$

Where E is the stiffness of the kelp stipe (Pa), a measured empirical property, L_k is the unstretched length of the kelp frond (m), ΔL_k is the change in length of the kelp frond (m), and c is an empirically determined exponent(Utter and Denny, 1996; Denny et al., 1997).

For bull kelp specifically:

$$F_t = 1.2x10^7[(L_k+\Delta L_k)/L_k]^1 A_{xs\,k} \qquad [8]$$

In the static solution of the force balance used in this study, the kelp is not accelerating, and has reached a stable position within the water column. In this configuration, the tension force will balance the drag and buoyant forces acting on the frond.

Forces on the Grain

The forces acting on a sediment particle are gravity, F_g, buoyancy, F_b, and lift and drag due to flow over the bed, F_l and F_d, respectively, and a resisting force, F_r.

The Gravitational Force

The gravitational force is given by the submerged weight of the grain, where

$$F_g' = F_g - F_b = (\rho_s - \rho)gV \qquad [9]$$

where ρ_s is sediment density (kg/m^3), typically 2650 kg/m^3 for coarse sand, ρ is fluid density, 1000 kg/m^3 for water, g is acceleration due to gravity (m/s^2), and V is grain volume (m^3).

The Drag Force

The formulation of the drag force is similar to that presented for kelp, though the shape parameter replaced with a drag coefficient, C_d, typically 0.4 for sediment grains. Further, the drag acting on the grain depends on the square of the velocity averaged over the grain cross-section.

$$F_d = 0.5\rho_f C_d u^2 A_{xs} \qquad [10]$$

The Lift Force

The formulation of the lift force is similar to that the drag force, with slight modification

$$F_l = 0.5\rho_f C_l(u_{top}^2 - u_{bottom}^2)A_{xs} \qquad [11]$$

where C_l is the lift coefficient, typically 0.2 for sediment grains, u_{top} specifies the velocity on the top of the grain (m/s), and u_{bottom} specifies the velocity at the bottom of the grain (m/s).

The Resisting Force

The force resisting downstream motion of the grain is specified as follows

$$F_r = F_n \tan\phi = (F_g'\cos\beta - F_l)\tan\phi \qquad [12]$$

where F_n is the effective weight of the sediment grain (gravity minus buoyancy and lift), β is the bed slope, and $\tan\phi$ is the angle of repose, which is analogous to a coefficient of friction, typically about 30°.

The Onset of Motion of only a Grain

A sediment grain at the surface of a riverbed will begin to move when the force resisting downstream motion is equal to the force driving downstream motion, such that

$$(F_g'\cos\beta - F_l)\tan\phi = F_d + F_g'\sin\beta \qquad [13]$$

Solution Method for Kelp Force Balance

It should be noted that we model the kelp frond as a point mass on an elastic string in a 2-dimensional, x,z coordinate space. We first determine the force balance for the point mass at every x,z pair in the coordinate space. We impose a law of the wall velocity profile through the water column, which has the form

$$u(z) = (u_*/\kappa)\, ln(z/z_0) \qquad [14]$$

where u_* is the shear velocity (m/s), κ is von Karman's constant, typically 0.4, z is the specified depth within the water column (m), and z_0 is the median grain size over 30, for hydraulically rough flows (Wiberg and Smith, 1987). Given this velocity profile, and the assumption of steady and uniform flow, we solve equations [6] and [8] for each point within the coordinate space. Since the buoyant force is imposed and constant, we do not need to explicitly solve for it in our model.

We then determine the point in the coordinate space in which the drag, buoyant, and tension forces balance, resulting in a net force of zero acting on the point mass. To do this, we split the tension force into the x and z components, and balance them separately, as follows

$$F_{net\,x} = F_{d\,k} - F_{t\,x} \qquad [15]$$

$$F_{net\,z} = F_b - F_{t\,z} \qquad [16]$$

We then locate the coordinate pair where the net force in both x and z are zero. This location represents the static solution to the kelp force balance. The tension force

acting along the length of the stipe is then applied to the grain force balance as and additional driving force. The new force balance on the grain is calculated as follows

$$[F_g'\cos\beta - (F_l + F_{tz})]\tan\phi = F_d + F_g'\sin\beta + F_{tx} \qquad [17]$$

The tension force acting in the z direction reduces the resisting force, similar to the lift force, ultimately making the grain more mobile. The tension force acting in the x direction adds to the driving forces of drag and gravity, further increasing the mobility of sediment grains.

Appendix B

Chapter 3 Supplementary Information

B.1 Introduction

The supplementary file includes six figures and two tables supporting the main text. B.1 illustrates the experimental grain size distribution. B.2 shows the data used to calculate the root-mean-square (RMS) error of the digital elevation models (DEMs) generated from Structure from Motion Photogrammetry. B.3 compares bed slopes between two phases of the experiments. B.4 shows the number of 11 and 12 mm protruding grains against sediment flux measurements. B.5 illustrates examples of enhanced erosion around high protruding particles. B.6 illustrates the change in elevation at every point in the experimental DEM compared to the change in elevation only surrounding the highest protruding points between the conditioning and transport phases of the experiments. Table B.1 provides data related to estimating the mass/volume eroded by different portions of the experimental bed during the experiments. This table was also used to create Figure 3.7. Table B.2 provides data used in the creations of Figures B.2, B.4, B.5, and B.6.

B.2 Figures and Tables

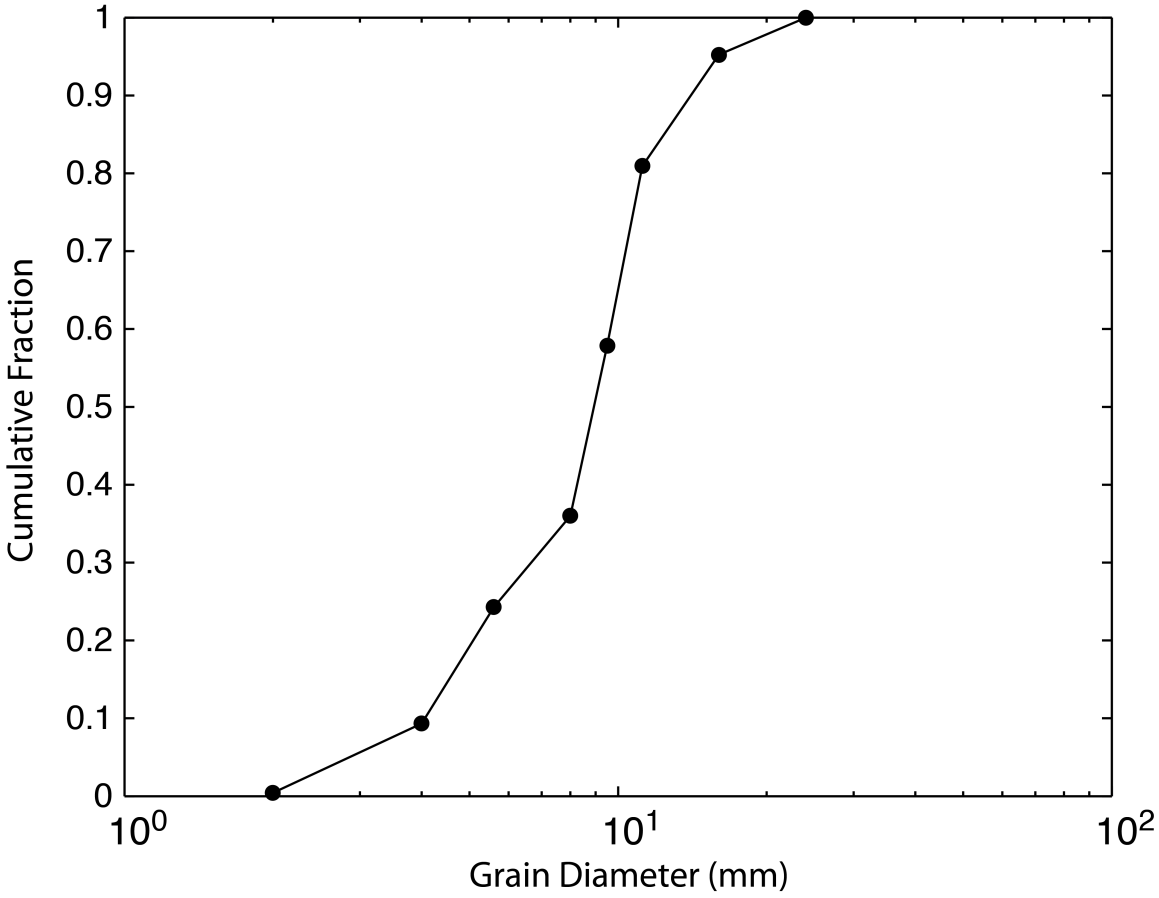

Figure B.1. Experimental grain size distribution.

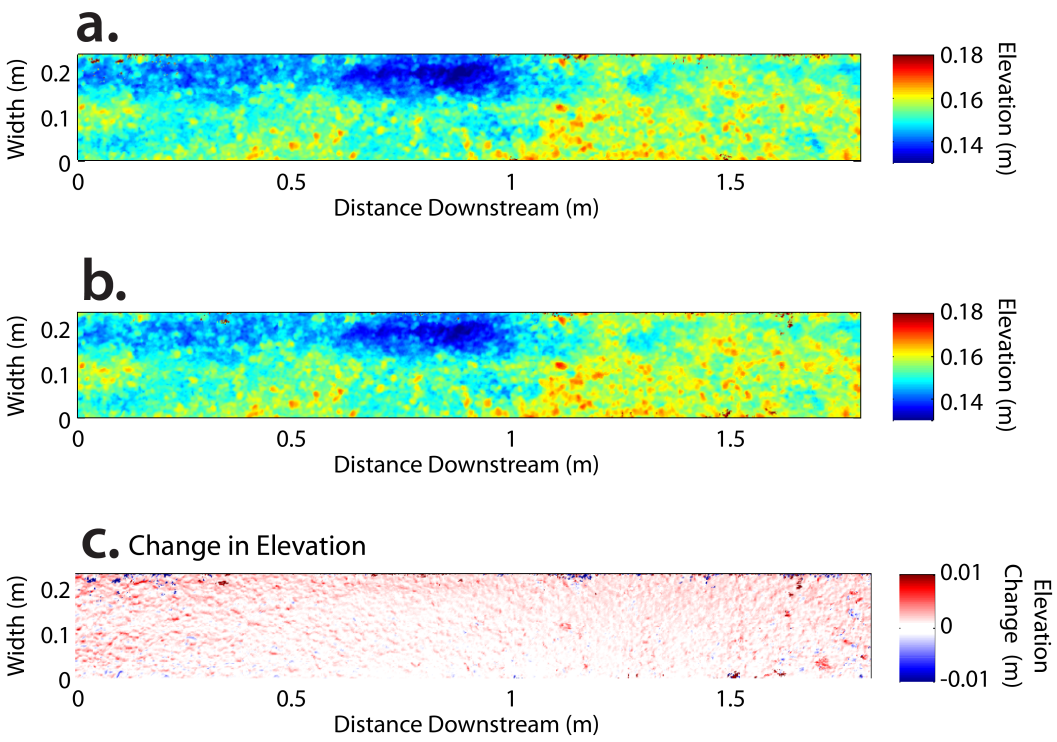

Figure B.2. Repeat Digital Elevation Models (DEMs) of the experimental bed created using Structure from Motion Photogrammetry **a,b)** Two independently

constructed DEMS of the same flume bed used to calculate RMS error. **c)** Differenced DEMs

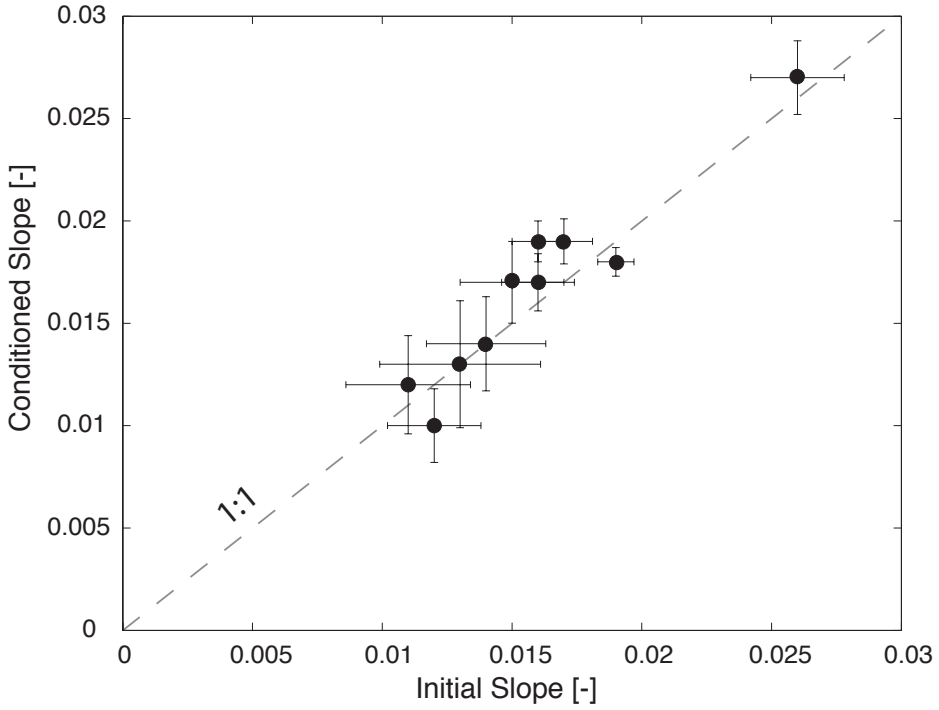

Figure B.3. Comparison of initial and conditioned bed slopes for each experiment measured from SFM DEMs. Error bars represent standard deviation associated with each slope calculation.

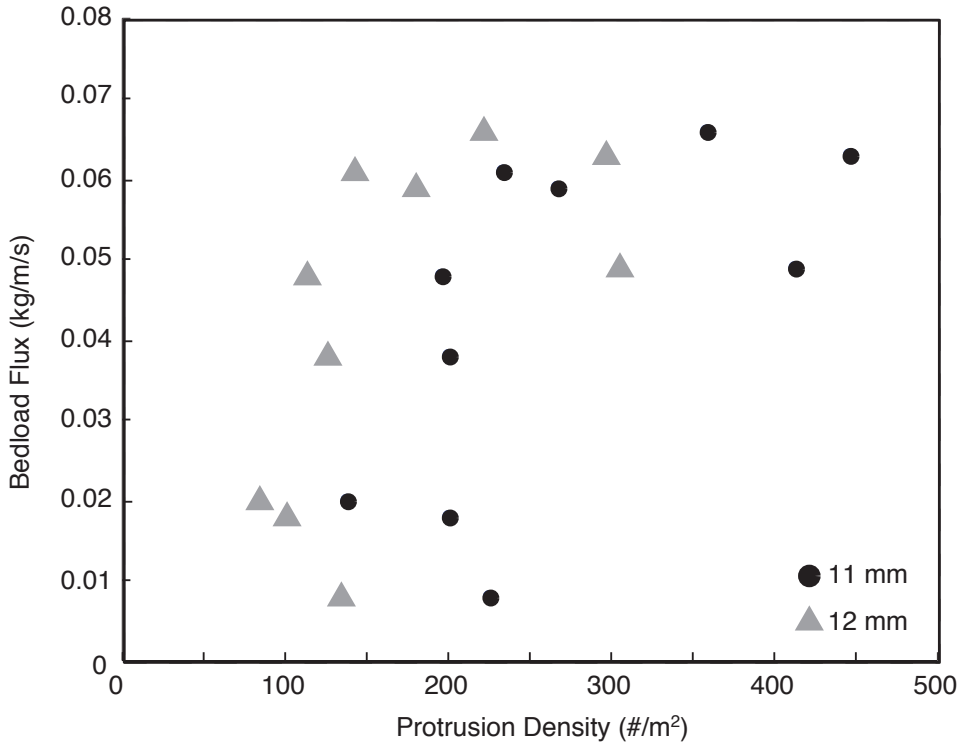

Figure B.4. Plot of density of grains protruding >11 or 12 mm above mean detrended bed elevation measured after the conditioning stage against sediment flux during the transport phase.

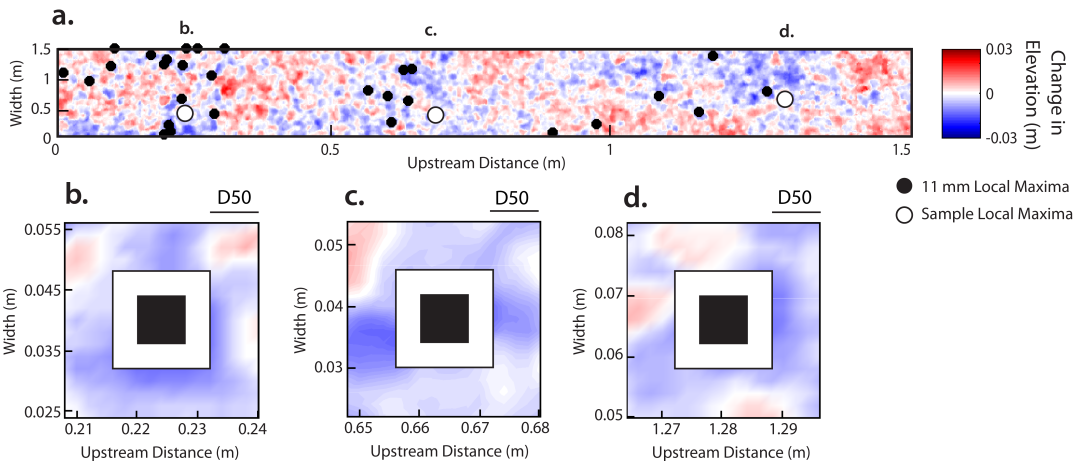

Figure B.5. Examples of keystone grains for a sample bed (10 minute conditioning time). **a)** Erosion and deposition during the transport stage across entire flume sample area with 11 mm local maxima identified. **b-d)** Three 4 D50 diameter samples of enhanced erosion surrounding 11 mm local maxima, or keystone grains. Black squares are unsampled areas which have a diameter of D50. White squares are unsampled areas with a diameter of 2D50. Sample areas b-d are identified as white circles in Figure pane A.

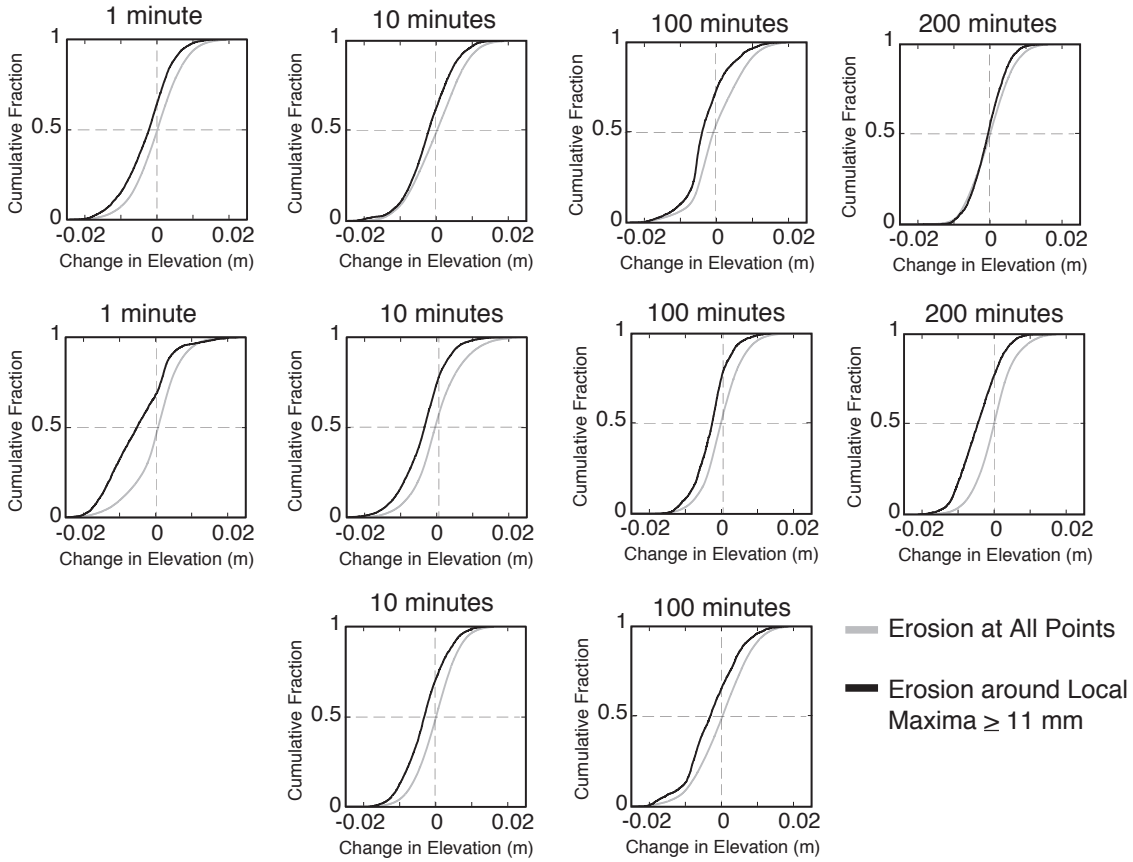

Figure B.6. Distribution of change in elevation across all points in each experimental DEM (grey) and in areas surrounding points protruding 11 mm or above mean bed elevation (black) for all 10 experiments.

Table B.1. Estimates of volume of surface layer eroded during transport, mass contributions from protruding points >11 mm, and total mass contribution from protruding points and their neighbors.

Conditioning Time	Bedload Flux (kg/m/s)	% Vol. of surface layer eroded	% Mass contribution from >11 mm local maxima	% Mass contribution of local max and neighbors
1	0.063	10.7	16.7	99.3
1	0.066	11.1	12.9	146.4
10	0.049	8.2	20.1	149.9
10	0.061	10.3	9.1	56.0
10	0.059	9.9	10.8	47.8
100	0.038	6.5	12.4	89.8
100	0.048	8.1	9.7	63.9
100	0.018	3.0	26.5	174.5
200	0.020	3.4	16.5	23.5
200	0.008	1.3	70.8	664.6

Table B.2. Data used to create Figure 3.2, Figure 3.4, Figure 3.5, and Figure 3.6 in the main text.

Protrusion Threshold (mm)		0	1	2	3	4	5	6	7
Conditoning Time	**Cumulative Bedload (kg)**	**Protrusion Density (#/m^2)**							
1	3411.3	3750.0	3320.8	2925.0	2554.2	2141.7	1770.8	1554.2	1262.5
1	3540	3612.5	3191.7	2775.0	2425.0	2091.7	1683.3	1379.2	1058.3
10	2620	3708.3	3395.8	3079.2	2737.5	2433.3	1954.2	1570.8	1237.5
10	3280	3975.0	3491.7	3016.7	2562.5	2062.5	1666.7	1304.2	1000.0
10	3163	3762.5	3287.5	2783.3	2320.8	1908.3	1570.8	1183.3	933.3
100	2060	4045.8	3554.2	3008.3	2562.5	2050.0	1612.5	1216.7	937.5
100	2581	3745.8	3300.0	2779.2	2337.5	1895.8	1508.3	1166.7	854.2
100	965.1	3704.2	3262.5	2845.8	2379.2	1991.7	1575.0	1233.3	962.5
200	1067	3862.5	3408.3	2945.8	2466.7	2079.2	1687.5	1362.5	1058.3
200	406	3979.2	3541.7	3083.3	2637.5	2175.0	1787.5	1420.8	1095.8
Correlation Coefficient		**0.10**	**0.18**	**0.32**	**0.52**	**0.43**	**0.48**	**0.49**	**0.48**
P-value		**0.775**	**0.625**	**0.375**	**0.123**	**0.214**	**0.157**	**0.154**	**0.159**

Protrusion Threshold (mm)		8	9	10	11	12	13	14	15
Conditoning Time	**Cumulative Bedload (kg)**	**Protrusion Density (#/m^2)**							
1	3411.3	950.0	737.5	570.8	445.8	295.8	195.8	100.0	50.0
1	3540	833.3	620.8	487.5	358.3	220.8	137.5	83.3	33.3
10	2620	1025.0	733.3	529.2	412.5	304.2	225.0	154.2	91.7
10	3280	737.5	512.5	333.3	233.3	141.7	75.0	29.2	12.5
10	3163	675.0	437.5	320.8	200.0	125.0	87.5	45.8	20.8
100	2060	667.0	441.7	291.7	195.8	112.5	50.0	20.8	8.3
100	2581	604.2	429.2	254.2	137.5	83.3	41.7	12.5	12.5
100	965.1	675.0	458.3	295.8	200.0	100.0	58.3	50.0	29.2
200	1067	733.3	579.2	408.3	225.0	133.3	83.3	58.3	37.5
200	406	795.8	570.8	379.2	266.7	179.2	133.3	91.7	54.2
Correlation Coefficient		**0.57**	**0.47**	**0.50**	**0.65**	**0.66**	**0.58**	**0.38**	**0.15**
P-value		**0.084**	**0.175**	**0.141**	**0.044**	**0.036**	**0.081**	**0.285**	**0.679**

References

Albertson, L.K., Sklar, L.S., Pontau, P., Dow, M., and Cardinale, B.J., 2014, A mechanistic model linking insect (Hydropsychidae) silk nets to incipient sediment motion in gravel-bedded streams: Journal of Geophysical Research: Earth Surface, v. 119, no. 9, p. 1833–1852, doi: 10.1002/2013JF003024.

Allan, A.F., and Frostick, L., 1999, Framework dilation, winnowing, and matrix particle size; the behavior of some sand-gravel mixtures in a laboratory flume: Journal of Sedimentary Research, v. 69, no. 1, p. 21–26, doi: 10.2110/jsr.69.21.

Ancey, C., Böhm, T., Jodeau, M., and Frey, P., 2006, Statistical description of sediment transport experiments.: Physical review. E, Statistical, nonlinear, and soft matter physics, v. 74, no. 1 Pt 1, p. 11302, doi: 10.1103/PhysRevE.74.011302.

Bathurst, J.C., 2007, Effect of Coarse Surface Layer on Bed-Load Transport: Journal of Hydraulic Engineering, v. 133, no. 11, p. 1192–1205, doi: 10.1061/(ASCE)0733-9429(2007)133:11(1192).

Booth, A.M., Hurley, R., Lamb, M.P., and Andrade, J.E., 2014, Force chains as the link between particle and bulk friction angles in granular material: Geophysical Research Letters, v. 41, no. 24, p. 8862–8869, doi: 10.1002/2014GL061981.

Boyer, F., Guazzelli, E., and Pouliquen, O., 2011, Unifying Suspension and Granular Rheology: Physical Review Letters, v. 107.

Brayshaw, A.C., 1985, Bed microtopography and entrainment thresholds in gravel-bed rivers: Geological Society of America Bulletin, v. 96, no. 2, p. 218, doi: 10.1130/0016-7606(1985)96<218:BMAETI>2.0.CO;2.

Brayshaw, A.C., 1984, Characteristics and Origin of Cluster Bedforms in Coarse-Grained Alluvial Channels: , p. 77–85.

Brayshaw, A.C., Frostick, L.E., and Reid, I., 1983, The hydrodynamics of particle clusters and sediment entrapment in coarse alluvial channels: Sedimentology, v. 30, no. 1, p. 137–143, doi: 10.1111/j.1365-3091.1983.tb00656.x.

Buffington, J.M., Dietrich, W.E., and Kirchner, J.W., 1992, Friction angle measurements on a naturally formed gravel streambed: Implications for critical boundary shear stress: Water Resources Research, v. 28, no. 2, p. 411–425, doi: 10.1029/91WR02529.

Buffington, J.M., and Montgomery, D.R., 1997, A systematic analysis of eight

decades of incipient motion studies, with special reference to gravel-bedded rivers: Water Resources Research, v. 33, no. 8, p. 1993–2029, doi: 10.1029/96WR03190.

Buffington, J.M., and Montgomery, D.R., 1999, Effects of sediment supply on surface textures of gravel-bed rivers: Water Resources Research, v. 35, no. 11, p. 3523–3530, doi: 10.1029/1999WR900232.

Buscombe, D., 2013, Transferable wavelet method for grain-size distribution from images of sediment surfaces and thin sections, and other natural granular patterns: Sedimentology, v. 60, no. 7, p. 1709–1732, doi: 10.1111/sed.12049.

Campbell, C.S., 2006, Granular material flows – An overview: Powder Technology, v. 162, no. 3, p. 208–229, doi: 10.1016/j.powtec.2005.12.008.

Carling, P.A., 2014, The role of attached kelp (seaweed) in lowering threshold of coarse gravel entrainment in tidal flows: Marine Geology, v. 357, p. 101–107, doi: 10.1016/j.margeo.2014.08.002.

Charru, F., Mouilleron, H., and Eiff, O., 2004, Erosion and deposition of particles on a bed sheared by a viscous flow: Journal of Fluid Mechanics, v. 519, p. 55–80, doi: 10.1017/S0022112004001028.

Chen, L., and Stone, M.C., 2008, Influence of bed material size heterogeneity on bedload transport uncertainty: Water Resources Research, v. 44, no. 1, doi: 10.1029/2006WR005483.

Church, M., Hassan, M.A., and Wolcott, J.F., 1998, Stabilizing self-organized structures in gravel-bed stream channels: Field and experimental observations: Water Resources Research, v. 34, no. 11, p. 3169–3179, doi: 10.1029/98WR00484.

Dancey, C.L., Diplas, P., Papanicolaou, A., and Bala, M., 2002, Probability of Individual Grain Movement and Threshold Condition: Journal of Hydraulic Engineering, v. 128, no. 12, p. 1069–1075, doi: 10.1061/(ASCE)0733-9429(2002)128:12(1069).

Denny, M.W., Gaylord, B.P., and Cowen, E.A., 1997, Flow and Flexibility: II. The roles of size and shape in determining wave forces on the bull kelp Nereocystis luetkeana: Journal of Experimental Biology, v. 200, p. 3165–3183.

Denny, M., Gaylord, B., Helmuth, B., and Daniel, T., 1998, The menace of momentum : Dynamic forces on flexible organisms: Limnology and Oceanography, v. 43, no. 5, p. 955–968.

Dieterich, J., 1994, A constitutive law for rate of earthquake production and its application to earthquake clustering: Journal of Geophysical Research: Solid

Earth, v. 99, no. B2, p. 2601–2618, doi: 10.1029/93JB02581.

Dietrich, W.E., Kirchner, J.W., Ikeda, H., and Iseya, F., 1989, Sediment supply and the development of the coarse surface layer in gravel-bedded rivers: Nature, v. 340, no. 6230, p. 215–217, doi: 10.1038/340215a0.

Dietrich, W.E., and Perron, J.T., 2006, The search for a topographic signature of life.: Nature, v. 439, no. 7075, p. 411–8, doi: 10.1038/nature04452.

Duda, J.J., Warrick, J.A., and Magirl, 2011, USGS Scientific Investigations Report 2011–5120: Coastal Habitats of the Elwha River, Washington—Biological and Physical Patterns and Processes Prior to Dam Removal.:

East, A.E., Pess, G.R., Bountry, J.A., Magirl, C.S., Ritchie, A.C., Logan, J.B., Randle, T.J., Mastin, M.C., Minear, J.T., Duda, J.J., Liermann, M.C., McHenry, M.L., Beechie, T.J., and Shafroth, P.B., 2015, Large-scale dam removal on the Elwha River, Washington, USA: River channel and floodplain geomorphic change: Geomorphology, v. 228, p. 765–785, doi: 10.1016/j.geomorph.2014.08.028.

Einstein, H., 1950, The bed-load function for sediment transportation in open channel flows: U.S. Dept. of Agriculture, Washington.

Elowyn Yager, 2006, Prediction of sediment transport in steep, rough streams: University of California, Berkeley.

van der Elst, N.J., Brodsky, E.E., Le Bas, P.-Y., and Johnson, P.A., 2012, Auto-acoustic compaction in steady shear flows: Experimental evidence for suppression of shear dilatancy by internal acoustic vibration: Journal of Geophysical Research: Solid Earth, v. 117, no. B9, p. n/a-n/a, doi: 10.1029/2011JB008897.

Emery, K.O., and Tschudy, R.H., 1941, Transportation of rock by kelp: Geological Society of America Bulletin, v. 52, no. 6, p. 855–862, doi: 10.1130/GSAB-52-855.

Engelund, F., and Fredsøe, J., 1975, A Sediment Transport Model for Straight Alluvial Channels: Hydrology Research, v. 7, no. 5, p. 293–306.

Estes, J.A., and Duggins, D.O., 1995, Sea Otters and Kelp Forests in Alaska: Generality and Variation in a Community Ecological Paradigm: Ecological Monographs, v. 65, no. 1, p. 75, doi: 10.2307/2937159.

Fenton, J.D., and Abbott, J.E., 1977, Initial Movement of Grains on a Stream Bed: The Effect of Relative Protrusion: Proceedings of the Royal Society A: Mathematical, Physical and Engineering Sciences, v. 352, no. 1671, p. 523–537, doi: 10.1098/rspa.1977.0014.

Ferguson, R.I., 1994, Critical discharge for entrainment of poorly sorted gravel: Earth Surface Processes and Landforms, v. 19, no. 2, p. 179–186, doi: 10.1002/esp.3290190208.

Fernandez Luque, R., and Van Beek, R., 2010, Erosion And Transport Of Bed-Load Sediment: Journal of Hydraulic Research, v. 14, no. 2, p. 127–144, doi: 10.1080/00221687609499677.

Frey, P., and Church, M., 2009, How River Beds Move: Science, v. 325, no. 5947.

Frey, S.E., and Dashtgard, S.E., 2012, Seaweed-assisted , benthic gravel transport by tidal currents British Columbia: Sedimentary Geology, v. 265–266, p. 121–125, doi: 10.1016/j.sedgeo.2012.04.002.

Friedland, M.T., and Denny, M.W., 1995, Surviving hydrodynamic forces in a wave-swept environment: Consequences of morphology in the feather boa kelp, Egregia menziesii (Turner): Journal of Experimental Marine Biology and Ecology, v. 190, no. 1, p. 109–133, doi: 10.1016/0022-0981(95)00038-S.

Furbish, D.J., Haff, P.K., Roseberry, J.C., and Schmeeckle, M.W., 2012, A probabilistic description of the bed load sediment flux: 1. Theory: Journal of Geophysical Research: Earth Surface, v. 117, no. F3, p. n/a-n/a, doi: 10.1029/2012JF002352.

Garden, C.J., and Smith, A.M., 2011, The role of kelp in sediment transport: Observations from southeast New Zealand: Marine Geology, v. 281, no. 1–4, p. 35–42, doi: 10.1016/j.margeo.2011.01.006.

Gaylord, B., and Denny, M.W., 1997, Flow and flexibility I. Effects of size, shape and stiffnes in determining wave forces on the stipitate kelps Eisenia arborea and Pterygophora californica: The Journal of Experimental Biology, v. 3164, p. 3141–3164.

Gaylord, B., Denny, M.W., and Koehl, M.A.R., 2008, Flow forces on seaweeds: Field evidence for roles of wave impingement and organism inertia.: The Biological Bulletin, v. 215, p. 295–308.

Gelfenbaum, G., Stevens, A.W., Miller, I., Warrick, J.A., Ogston, A.S., and Eidam, E., 2015, Large-scale dam removal on the Elwha River, Washington, USA: Coastal geomorphic change: Geomorphology, doi: 10.1016/j.geomorph.2015.01.002.

Gilbert, R., 1984, The Movement of Gravel by the Alga Fucus Vesiculosus (L.) on an Arctic Intertidal Flat: Journal of Sedimentary Petrology, v. 54, no. 2, p. 463–468.

Gilbert, G.K., and Murphy, E.C., 1914, The Transportation of Debris by Running Water.:

Gomez, B., and Church, M., 1989, An assessment of bed load sediment transport formulae for gravel bed rivers: Water Resources Research, v. 25, no. 6, p. 1161–1186, doi: 10.1029/WR025i006p01161.

Gomez, B., Naff, R.L., and Hubbell, D.W., 1989, Temporal variations in bedload transport rates associated with the migration of bedforms: Earth Surface Processes and Landforms, v. 14, no. 2, p. 135–156, doi: 10.1002/esp.3290140205.

Grady, D.E., and Kipp, M.E., 1987, 10 – Dynamic Rock Fragmentation, *in* Fracture Mechanics of Rock, p. 429–475.

Harrold, C., and Reed, D.C., 1985, Food Availability, Sea Urchin Grazing, and Kelp Forest Community Structure: Ecology, v. 66, no. 4, p. 1160, doi: 10.2307/1939168.

Haynes, H., and Pender, G., 2007, Stress History Effects on Graded Bed Stability: Journal of Hydraulic Engineering, v. 133, no. 4, p. 343–349, doi: 10.1061/(ASCE)0733-9429(2007)133:4(343).

Hegg, C., McArdell, B.W., and Badoux, A., 2006, One hundred years of mountain hydrology in Switzerland by the WSL: Hydrological Processes, v. 20, no. 2, p. 371–376, doi: 10.1002/hyp.6055.

Heyman, J., Mettra, F., Ma, H.B., and Ancey, C., 2013, Statistics of bedload transport over steep slopes: Separation of time scales and collective motion: Geophysical Research Letters, v. 40, no. 1, p. 128–133, doi: 10.1029/2012GL054280.

Hodge, R.A., Sear, D.A., and Leyland, J., 2013, Spatial variations in surface sediment structure in riffle-pool sequences: a preliminary test of the Differential Sediment Entrainment Hypothesis (DSEH): Earth Surface Processes and Landforms, v. 38, no. 5, p. 449–465, doi: 10.1002/esp.3290.

Houssais, M., Ortiz, C.P., Durian, D.J., and Jerolmack, D.J., 2015, Onset of sediment transport is a continuous transition driven by fluid shear and granular creep.: Nature communications, v. 6, p. 6527, doi: 10.1038/ncomms7527.

Hsu, L., Dietrich, W.E., and Sklar, L.S., 2008, Experimental study of bedrock erosion by granular flows: Journal of Geophysical Research, v. 113, no. F2, p. F02001, doi: 10.1029/2007JF000778.

Iverson, R.M., 1997, The physics of debris flows: Reviews of Geophysics, v. 35, no. 3, p. 245–296, doi: 10.1029/97RG00426.

Jaeger, H.M., Nagel, S.R., and Behringer, R.P., 1996, Granular solids, liquids, and gases: Reviews of Modern Physics, v. 68, no. 4, p. 1259–1273, doi: 10.1103/RevModPhys.68.1259.

Jerolmack, D.J., and Paola, C., 2010, Shredding of environmental signals by sediment transport: Geophysical Research Letters, v. 37, no. 19, p. n/a-n/a, doi: 10.1029/2010GL044638.

Johnson, J.P.L., 2016, Gravel threshold of motion: a state function of sediment transport disequilibrium? Earth Surface Dynamics, v. 4, no. 3, p. 685–703, doi: 10.5194/esurf-4-685-2016.

Katsuragi, H., Abate, A.R., and Durian, D.J., 2010, Jamming and growth of dynamical heterogeneities versus depth for granular heap flow: , doi: 10.1039/b918991b.

Kirchner, J.W., Dietrich, W.E., Iseya, F., and Ikeda, H., 1990, The variability of critical shear stress, friction angle, and grain protrusion in water-worked sediments: Sedimentology, v. 37, no. 4, p. 647–672, doi: 10.1111/j.1365-3091.1990.tb00627.x.

Knight, J.B., Fandrich, C.G., Lau, C.N., Jaeger, H.M., and Nagel, S.R., 1995, Density relaxation in a vibrated granular material: Physical Review E, v. 51, no. 5, p. 3957–3963, doi: 10.1103/PhysRevE.51.3957.

Kudrass, H.-R., 1974, Experimental study of nearshore transportation of pebbles with attached algae: Marine Geology, v. 16, p. M9–M12, doi: 10.1016/0025-3227(74)90019-X.

Lacey, R.W.J., and Roy, A.G., 2008, The spatial characterization of turbulence around large roughness elements in a gravel-bed river: Geomorphology, v. 102, no. 3, p. 542–553, doi: 10.1016/j.geomorph.2008.05.045.

Lamb, M.P., Dietrich, W.E., and Sklar, L.S., 2008a, A model for fluvial bedrock incision by impacting suspended and bed load sediment: Journal of Geophysical Research, v. 113, no. F3, p. F03025, doi: 10.1029/2007JF000915.

Lamb, M.P., Dietrich, W.E., and Venditti, J.G., 2008b, Is the critical Shields stress for incipient sediment motion dependent on channel-bed slope? Journal of Geophysical Research, v. 113, no. F2, p. F02008, doi: 10.1029/2007JF000831.

Laronne, J., Alexandrov, Y., Bergman, N., Cohen, H., Garcia, C., and Habersack, H., 2003, The continuous monitoring of bed load flux in various fluvial environments, *in* Bogen, J., Fergus, T., and Walling, D.E. eds., Erosion and Sediment Transport Measurement in Rivers: Technological and Methodological Advances, Int'l. Assoc. Hydrol. Sci., p. 134–145.

Laronne, J.B., and Carson, M.A., 1976, Interrelationships between bed morphology and bed-material transport for a small, gravel-bed channel: Sedimentology, v. 23, no. 1, p. 67–85, doi: 10.1111/j.1365-3091.1976.tb00039.x.

Lavelle, J.W., and Mofjeld, H.O., 1987, Do Critical Stresses for Incipient Motion and Erosion Really Exist? Journal of Hydraulic Engineering, v. 113, no. 3, p. 370–385, doi: 10.1061/(ASCE)0733-9429(1987)113:3(370).

Lenzi, A, M., D 'agostino, V., and Billi, P., 1999, Bedload transport in the instrumented catchment of the Rio Cordon Part I: Analysis of bedload records, conditions and threshold of bedload entrainment: Catena, v. 36, p. 171–190.

Lenzi, M.A., Mao, L., and Comiti, F., 2006, When does bedload transport begin in steep boulder-bed streams? Hydrological Processes, v. 20, no. 16, p. 3517–3533, doi: 10.1002/hyp.6168.

Liu, Y., Métivier, F., Lajeunesse, É., Lancien, P., Narteau, C., Ye, B., and Meunier, P., 2008, Measuring bedload in gravel-bed mountain rivers: averaging methods and sampling strategies: Geodinamica Acta, v. 21, no. 1–2, p. 81–92, doi: 10.3166/ga.21.81-92.

Masteller, C.C., and Finnegan, N.J., 2017, Interplay between grain protrusion and sediment entrainment in an experimental flume: Journal of Geophysical Research: Earth Surface, v. 122, no. 1, p. 274–289, doi: 10.1002/2016JF003943.

Masteller, C.C., Finnegan, N.J., Warrick, J.A., and Miller, I.M., 2015, Kelp, cobbles, and currents: Biologic reduction of coarse grain entrainment stress: Geology, v. 43, no. 6, p. 543–546, doi: 10.1130/G36616.1.

Métivier, F., Meunier, P., Moreira, M., Crave, A., Chaduteau, C., Ye, B., and Liu, G., 2004, Transport dynamics and morphology of a high mountain stream during the peak flow season: The Ürümqi River (Chinese Tian Shan): Draft, p. 1–8.

Meunier, P., Métivier, F., Lajeunesse, E., Mériaux, a. S., and Faure, J., 2006, Flow pattern and sediment transport in a braided river: The "torrent de St Pierre" (French Alps): Journal of Hydrology, v. 330, no. 3–4, p. 496–505, doi: 10.1016/j.jhydrol.2006.04.009.

Meyer-Peter, E., and Müller, R., 1948, Formulas for bedload transport: Proceedings of the 2nd Meeting of the International Association for Hydraulic Structures Research, p. 39–64.

Middleton, R., Brasington, J., Murphy, B.., and Frostick, L.., 2000, Monitoring gravel framework dilation using a new digital particle tracking method: Computers & Geosciences, v. 26, no. 3, p. 329–340, doi: 10.1016/S0098-3004(99)00136-3.

Miller, I.M., Warrick, J. a., and Morgan, C., 2011, Observations of coarse sediment movements on the mixed beach of the Elwha Delta, Washington: Marine Geology, v. 282, p. 201–214, doi: 10.1016/j.margeo.2011.02.012.

Monsalve, A., Yager, E.M., Turowski, J.M., and Rickenmann, D., 2016, A

probabilistic formulation of bed load transport to include spatial variability of flow and surface grain size distributions: Water Resources Research, v. 52, no. 5, p. 3579–3598, doi: 10.1002/2015WR017694.

Monteith, H., and Pender, G., 2005, Flume investigations into the influence of shear stress history on a graded sediment bed: Water Resources Research, v. 41, no. 12, p. n/a-n/a, doi: 10.1029/2005WR004297.

Montgomery, D.R., Buffington, J.M., Peterson, N.P., Schuett-Hames, D., and Quinn, T.P., 2011, Stream-bed scour, egg burial depths, and the influence of salmonid spawning on bed surface mobility and embryo survival: Canadian Journal of Fisheries and Aquatic Sciences,.

Moog, D.B., and Whiting, P.J., 1998, Annual hysteresis in bed load rating curves: Water Resources Research, v. 34, no. 9, p. 2393–2399, doi: 10.1029/98WR01658.

Morrison, L., Feely, M., Stengel, D.B., Blamey, N., Dockery, P., Sherlock, A., and Timmins, E., 2009, Seaweed attachment to bedrock: biophysical evidence for a new geophycology paradigm.: Geobiology, v. 7, p. 477–87, doi: 10.1111/j.1472-4669.2009.00206.x.

Naylor, L.A., Coombes, M.A., and Viles, H.A., 2012, Reconceptualising the role of organisms in the erosion of rock coasts: A new model: Geomorphology, v. 157–158, p. 17–30, doi: 10.1016/j.geomorph.2011.07.015.

Ockelford, A.-M., and Haynes, H., 2013, The impact of stress history on bed structure: Earth Surface Processes and Landforms, v. 38, no. 7, p. 717–727, doi: 10.1002/esp.3348.

Papanicolaou, A.N., Diplas, P., Evaggelopoulos, N., and Fotopoulos, S., 2002, Stochastic Incipient Motion Criterion for Spheres under Various Bed Packing Conditions: Journal of Hydraulic Engineering, v. 128, no. 4, p. 369–380, doi: 10.1061/(ASCE)0733-9429(2002)128:4(369).

Paphitis, D., and Collins, M.B., 2005, Sand grain threshold, in relation to bed "stress history": an experimental study: Sedimentology, v. 52, no. 4, p. 827–838, doi: 10.1111/j.1365-3091.2005.00710.x.

Parker, G., 1979, Hydraulic Geometry of Active Gravel Rivers: Journal of the Hydraulics Division, v. 105, no. 9, p. 1185–1201.

Parker, G., and Klingeman, P.C., 1982, On why gravel bed streams are paved: Water Resources Research, v. 18, no. 5, p. 1409–1423, doi: 10.1029/WR018i005p01409.

Parker, G., and Sutherland, A.J., 1990, Fluvial armor: Journal of Hydraulic Research,

v. 28, no. 5, p. 529–544, doi: 10.1080/00221689009499044.

Parker, G., Wilcock, P.R., Paola, C., Dietrich, W.E., and Pitlick, J., 2007, Physical basis for quasi-universal relations describing bankfull hydraulic geometry of single-thread gravel bed rivers: Journal of Geophysical Research, v. 112, no. F4, p. F04005, doi: 10.1029/2006JF000549.

Pearse, J.S., and Hines, A.H., 1979, Expansion of a central California kelp forest following the mass mortality of sea urchins: Marine Biology, v. 51, p. 83–91, doi: 10.1007/BF00389034.

Phillips, C.B., Jerolmack, D.J., Molnar, P., Whipple, K.X., Peizhen, Z., Molnar, P., Downs, W.R., Burbank, D.W., Blythe, A.E., Putkonen, J., Pratt-Sitaula, B., Gabet, E., Oskin, M., Barros, A., et al., 2016, Self-organization of river channels as a critical filter on climate signals.: Science (New York, N.Y.), v. 352, no. 6286, p. 694–697, doi: 10.1126/science.aad3348.

Recking, A., Liébault, F., Peteuil, C., and Jolimet, T., 2012, Testing bedload transport equations with consideration of time scales: Earth Surface Processes and Landforms, v. 37, no. 7, p. 774–789, doi: 10.1002/esp.3213.

Reid, I., Frostick, L.E., and Layman, J.T., 1985, The incidence and nature of bedload transport during flood flows in coarse-grained alluvial channels: Earth Surface Processes and Landforms, v. 10, no. 1, p. 33–44, doi: 10.1002/esp.3290100107.

Reid, I., and Laronne, J.B., 1995, Bed Load Sediment Transport in an Ephemeral Stream and a Comparison with Seasonal and Perennial Counterparts: Water Resources Research, v. 31, no. 3, p. 773–781, doi: 10.1029/94WR02233.

Richard, P., Nicodemi, M., Delannay, R., Ribière, P., and Bideau, D., 2005, Slow relaxation and compaction of granular systems.: Nature materials, v. 4, no. 2, p. 121–8, doi: 10.1038/nmat1300.

Rickenmann, D., and McArdell, B.W., 2008, Calibration of piezoelectric bedload impact sensors in the Pitzbach mountain stream: Geodinamica Acta, v. 21, no. 1–2, p. 35–52, doi: 10.3166/ga.21.35-52.

Rickenmann, D., and McArdell, B.W., 2007, Continuous measurement of sediment transport in the Erlenbach stream using piezoelectric bedload impact sensors: Earth Surface Processes and Landforms, v. 32, no. 9, p. 1362–1378, doi: 10.1002/esp.1478.

Riebe, C.S., Sklar, L.S., Overstreet, B.T., and Wooster, J.K., 2014, Optimal reproduction in salmon spawning substrates linked to grain size and fish length: Water Resources Research, v. 50, no. 2, p. 898–918, doi: 10.1002/2013WR014231.

Rouse, H., 1961, Fluid Mechanics for Hydraulic Engineers: Dover, New York.

Saletti, M., Molnar, P., Zimmermann, A., Hassan, M.A., and Church, M., 2015, Temporal variability and memory in sediment transport in an experimental step-pool channel: Water Resources Research, v. 51, no. 11, doi: 10.1002/2015WR016929.

Scheibling, R.E., Kelly, N.E., and Raymond, B.G., 2009, Physical disturbance and community organization on a subtidal cobble bed: Journal of Experimental Marine Biology and Ecology, v. 368, p. 94–100, doi: 10.1016/j.jembe.2008.10.017.

Scheingross, J.S., Winchell, E.W., Lamb, M.P., and Dietrich, W.E., 2013, Influence of bed patchiness, slope, grain hiding, and form drag on gravel mobilization in very steep streams: Journal of Geophysical Research: Earth Surface, v. 118, no. 2, p. 982–1001, doi: 10.1002/jgrf.20067.

Scholz, C.H., 1998, Earthquakes and friction laws: Nature, v. 391, no. 6662, p. 37–42, doi: 10.1038/34097.

Shields, A., 1936, Application of similarity principles and turbulence research to bed-load movement: Mitt. Preuss. Versuchsanst. Wasserbau Schiffbau, v. 26, no. 26.

Sklar, L.S., and Dietrich, W.E., 2004, A mechanistic model for river incision into bedrock by saltating bed load: Water Resources Research, v. 40, no. 6, p. W06301, doi: 10.1029/2003WR002496.

Sklar, L.S., and Dietrich, W.E., 2008, Implications of the saltation–abrasion bedrock incision model for steady-state river longitudinal profile relief and concavity: Earth Surface Processes and Landforms, v. 33, no. 7, p. 1129–1151, doi: 10.1002/esp.1689.

Steneck, R.S., Graham, M.H., Bourque, B.J., Corbett, D., Erlandson, J.M., Estes, J.A., and Tegner, M.J., 2003, Kelp forest ecosystems: biodiversity, stability, resilience and future: Environmental Conservation, v. 29, no. 4, p. 436–459, doi: 10.1017/S0376892902000322.

Stevens, C.L., Hurd, C.L., and Smith, M.J., 2001, Water motion relative to subtidal kelp fronds: Limnology and Oceanography, v. 46, no. 3, p. 668–678, doi: 10.4319/lo.2001.46.3.0668.

Turowski, J.M., Badoux, A., and Rickenmann, D., 2011, Start and end of bedload transport in gravel-bed streams: Geophysical Research Letters, v. 38, no. 4, p. n/a-n/a, doi: 10.1029/2010GL046558.

Turowski, J.M., Yager, E.M., Badoux, A., Rickenmann, D., and Molnar, P., 2009, The impact of exceptional events on erosion, bedload transport and channel

stability in a step-pool channel: Earth Surface Processes and Landforms, v. 34, no. 12, p. 1661–1673, doi: 10.1002/esp.1855.

Utter, B., and Denny, M., 1996, Wave-induced forces on the giant kelp Macrocystis pyrifera (Agardh): field test of a computational model: The Journal of Experimental Biology, v. 199, p. 2645–2654.

Vogel, S., 1984, Drag and Flexibility in Sessile Organisms: Integrative and Comparative Biology, v. 24, p. 37–44, doi: 10.1093/icb/24.1.37.

Westoby, M.J., Brasington, J., Glasser, N.F., Hambrey, M.J., and Reynolds, J.M., 2012, "Structure-from-Motion" photogrammetry: A low-cost, effective tool for geoscience applications: Geomorphology, v. 179, p. 300–314, doi: 10.1016/j.geomorph.2012.08.021.

Wiberg, P.L., and Smith, J.D., 1987, Calculations of the Critical Shear Stress for Motion of Uniform and Heterogenous Sediments: Water Resources Research, v. 23, no. 8, p. 1471–1480.

Wilcock, P.R., and Crowe, J.C., 2003, Surface-based Transport Model for Mixed-Size Sediment: Journal of Hydraulic Engineering, v. 129, no. 2, p. 120–128, doi: 10.1061/(ASCE)0733-9429(2003)129:2(120).

Wong, M., and Parker, G., 2006, Reanalysis and Correction of Bed-Load Relation of Meyer-Peter and Müller Using Their Own Database: Journal of Hydraulic Engineering, v. 132, no. 11, p. 1159–1168, doi: 10.1061/(ASCE)0733-9429(2006)132:11(1159).

Woodborne, M.W., Rogers, J., and Jarman, N., 1989, The Geological Significance of Kelp-Rafted Rock along the West Coast of South Africa: Geo-Marine Letters, v. 9, p. 109–118.

Wyss, C.R., Rickenmann, D., Fritschi, B., Turowski, J.M., Weitbrecht, V., Travaglini, E., Bardou, E., and Boes, R.M., 2016, Laboratory flume experiments with the Swiss plate geophone bed load monitoring system: 2. Application to field sites with direct bed load samples: Water Resources Research, v. 52, no. 10, p. 7760–7778, doi: 10.1002/2016WR019283.

Yager, E.M., Dietrich, W.E., Kirchner, J.W., and McArdell, B.W., 2012a, Patch dynamics and stability in steep, rough streams: Journal of Geophysical Research, v. 117, no. F2, p. F02010, doi: 10.1029/2011JF002253.

Yager, E.M., Kirchner, J.W., and Dietrich, W.E., 2007, Calculating bed load transport in steep boulder bed channels: Water Resources Research, v. 43, no. 7, p. W07418, doi: 10.1029/2006WR005432.

Yager, E.M., Turowski, J.M., Rickenmann, D., and McArdell, B.W., 2012b,

Sediment supply, grain protrusion, and bedload transport in mountain streams: Geophysical Research Letters, v. 39, no. 10, p. L10402, doi: 10.1029/2012GL051654.

Yalin, M.S., 1972, Mechanics of Sediment Transport: Pergamon Press, Oxford.